SYNTHESIS, CHARACTERIZATION AND PHOTOLUMINESCENCE PROPERTIES OF LANTHANIDE-*β*-DIKETONATE COMPLEXES

Thesis Submitted to AcSIR for the Award of the Degree of
DOCTOR OF PHILOSOPHY
in Chemical Sciences

By

GEORGE T. M.

Registration No: 10CC11A39006

Under the guidance of

Dr. M. L. P. REDDY

CSIR-NATIONAL INSTITUTE FOR INTERDISCIPLINARY SCIENCE AND TECHNOLOGY (CSIR-NIIST)
THIRUVANANTHAPURAM-695 019, KERALA, INDIA

2016

….Dedicated to

My Family….

DECLARATION

I hereby declare that the Ph.D. thesis entitled: "**Synthesis, characterization and photoluminescence properties of lanthanide-*β*-diketonate complexes**" is the result of the investigations carried out by me at the Materials Science and Technology Division, CSIR-National Institute for Interdisciplinary Science and Technology (CSIR-NIIST), Trivandrum, under the supervision of Dr. M. L. P. Reddy and the same has not been submitted elsewhere for any other degree.

In keeping with the general practice of reporting scientific observations, due acknowledgement has been made wherever the work described is based on the findings of other investigators.

GEORGE T. M.

COUNCIL OF SCIENTIFIC & INDUSTRIAL RESEARCH
NATIONAL INSTITUTE FOR INTERDISCIPLINARY SCIENCE AND TECHNOLOGY (CSIR-NIIST)
Industrial Estate P.O., Trivandrum - 695 019, India

Dr. M. L. P. Reddy, FAPSc
Chief Scientist

Tel: 91-471-2515 360
Fax: +91-471-2491 712
E-mail: mlpreddy55@gmail.com

CERTIFICATE

This is to certify that the work incorporated in this Ph.D. thesis entitled "**Synthesis, characterization and photoluminescence properties of lanthanide *β*-diketonate complexes**" submitted by **Mr. GEORGE T. M.** to Academy of Scientific and Innovative Research (AcSIR), in partial fulfilment of the requirements for the award of the **Degree of Doctor of Philosophy in Chemical Sciences**, embodies original research work under my supervision and guidance at the Materials Science and Technology Division of the CSIR-National Institute for Interdisciplinary Science and Technology (CSIR-NIIST), Trivandrum. I further certify that this work has not been submitted to any other University or Institution in part or full for the award of any degree or diploma. Research material obtained from other sources has been duly acknowledged in the thesis. Any text, illustration, table etc., used in the thesis from other sources, have been duly cited and acknowledged.

GEORGE T. M.

Thiruvananthapuram
October, 2016

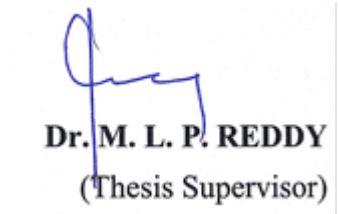

ACKNOWLEDGEMENTS

It gives me great pleasure to express my deepest gratitude to my research supervisor, Dr. M. L. P. Reddy, for suggesting the research problem and his valuable guidance and encouragement leading to the successful completion of this work.

I am grateful to Dr. A. Ajayaghosh, Director, NIIST, and former Directors Dr. Suresh Das and Dr. Gangan Pratap, for providing the necessary facilities and infrastructure to carry out this investigation.

My sincere thanks to:

- *Dr. R. Luxmi Varma and Dr. Mangalam S. Nair, present and former AcSIR co-ordinators.*
- *Dr. K. V Radhakrishnan, Dr. Ravi Shankar L. and Dr. Luxmi Varma, my DAC members.*
- *Dr. Sunil Varughese of Chemical Sciences and Technology Division, NIIST for X-ray single crystal measurements.*
- *Dr. Mahesh S. Krishna from Rajiv Gandhi Centre for Biotechnology (RGCB) Thiruvananthapuram for the imaging experiments.*
- *Dr. N. Gopakumar and Mr. S. J. Sajan from Mahatma Gandhi College, Thiruvananthapuram for Triboluminescence measurements.*
- *Dr. C. K. Jayasankar and Mr. Suresh K, Sree Venkateswara University for NIR luminescence measurements.*
- *Dr. V. Divya, Dr. S. Sarika, Dr. A. R. Ramya, Dr. Biju Francis, Dr. Sheethu Jose, Ms. P. Aiswaria, Mr. K. S. Bejoymohandas, Ms. T. V. Usha Gangan, Mrs. J. Anaswara, Mr. K. R. Ajay, Mr. S. Sreenadh, Mrs. M. V. Lucky, Mr. P. K. Thejus, Mr. Alikunhi, Mrs. S. Surya, Ms. S. Anila, Ms. Syamasrit Dash, Ms. Amala Augustine my roommates and all other friends at NIIST family for their help and cooperation.*
- *All technical supportive staff of CSIR-NIIST for their timely help in the utilization of sophisticated analytical instruments.*
- *All my teachers for their encouragement at different stages of my academic career.*
- *University Grants Commission (UGC), New Delhi, Government of India for financial assistance.*

I wish to thank my parents for their love encouragement and blessings, without whom I would never have enjoyed so many opportunities. Finally I would like to thank, my beloved brothers, my sisters in law, friends and relatives for their excellent support and encouragement.

Above all, I thank Almighty for his showers of blessings throughout my research work to complete the research successfully.

GEORGE T. M.

CONTENTS

List of Schemes

List of Figures

List of Tables

ABBREVIATIONS

UV	Ultra Violet
OLED	Organic Light Emitting Diode
EL	Electroluminescence
PL	Photoluminescence
ET	Energy Transfer
Ln^{3+}	Trivalent Lanthanide ion
Eu^{3+}	Trivalent Europium ion
Nd^{3+}	Trivalent Neodymium ion
Yb^{3+}	Trivalent Ytterbium ion
Gd^{3+}	Trivalent Gadolinium ion
S_1	Singlet
T_1	Triplet
fod	6,6,7,7,8,8,8-heptafluoro-2,2-dimethyloctane-3,5-dione
XRD	X-Ray Diffraction
$CHCl_3$	Chloroform
$CDCl_3$	Chloroform-d
ESI-MS	Electro Spray Ionization Mass Spectroscopy
NMR	Nuclear Magnetic Resonance
DMSO	Dimethyl sulphoxide
DMEM	Dulbecco's Minimal Essential Medium
NaH	Sodium hydride

HCl	Hydrochloric acid
DPEPO	bis(2-(diphenylphosphino)phenyl) ether oxide
2-TFDBC	2-(4′4′4′-trifluoro-1′3′-dioxobutyl)-carbazole
2,7-BTFDBC	2,7-bis(4′4′4′-trifluoro-1′3′-dioxobutyl)-carbazole
Phen	1,10-phenanthroline
NTA	1-(2-naphthoyl)-3,3,3-trifluoroacetonate
PMMA	poly(methyl methacrylate)
DDXPO	4,5-bis(diphenylphosphino)-9,9-dimethylxanthene oxide
bpy	2,2′- bipyridine
DBM	Dibenzoylmethane
TTA	Theonyltrifluoroacetylacetone
tpy	2,2':6,6"-terpyridine
CIE	International Commission on Emission
THF	Tetrahydrofuran
IR	Infrared
NIR	Near-Infrared
FT-IR	Fourier Transform Infrared spectrophotometer
FT-Raman	Fourier Transform Raman spectrophotometer
GFP	Green fluorescent protein
MTT	3-[4,5-dimethylthiazol-2-yl]-2,5-diphenyltetrazoliumbromide
FBS	Fetal Bovine Serum
TL	Triboluminescence

PREFACE

The unique electronic structures of lanthanide cations ligated with conjugated organic ligands continue to stimulate an ever increasing number of important technological applications in fields as diverse as biomedicine and materials science. Moreover, the long excited-state lifetimes and the high chromaticities of the lanthanides are also pertinent to applications in the domain of solid-state photonic materials. For instance, Tb^{3+}, Eu^{3+} and Tm^{3+} cations are used as green, red, and blue emitters, respectively, in multicolour displays and organic light-emitting diodes (OLEDs). However, since f-f transitions are parity forbidden, unligated luminescent lanthanide cations have extremely low molar extinction coefficients; hence, direct lanthanide excitation results only in modest luminescence intensities. Therefore, over the past few years, efforts have been made to augment the absorption coefficients and thereby obtain significantly more intense lanthanide ion emissions. Fortunately, this objective can be accomplished by prudent selection and synthesis of organic ligands with conjugated motifs. β-diketones are particularly valuable in this context because such ligands can absorb ultraviolet light and transfer the absorbed energy to the central lanthanide ions in an appropriately effective manner (the so-called antenna effect). Therefore the objective of the current research work is to design and develop efficient light emitting materials based on lanthanide aromatic β-diketones with superior photophysical properties.

The present thesis has been divided into four chapters. In the first chapter, general principles for improving the light harvesting feature in the design of luminescent lanthanide complexes were discussed with a specific emphasis on how to take advantage of it for developing "robust antenna molecules" based on *β*-diketones. Furthermore, the objectives of the thesis are also briefly presented in this chapter.

In the second chapter, a new polyfluorinated *β*-diketonate ligand containing a pyrene chromophore, namely, 4,4,5,5,6,6,6- heptafluoro-3-hydroxy-1-(pyren-1-yl)hex-2-en-1-one (Hhfpyr) has been designed and employed for the development of a series of near-infrared (NIR) emitting lanthanide complexes (Nd^{3+} and Yb^{3+}) in the absence and presence of an ancillary ligand, 4,7-diphenyl-1,10-phenanthroline (bath). The isolated NIR emitting lanthanide complexes [$Nd(hfpyr)_3(H_2O)$ **1**, $Nd(hfpyr)_3(bath)$ **2**, $Yb(hfpyr)_3(H_2O)$ **3** and $Yb(hfpyr)_3(bath)$ **4**] have been characterized by various spectroscopic techniques and evaluated their photoluminescence properties. The photophysical properties disclosed that the developed pyrene-based *β*-diketonate ligand is well suited for the sensitization of Nd^{3+} as well as Yb^{3+} emissions, thanks to the favourable position of the triplet state (T_1) of the ligand ($\Delta E = T_1 - {}^4F_{3/2} = 4700\ cm^{-1}$ for Nd^{3+} and $\Delta E = T_1 - {}^2F_{5/2} = 6200\ cm^{-1}$ for Yb^{3+}), as evidenced from the phosphorescence spectra of the corresponding Gd^{3+} complexes. Most importantly, the displacement of solvent molecules from the coordination sphere of the NIR emitting lanthanide binary complexes (**1** and **3**) with

an ancillary ligand markedly enhances the quantum yields ($\boldsymbol{\Phi}_{overall}$ = 0.45 for **1** to 1.07% for **2** and from 1.69 for **3** to 3.08% for **4**) and excited state lifetime values (τ = 2.80 for **1** to 6.16 μs for **2** and from 6.88 for **3** to 13.45 μs for **4**). Notably, Yb^{3+} ternary compound **4** with promising NIR luminescence properties was embedded into PMMA matrices, giving rise to a series of PMMA-supported hybrid materials (PMMA@**4**), where the thermal stability and the film-forming properties were significantly enhanced.

The third chapter deals with the synthesis and characterization of a novel lysosome targetable luminescent bioprobe derived from a europium coordination compound, namely, $Eu(pfphOCH_3IN)_3(DDXPO)$ [where $HpfphOCH_3IN$ = 4,4,5,5,5-pentafluoro-3-hydroxy-1-(1-(4-methoxyphenyl)-1H-indol-3-yl)pent-2-en-1-one and DDXPO = 4,5-bis(diphenylphosphino)-9,9-dimethylxanthene oxide]. Notably, the newly designed europium complex exhibits significant quantum yield ($\boldsymbol{\Phi}_{overall}$ = 25 ± 3%) and $^5D_0$ excited state lifetime (τ = 398 ± 3 μs) values under physiological pH (7.2) conditions when excited at 405 nm. Hence the developed europium complex has been evaluated for the live cell imaging application using mouse pre-adipocyte cell lines (3T3L1). Most importantly, the developed bioprobe exhibits good cell permeability, photostability and non-cytotoxicity. Colocalization studies of the designed bio-probe with commercial Lysosome-GFP in 3T3L1 cells demonstrated the specific localization of the probe in the lysosome with a high colocalization coefficient (A = 0.83).

The fourth chapter describes the synthesis of a new *β*-diketonate ligand, namely, 1-(4-(diphenylphosphino)phenyl)-4,4,5,5,5-pentafluoro- pentane-1,3-dione (DPPFH) and utilized for the construction of an antenna complex of Eu^{3+} [$Eu(DPPF)_3(DDXPO)$] in the presence of a chelating ligand, 4,5-bis(diphenylphosphino)- 9,9 - dimethylxanthene oxide (DDXPO). The developed Eu^{3+} compound has been well characterized and investigated the photophysical properties. The designed Eu^{3+} complex displays bright red luminescence upon irradiation at the ligand-centered band at 375 nm with a quantum yield of 39% in the solid-state. Interestingly, the ternary Eu^{3+} complex also exhibits brilliant triboluminescence in the daylight, which could be useful in the design of pressure and damage detection probes. In addition, the newly obtained Eu^{3+} complex was embedded into a PMMA matrix to form highly luminescent films having quantum yields as high as 45–50%. These plastic materials display enhanced thermal stability as compared to parent compound. The ground state coordination geometry of the typical Eu^{3+} complex was calculated using the Sparkle/RM1 model. The excellent agreement between the experimental and theoretically predicted photophysical data, attesting the efficacy of the theoretical approach implemented in the LUMPAC software (http://lumpac.pro.br).

Chapter 1

Introduction to Lanthanide Luminescence

Lanthanide ions (Ln^{3+}) possess fascinating optical properties and their discovery, first industrial uses and present high technological applications are largely governed by their interaction with light.[1] Lighting devices (economical luminescent lamps, light emitting diodes),[2] television and computer displays,[3] optical fibres,[1b, 4] optical amplifiers,[1b, 4a, 5] lasers,[1b, 4a, 5] as well as responsive luminescent stains for biomedical analysis,[2d, 6] medical diagnosis,[7] and cell imaging[8] rely heavily on lanthanide ions (Figure 1.1).

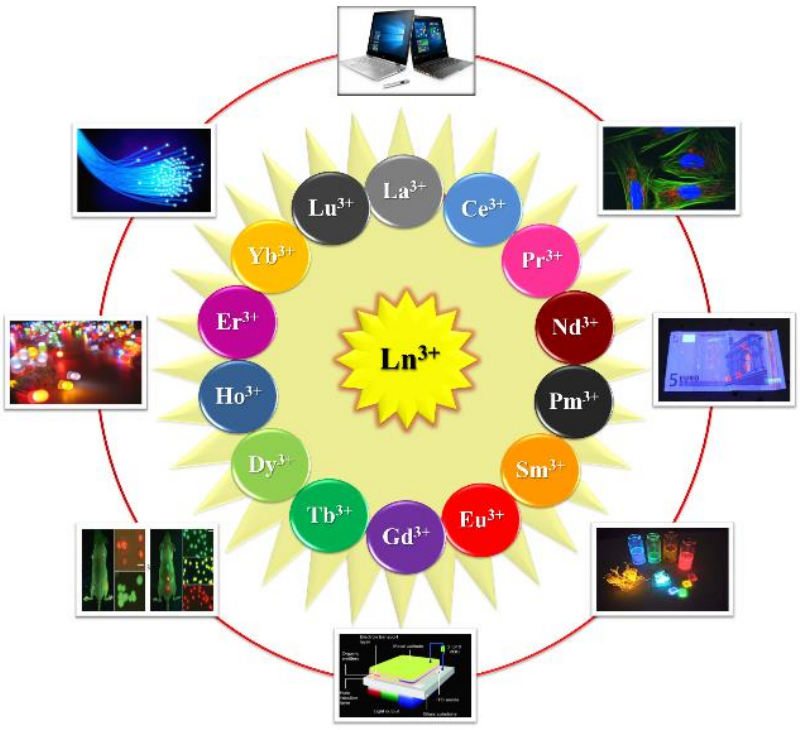

Figure 1.1. Applications of Ln^{3+} coordination complexes.

Lanthanides possess intrinsic luminescence that originates from f−f electron transitions in the $4f^n$ shell of the $[Xe]5s^25p^6$ configuration and offer unique properties for optical imaging contrast agents that address current limitations of their organic counterparts.[8d,9] First, due to shielding by the 5s and 5p orbitals, the 4f orbitals do not directly participate in chemical bonding. Hence the emission wavelengths of lanthanides are minimally perturbed by the surrounding matrix and ligand field, resulting in sharp, line-like emission bands with the same fingerprint wavelengths and narrow peak widths of the corresponding free Ln^{3+} salts. Second, the f−f transitions are formally forbidden by the spin and Laporte rule and feature long excited-state lifetimes in the milli to microsecond range.[9b, 10] Although the excited-state lifetimes of Ln^{3+} complexes are long, the forbidden f−f transitions suffer the consequence of weak intrinsic luminescence due to low molar absorptivity.[1d, 9a, 11] Intense light sources such as lasers are required to populate the excited states of Ln^{3+} ions by direct excitation and are impractical for the majority of biological imaging. Attachment of a light-harvesting antenna circumvents this limitation by sensitizing the Ln^{3+} ion in what has been termed as the antenna effect (Figure 1.2).[12] Light absorbed to the short-lived singlet excited state of the antenna ($S_0 \rightarrow S_1$) can undergo intersystem crossing to the longer-lived triplet excited state ($S_1 \rightarrow T_1$). Sensitization occurs by population of the lowest excited state of the lanthanide through energy transfer from the T_1 state of the antenna. Energy transfer can also occur from the S_1 state, but energy transfer from the T_1 state is generally accepted as the mechanism due to its longer lifetime.[1e, 13] Electronic transitions from the excited

state to the ground state of the lanthanide ion emit photons characterized by a series of bands in the visible (Eu^{3+} and Tb^{3+}), near-IR wavelengths ((Dy^{3+}, $Sm^{3+,}$ Nd^{3+} and Yb^{3+}).[14] On the basis of this mechanism, most existing lanthanide-based optical probes comprise three major components: a luminescent metal center, a protective chelate, and a sensitizing antenna.[1c, 15]

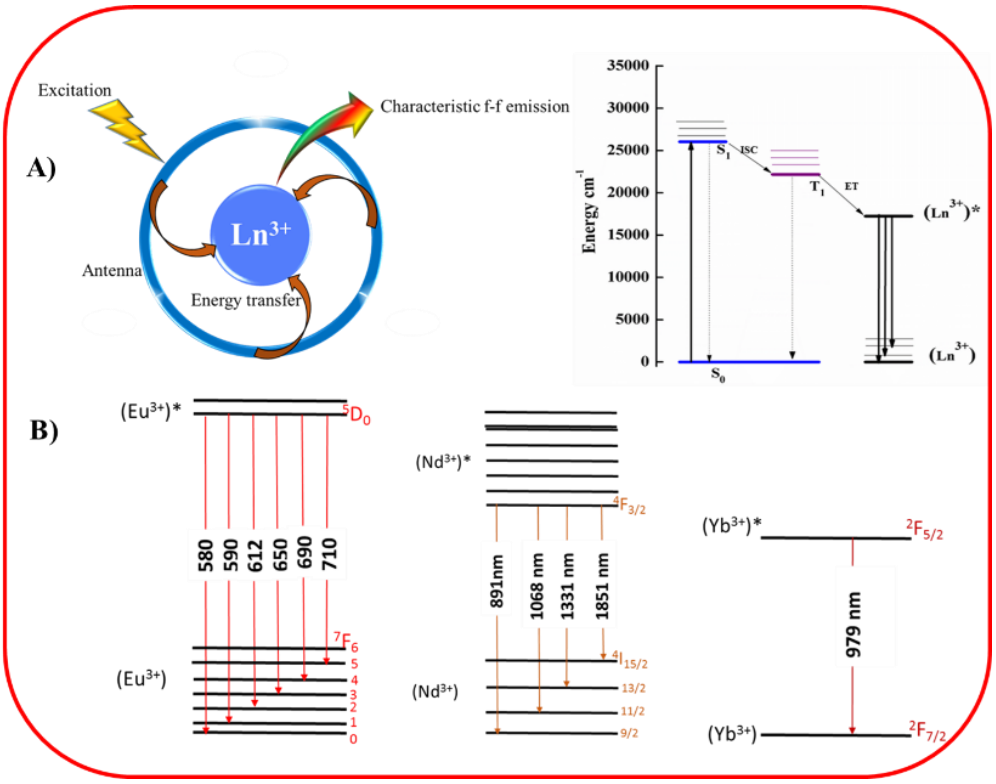

Figure 1.2. (A) The antenna effect. The general architecture of emissive lanthanide complexes consists of the metal center surrounded by an antenna molecule. The antenna harvests energy through high molar absorption to the singlet excited state. After undergoing intersystem crossing to the triplet state, the antenna transfers energy to the excited state of the lanthanide. The radiative transition of electrons from the excited state to the ground states results in luminescent emission from the lanthanide ion. (B) Luminescent 4f−4f transitions of europium, neodymium and ytterbium complexes.

The most important point to consider in the design of luminescent Ln^{3+} complexes is the crucial role played by OH, NH and CH oscillators in the possible quenching of the Ln^{3+} emission. In the late 1970s, Horrocks and co-workers demonstrated that the photoluminescence lifetime of Eu and Tb complexes was directly related to the number of O–H oscillators in the first coordinating sphere of the cations.[16] By comparing lifetimes measured in H_2O and D_2O, they derived empirical rules that allowed us to determine the number of water molecules in the first coordination sphere. This pioneering work was followed by numerous others, including the influence of other oscillators (NH, amide NH, CH) and outer sphere contributions[17] as well as other Ln^{3+} cations (Dy^{3+}, Sm^{3+}),[18] among which are some NIR emitters (Yb^{3+} and Nd^{3+}).[19] The coordination of the ligands will be essentially guided by a subtle balance between the strength of the electrostatic interactions between the Ln^{3+} and the ligands and steric repulsion interactions between the ligands around the cation. In summary, the main pre-requisites to build a ligand that will afford an efficient Ln^{3+} luminescent label are:

- ✓ High absorption coefficient.
- ✓ Fine tuning of the singlet and triplet energy levels depending on the targeted Ln^{3+} cation.
- ✓ Good shielding of the Ln^{3+} cation by the ligand (CN = 7 to 10).
- ✓ High thermodynamic and kinetic stabilities.
- ✓ Compatible physicochemical properties with biological media.

1.1. Overview On the Luminescent Lanthanide *β*-Diketonate Complexes

The luminescent properties of lanthanide *β*-diketonate complexes have been extensively investigated and these data are well documented in many pioneering review articles.[2c, 2d, 8a, 20]

1.1.1. Luminescent Properties of Carbazole Based Eu^{3+}-*β*-diketonate Complexes

The carbazole moiety displays unique advantages for application in optoelectronic devices because of inexpensive starting material, good chemical stability, and being tailored with a wide variety of functional groups to tune the optical and electrical properties.[21] As a consequence, carbazole-containing *β*-diketones and their corresponding Eu^{3+} complexes have been extensively studied and it was concluded that Eu^{3+} complexes with these kinds of *β*-diketonates containing 1′,3′-dioxobutyl linked at the 3- and 6-positions failed to extend their excitation band to the visible region.[21a, 21b, 21d, 22] On the other hand, the introduction of 1′,3′-dioxobutyl linked at the 2- and 7-positions in a carbazole ring leads to a longer π-conjugation length, which results in a bathochromic shift in the excitation band. However, the synthesis of this type of compound is challenging.

Gong and co-workers[23] were successful in designing two new carbazole-based *β*-diketonates with 2- or 2,7-substituted groups in the carbazole ring, 2-(4′,4′,4′-

trifluoro-1′,3′-dioxobutyl)-carbazole (2-TFDBC) and 2,7-bis(4′,4′,4′-trifluoro-1′,3′-dioxobutyl)- carbazole (2,7-BTFDBC), and their Eu^{3+} ternary complexes Eu(2-TFDBC)$_3$(phen) and Eu_2(2,7-BTFDBC)$_3$(phen)$_2$. Compared with the similar *β*-diketonate complexes linked at 3- and 6-positions in the carbazole ring,[24] the excitation bands of Eu(2-TFDBC)$_3$(phen) and Eu_2(2,7-BTFDBC)$_3$(phen)$_2$ showed a remarkable red shift by about 30 nm and were extended to 500 nm because of the larger π-conjugation in the molecules (Figure 1.3). However, the strongest excitation peak of these two complexes was not long enough to avoid the photodecomposition efficiently. The luminescence application of the complexes Eu(2-TFDBC)$_3$(phen) and Eu_2(2,7-BTFDBC)$_3$(phen)$_2$ is confirmed by the high decomposition temperatures obtained (361.4 and 367.3 °C in air, respectively) by thermo-gravimetric analysis. The ancillary ligand, phen, enhances the luminescence intensity and thermal stabilities of the complexes and satisfies the high coordination number of the central Eu^{3+} ion. The quantum yields are found to be 28% for Eu(2-TFDBC)$_3$(phen) and 10% for Eu_2(2,7-BTFDBC)$_3$(phen)$_2$. This quantum yield reduction can be explained by the closer Eu^{3+}-Eu^{3+} distance in the Eu_2(2,7-BTFDBC)$_3$(phen)$_2$ molecule than that in Eu(2-TFDBC)$_3$(phen), and thus, the concentration quenching more easily happens in the former molecule.

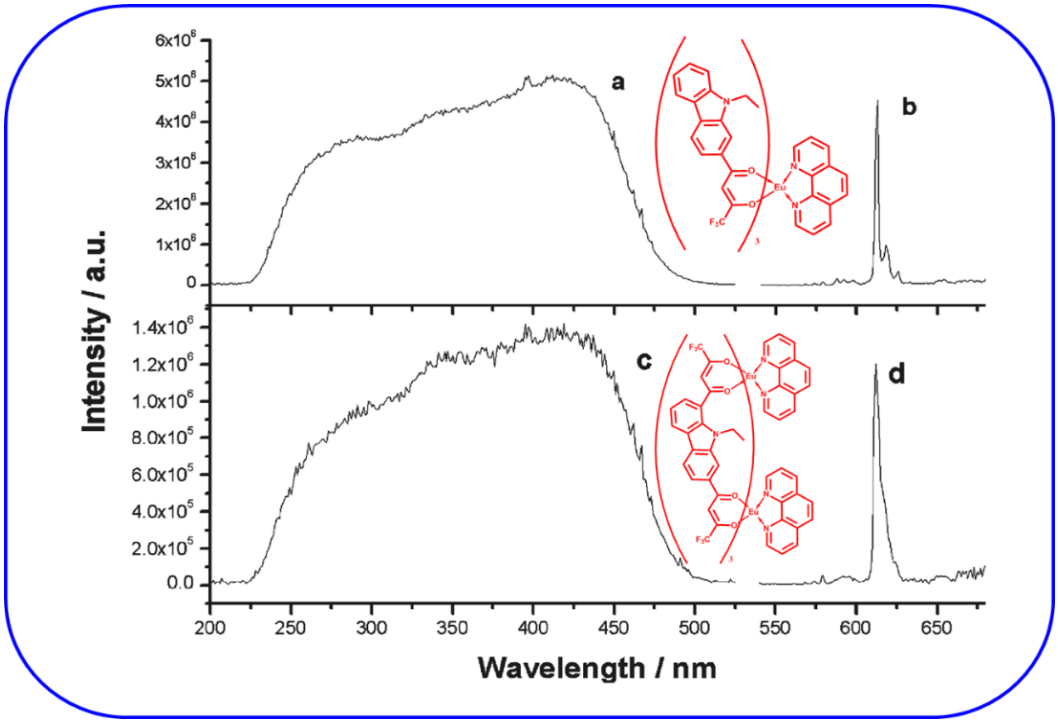

Figure 1.3. Excitation (a and c) and emission (b and d) spectra of Eu(2-TFDBC)$_3$(phen) and Eu$_2$(2,7-BTFDBC)$_3$(phen)$_2$ respectively in the solid state (λ_{exc} =429 nm and λ_{em}=613 nm).

In order to minimize the photodecomposition and also to extend the excitation band to the blue region, in the subsequent studies Gong and coworkers[21c] introduced a methoxyl moiety at the 7-position of β-diketone; thus a new organic ligand, 1-(9-ethyl-7-methoxyl-9H-carbazol-2-yl)-4,4,4-trifluorobutane-1,3-dione (EMOCTFBD), and its Eu^{3+} ternary complex Eu(EMOCTFBD)$_3$(phen) were synthesized and their photophysical properties have been investigated. The introduction of a methoxyl in the 7-position of the carbazole ring remarkably enhanced the excitation band intensity in the blue region, and the complex exhibited intense red emission under blue-light excitation. The integrated emission intensity of Eu(EMOCTFBD)$_3$(phen) has been

enhanced by 60% as compared with the complex Eu(2-TFDBC)$_3$(phen) without a methoxyl at the 7-position of the ligand. This may be due to the modification of the molecular structure of the ligand. Substitution of the 7-positional hydrogen atom with a methoxyl leads to the increase of the electronic density in the carbazole ring, and thus increases the electron transition probability, which in turn enhances the excitation intensity. Finally, a bright red-emitting diode was fabricated by coating the complex phosphor onto a ~460 nm emitting InGaN chip (Figure 1.4). All the results indicate that Eu (EMOCTFBD)$_3$(phen) is an interesting red-emitting material excited by blue light, and therefore may be applied in many fields without UV radiation.

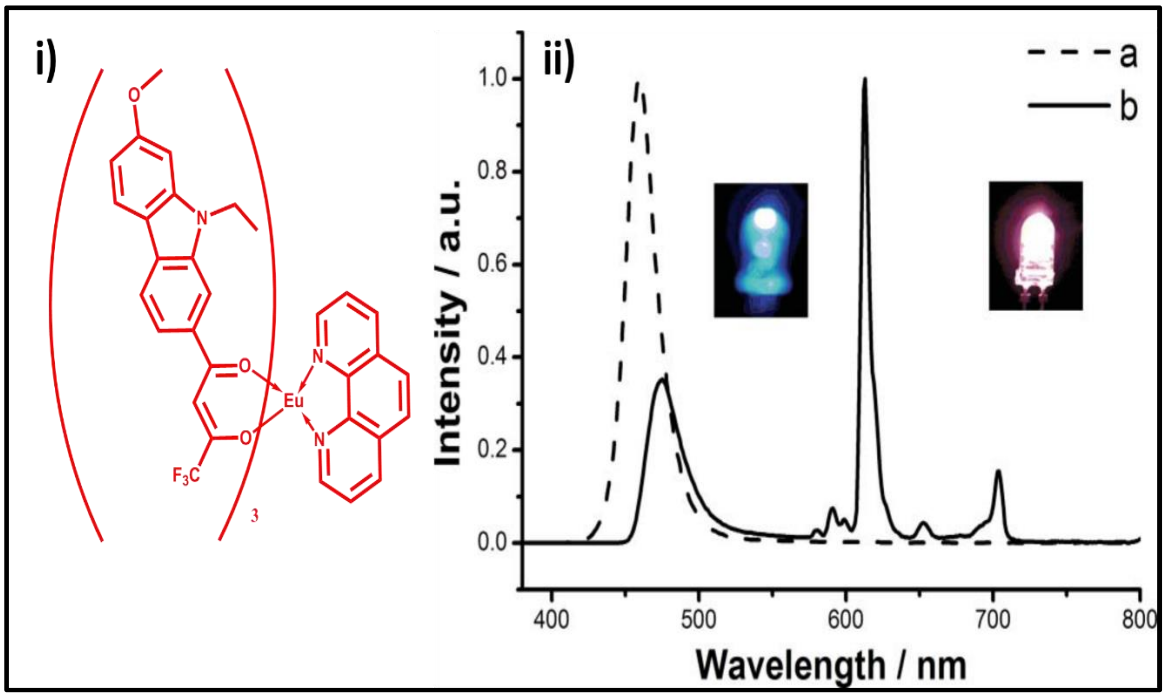

Figure 1.4. (i) Molecular structure, (ii) Emission spectra and the photographs of the original InGaN LED without phosphor (a and left) and the LED with Eu(EMOCTFBD)$_3$(phen) (b and right) under excitation of 20 mA forward bias. Inset: photographs of the lighting LEDs.

Liu and co-workers[25] have developed a new ligand which contains carbazole group, 1-(7-(tert-butyl)-9-ethyl-9H-carbazol-2-yl)-4,4,4-trifluorobutane-1,3-dione (HL), and is utilized for the construction of a new complex, $EuL_3(phen)$. Photoluminescent measurement indicates that the Eu^{3+} complex exhibits intense red-emission and extends their excitation bands to the visible region. Compared with the similar 3-(*β*-diketonato)carbazole complexes, the excitation bands of the complex show a remarkable red-shift by about 30 nm and were extended to 500 nm. Complex $EuL_3(phen)$ was employed as a phosphor to fabricate LEDs in a mass ratio of 1:20 of phosphor to silicone gel with 460 nm-emitting InGaN chips. The emission spectra of the original 460 nm LEDs without phosphor and the LED fabricated with the complex and a 460 nm chip under 20 mA forward bias are shown in figure 1.5. The sharp peak at 613 nm is due to the Eu^{3+} emission from the complex in the LEDs chip.

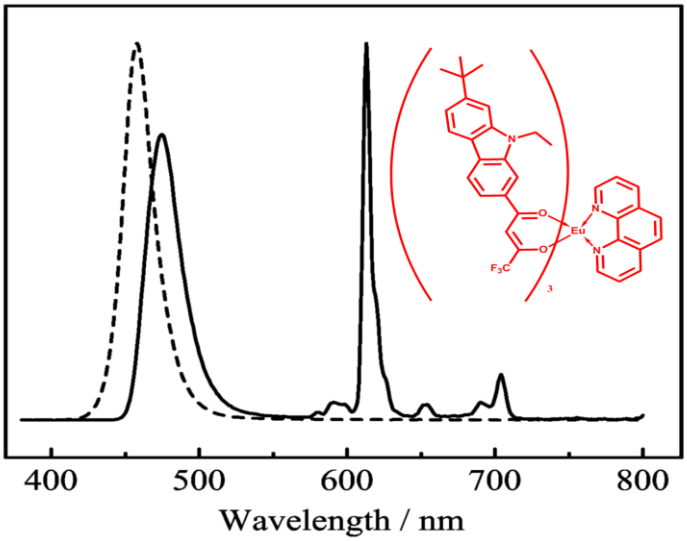

Figure 1.5. Molecular structure of $EuL_3(phen)$ and emission spectra of the original InGaN LEDs without phosphor (broken line) and the LEDs with $EuL_3(phen)$ (solid line) under excitation of 20 mA forward bias.

Reddy and co-workers[26] have synthesized a series of Eu^{3+} complexes based on novel carbazole-based fluorinated *β*-diketones, namely, 4,4,5,5,5-pentafluoro-3-hydroxy-1-(9-phenyl-9H-carbazol-2-yl)pent-2-en-1-one (L1) and 4,4,5,5,5-pentafluoro-3-hydroxy-1-(9-(4-methoxyphenyl)-9H-carbazol-2-yl)pent-2-en-1-one (L2) as primary ligands and a bidentate phosphine oxide molecule, 4,5-bis(diphenylphosphino)-9,9-dimethylxanthene oxide (DDXPO) as ancillary ligand (Figure 1.6). Using the Sparkle/PM3 model the molecular geometries of the designed complexes are optimized and the luminescent parameters are calculated by the LUMPAC software. The results demonstrated that suitably expanded π-conjugation in the developed Eu^{3+}–carbazole based *β*-diketonate complexes dramatically red-shifted the excitation maximum to the visible region (λ_{exc} = 420 nm) with an impressive quantum yield (34–42%). The triplet state energy levels of L1 and L2 in the complexes are higher than that of the lowest excited level of Eu^{3+} ion, $^5D_0$, so the photoluminescence mechanism of the Eu^{3+} complexes was proposed as a ligand-sensitized luminescence process. The predicted luminescent parameters from the Sparkle/PM3 structures are in agreement with the experimental data, which shows the efficacy of the theoretical models adopted in the present study. The improvements in the photophysical properties and excitation window, brought about by the introduction of extended conjugation and ancillary ligand; emphasize the significance of molecular engineering of ligand and complexes to achieve desired properties.

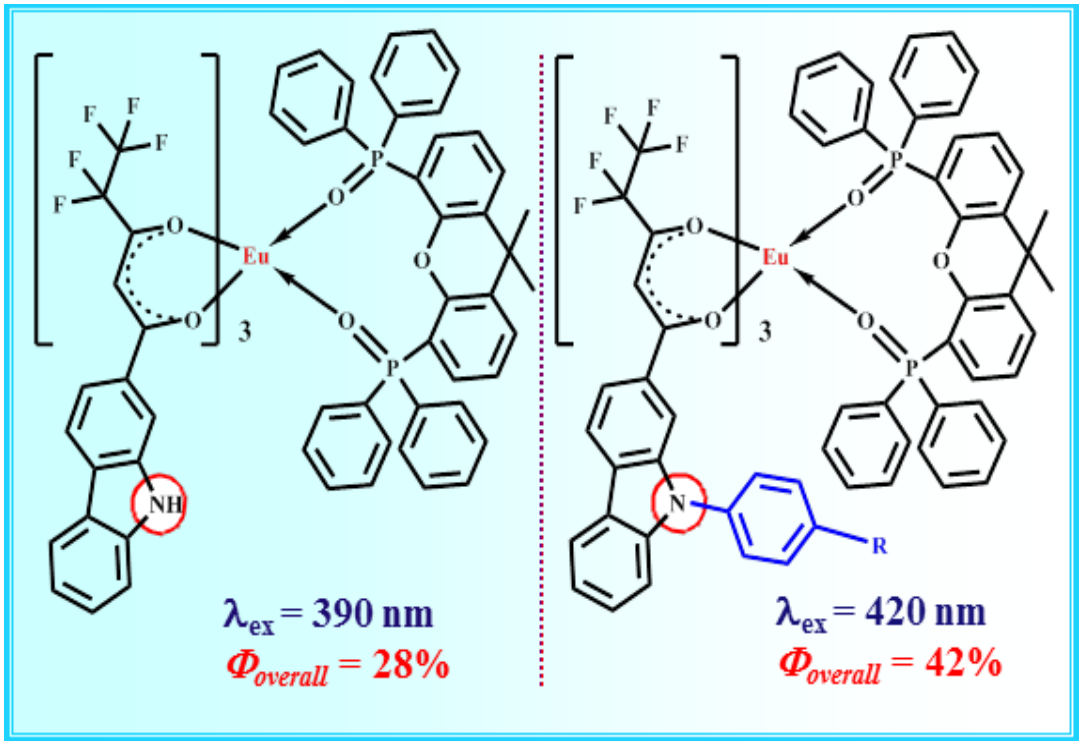

Figure 1.6. Molecular structures of $Eu(L1)_3(DDXPO)$ (left) and $Eu(L2)_3(DDXPO)$ (right).

1.1.2. Luminescent Properties of Phenanthrene Based Fluorinated Eu^{3+}-β-diketonate Complexes

Reddy and co-workers[27] have developed a novel β-diketonate ligand, namely, 4,4,5,5,5-pentafluoro-3-hydroxy-1-(phenanthren-3-yl)pent-2-en-1-one (Hpfppd), by incorporating a highly conjugated phenanthrene moiety as well as a polyfluorinated alkyl group in the complex molecule with a view to improve the quantum efficiency and especially to shift the excitation window to longer wavelengths in Eu^{3+}–β-diketonate complexes for use in bioassays. The synthesized ligand has been well characterized and utilized for the construction of two new europium complexes $Eu(pfppd)_3(H_2O)_2$ and $Eu(pfppd)_3(tpy)$ (where tpy = 2,2′:6,6″-terpyridine). The

photophysical studies demonstrated that the introduction of conjugated phenanthrene moiety in 3-position of the *β*-diketonate ligand remarkably extends the excitation window of the Eu^{3+} complexes towards the visible region (500 nm). The replacement of high-energy oscillators O–H in $Eu(pfppd)_3(H_2O)_2$ with an ancillary ligand, terpyridine, leads to an impressive enhancement in both overall quantum yield (from 31 to 75%) and $^5D_0$ lifetime (from 0.51 to 1.04 ms) values. It is interesting to note that the newly developed Eu^{3+} complex also exhibits a strong photoluminescence (quantum yield = 41%) and a long lifetime (0.88 ms) under physiological pH conditions (7.4) when excited under blue light (403 nm) and selectively stains cellular mitochondria of the rat embryonic heart cell line, H9c2. (Figure 1.7.) The ternary Eu^{3+} complex permeates into the H9c2 cells and co-localises with the mitochondria, as demonstrated by counterstaining experiments. The attractive feature of the developed Eu^{3+} complex is its chemical stability at ambient temperature and it requires less incubation time (30 min) as compared to commercial Mitotracker, CellLight™ Mitochondria-GFP (16 h). On the other hand, the commercially available Mitotracker Green has the typical problem of thawing and freezing and must be stored at −20 °C due to chemical instability. These properties of the designed Eu^{3+} ternary complex, together with its good cell membrane permeability and fast cellular uptake, suggest its potential as a mitochondria targeting probe excitable at visible light.

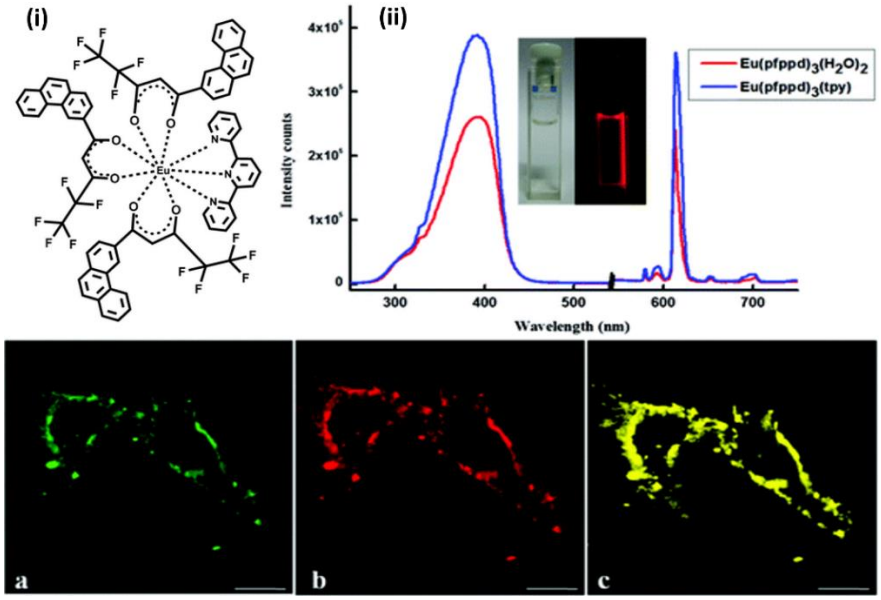

Figure 1.7. (i) Molecular structure of $Eu(pfppd)_3(tpy)$, (ii) excitation and emission spectrum of $Eu(pfppd)_3(tpy)$ and $Eu(pfppd)_3(H_2O)_2$ (a) An image of the H9c2 cells after 16 h incubation with Mitochondria tracker CellLight™ Mitochondria-GFP BacMam 2.0, (b) An image of the H9c2 cells after incubation with 30 μM of the $Eu(pfppd)_3(tpy)$ complex for 30 min, (c) The merged image. Scale bars: 25 μm.

1.1.3. Luminescent Properties of Triphenylamine Based Fluorinated Eu^{3+}-*β*-diketonate Complexes

Triphenylamine derivatives are widely used as hole-transporting materials in Organic Light Emitting Diodes (OLEDs) due to their high charge mobility, light-harvesting unit and high thermal stability. It is well documented that the replacement of C–H bonds in a *β*-diketonate ligand with lower-energy C–F oscillators is able to lower the vibration energy of the ligand, which decreases the energy loss caused by ligand vibration and enhances the emission intensity of the lanthanide ion. Further, due to the heavy-atom

effect, which facilitates intersystem crossing, the lanthanide-centered luminescent properties are enhanced. Based on the above considerations, Reddy and co-workers developed a new strategy that simultaneously incorporates highly conjugated triphenylamine and polyfluorinated alkyl groups into the *β*-diketonate ligand, expecting to obtain the resultant ligands possessing high luminescence efficiency and photochemical stability under visible light excitation upon coordination with trivalent lanthanides. Thus, a series of novel aminophenyl based *β*-diketonate ligands, namely, 1-(4-aminophenyl)-4,4,5,5,5-pentafluoro-3-hydroxypent-2-en-1-one (HAPFP), 1-(4-(dimethylamino)phenyl)-4,4,5,5,5-pentafluoro-3-hydroxypent-2-en-1-one (HDMAPFP) and 1-(4-(diphenylamino)phenyl)-4,4,5,5,5-pentafluoro-3-hydroxypent-2-en-1-one (HDPAPFP), have been synthesized and utilized for the construction of Eu^{3+}–*β*-diketonate coordination compounds in the presence and absence of an ancillary ligand, 4,5-bis(diphenylphosphino)-9,9-dimethylxanthene oxide (DDXPO), with a view to shift the excitation window to the visible region.[28] The origin of the 'amino conjugation effect' on the emission as well as other excited state properties in these complexes has also been elucidated and discussed. The results demonstrated that the triphenylamine based polyfluorinated Eu^{3+}–*β*-diketonate complexes dramatically red-shifted the excitation maximum to the visible region (λ_{exc} = 400 nm) with an impressive quantum yield (40%) as compared to the simple Eu^{3+}–aminophenyl-*β*-diketonate complexes (λ_{exc} = 370 nm). This can be explained on the basis of the conjugation between nitrogen lone pair electrons and the phenyl π-electrons in the *β*-diketonate

ligand system. On the other hand, the electron-donating dimethylamino group (Hammett constant: $\sigma_p = -0.83$) containing Eu^{3+}–β-diketonate complexes moderately shifted the excitation maximum in the UV region from 370 to 380 nm as compared to unsubstituted aminophenyl (Hammett constant: $\sigma_p = -0.66$) Eu^{3+} complexes (Figure 1.8.). The displacement of water molecules in aminophenyl based Eu^{3+}–β-diketonate binary complexes by a rigid phosphine oxide ligand richly enhances the photoluminescence quantum yields as well as the excited state lifetime values of the corresponding ternary complexes. As an integral part of this work, hybrid materials have been developed through a sol–gel route by encapsulating a ternary Eu^{3+} compound in a silica/polymer hybrid for high performance luminescence applications. In addition, a bright red-emitting diode was fabricated by coating the designed hybrid material onto a 400 nm emitting InGaN chip and the photoluminescence was examined.

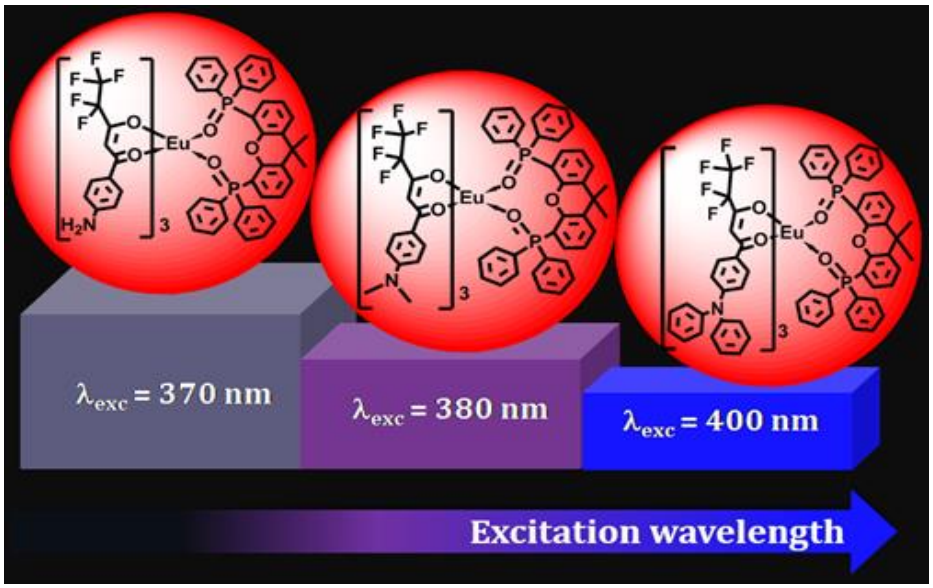

Figure 1.8. Molecular structures of $Eu(APFP)_3(DDXPO)$, $Eu(DMAPFP)_3(DDXPO)$ and $Eu(DPAPFP)_3(DDXPO)$.

1.1.4. Luminescent Properties of Biphenyl Based Fluorinated Eu^{3+}-β-diketonate Complexes

The compounds with aromatic–aromatic bond appended with functional moieties have attracted considerable interest owing to their intriguing structural motifs and unique luminescence properties. The intermolecular interactions in the solid state may promote the coplanar arrangements of aromatic rings in the biphenyl compounds, which may be accountable for the noted conjugation. Further, investigations disclosed that complexation with cations can control the conformation of the biphenyl. It is also well documented that the incorporation of electron-donating methoxy group on the phenyl ring of the biphenyl system allows oxygen electrons to be part of the delocalized system through resonance and increases the conjugation of the chromophore. Based on the above concepts, recently Reddy and co-workers[29] developed a new β-diketonate ligand, namely, 1-(4′-methoxy-[1,1′-biphenyl]-4-yl)-4,4,4-trifluoro-3-hydroxybut-2-en-1-one (HMeOBPhTFB), which contains a conjugated methoxy-substituted biphenyl unit, as well as a polyfluorinated alkyl group, and utilized for the construction of two new Eu^{3+} complexes $[Eu(MeOBPhTFB)_3(H_2O)(C_2H_5OH)]$ and $[Eu(MeOBPhTFB)_3(TPY)]$ where TPY denotes 2,2′:6′,2″- terpyridine. The synthesized compounds are well characterized by various spectroscopic techniques, and their solid-state photophysical properties were investigated. For comparison, Eu^{3+} complexes $[Eu(BPhTFB)_3(H_2O)(C_2H_5OH)]$ and $[Eu(BPhTFB)_3(TPY)]$ were also designed involving an unsubstituted biphenyl based β-diketonate ligand, 1-[1,1′-biphenyl]-4-yl)-

4,4,4-trifluoro-3-hydroxybut-2-en-1-one (HBPhTFB). The results disclosed that the methoxy-substituted biphenyl based polyfluorinated Eu^{3+}-*β*-diketonate complexes significantly red-shifted the excitation maximum to the visible region (λ_{exc} = 400 nm) with promising solid-state quantum yield ($\Phi_{overall}$ = 62%) as compared to simple Eu^{3+}-biphenyl *β*-diketonate ternary complex (λ_{exc} = 382 nm). In the current work, attempts also have been made to isolate luminescent molecular plastic materials by incorporating the unique photophysical properties of the developed visible-light excitable Eu^{3+}-*β*-diketonate complex with the mechanical, thermal and chemical stability, and flexibility and a film-forming tendency of poly(methylmethacrylate) [PMMA] (Figure 1.9.). The developed molecular plastic materials were characterized and evaluated their photoluminescence properties. Most importantly, the newly constructed polymer films exhibit remarkable quantum yields (75–79%) under blue-light excitation as compared to many of the existing Eu^{3+} based polymeric materials.

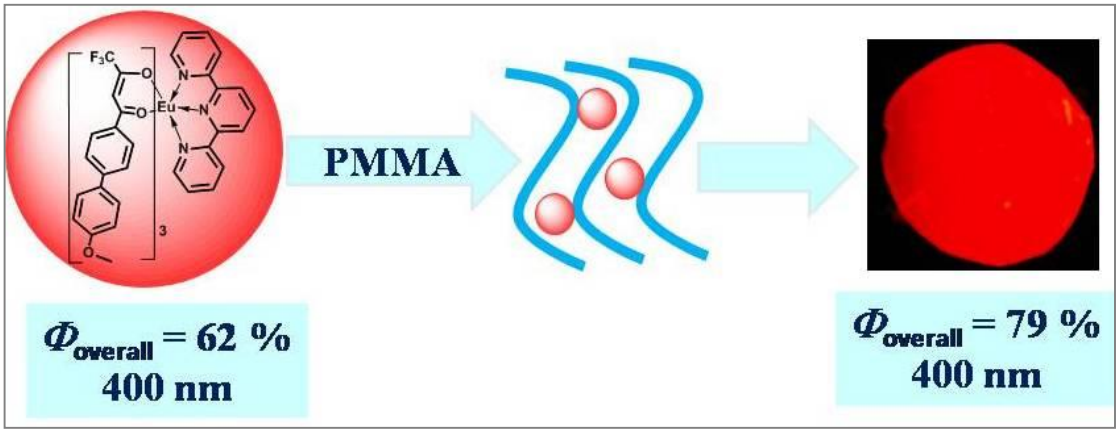

Figure 1.9. Luminescent molecular plastic materials derived from Eu^{3+}-biphenyl based *β*-diketonate ternary complex and poly(methylmethacrylate) display impressive quantum yield (79%) under blue-light excitation (400 nm).

1.1.5. Photophysical Properties of Visible Light Sensitized Fluorene Based Eu^{3+}-*β*-Diketonate Complexes

π-Conjugated polymers and oligomers based on fluorine building blocks have gained importance as the active materials in various types of organic optoelectronic devices, most notably in organic light-emitting diodes.[30] Reddy and co-workers[31] designed a series of near-visible light sensitized europium complexes $Eu(pffpd)_3(C_2H_5OH)(H_2O)$, $Eu(pffpd)_3$(DDXPO) and $Eu(pffpd)_3$(DPEPO) supported by a novel *β*-diketonate ligand, 4,4,5,5,5-pentafluoro-1-(9H-fluoren- 2-yl)-1,3-pentanedione (hpffpd), and a chelate phosphine oxide ligand [where DDXPO refers to 4,5-bis(diphenylphosphino)-9,9-dimethylxanthene oxide and DPEPO refers to bis(2-(diphenylphosphino)phenyl)ether oxide]. The single crystal X-ray diffraction analyses of $Eu(pffpd)_3$(DDXPO) and $Eu(pffpd)_3$(DPEPO) revealed that these complexes are mononuclear, and that the central Eu^{3+} ion is surrounded by eight oxygen atoms, six of which are from the three bidentate fluorinated *β*-diketonates and the other two oxygen atoms from the chelate phosphine oxide. The coordination polyhedral can be best described as distorted square-antiprism. These complexes display a broad excitation band between 250 and 450 nm (λ_{max} = 390 nm), which is attributed to singlet–singlet π–π* enol absorption of the *β*-diketonate ligand (Figure 1.10.). The displacement of the solvent molecules from the complex $Eu(pffpd)_3(C_2H_5OH)(H_2O)$ by the chelating phosphine oxide, DDXPO, leads to significant enhancement in the emission intensity (absolute quantum yield 3 to 48%) and lifetime values (328 to 820 μs). This may be

due to strong coordination of P=O in DDXPO with the central Eu^{3+} (average Eu–O = 2.34 Å), which might enable efficient energy transfer. On the other hand, in the presence of DPEPO these values are only moderately enhanced (quantum yield = 28% and lifetime to 742 μs) due to weak binding of DPEPO to the central Eu^{3+} ion (average Eu–O = 2.38 Å).

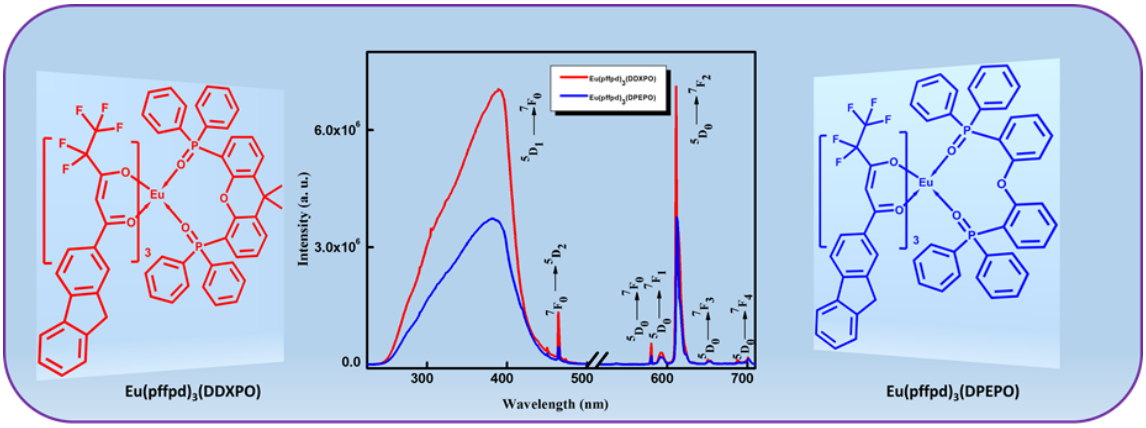

Figure 1.10. Molecular structures of $Eu(pffpd)_3(DDXPO)$ (left), $Eu(pffpd)_3(DPEPO)$ (right) and excitation and emission spectra of the complexes (centre).

In later studies, Reddy and co-workers[32] have constructed a new class of efficient visible light sensitized antenna complexes of Eu^{3+} based on the use of a series of highly conjugated *β*-diketonates, namely, 1-(1-phenyl)-3-(2-fluoryl)propanedione (HBFPD), 1-(2-naphthyl)-3-(2-fluoryl)propanedione (HNFPD), 1-(4-biphenyl)-3-(2-fluoryl)propanedione (HBPFPD) and 2,2′-bis(di-p-tolylphosphino)-1,1′-binaphthyl oxide (TBNPO), as the ancillary ligand. The substitution of the phenyl group with the naphthyl or biphenyl groups in the 3-position of the fluoryl based *β*-diketonate ligand remarkably shifts the excitation window from 275–440 nm (λ_{max} = 400 nm for Eu^{3+}

complexes containing HBFPD to the visible region 300–550 nm with an excitation maximum at 430 nm (for Eu^{3+} complexes containing HNFPD) and 440 nm (for Eu^{3+} complexes containing HBPFPD), respectively, in the corresponding Eu^{3+} complexes. (Figure 1.11.) Thus the structure of the conjugated *β*-diketonate ligand with suitably extended π-conjugation in the complex molecules dramatically influences and shifts the excitation window of the Eu^{3+} complexes towards the visible region, with an important application in biomedical analysis and lighting devices. The luminescence intensity of the ternary Eu^{3+} complexes is greatly enhanced as compared to the hydrated europium *β*-diketonate complexes by the displacement of the solvent molecules from the complexes by the rigid chelating phosphine oxide TBNPO, which in turn reduces the high frequency oscillators. As a consequence, the quantum yields (19–43%) and lifetime values (769–877 μs) of the ternary Eu^{3+} complexes are found to be significantly enhanced as compared to precursor Eu^{3+} complexes (quantum yields = 2–7%, lifetime = 399–376 μs).

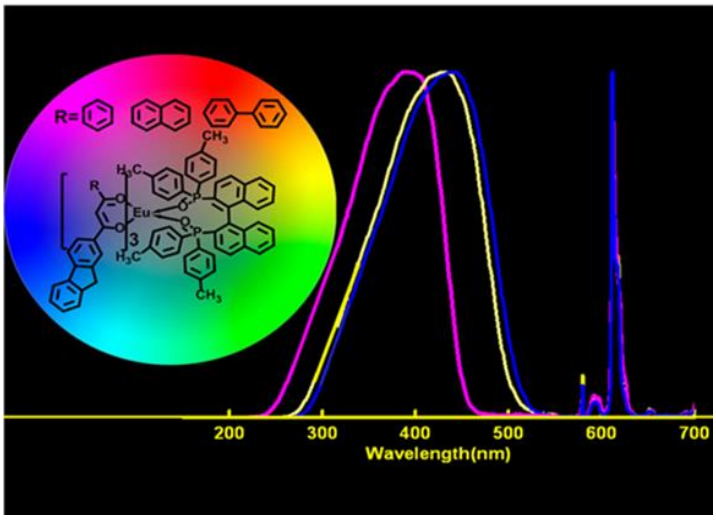

Figure 1.11. Molecular structures and excitation emission spectra of $Eu(BFPD)_3(TBNPO)$, $Eu(NFPD)_3(TBNPO)$ and $Eu(BPFPD)_3(TBNPO)$.

1.1.6. Photophysical Properties of Anthracene Based Eu^{3+}-β-diketonate Complexes

Sun et al.[33] have proposed a unique β-diketonate–Eu^{3+} complex, [Eu(pfdap)$_3$(tpy)], as a probe for the recognition and time-gated luminescence detection of $^1O_2$ in living cells. The new Eu^{3+} complex probe showed not only highly selective luminescence response ability to $^1O_2$, but also highly specific colocalization performance in mitochondria, which allowed it to be used for time-gated luminescence imaging to monitor the $^1O_2$ generation in mitochondria of living cells Figure (1.12.). Compared to the previously reported Eu^{3+} complex based luminescence probes for $^1O_2$, the new probe has several distinct advantages including synthetic simplicity, high luminescence turn-on ratio, cell membrane permeability, and mitochondria targetability. The results of time-gated luminescence imaging of $^1O_2$ in the ALA loaded HepG2 cells demonstrated the practical applicability of the probe for monitoring the $^1O_2$ generation during the photodynamic process in cancer cells, which could be anticipated to be a useful tool for the research of the PDT technique for improving cancer treatments.

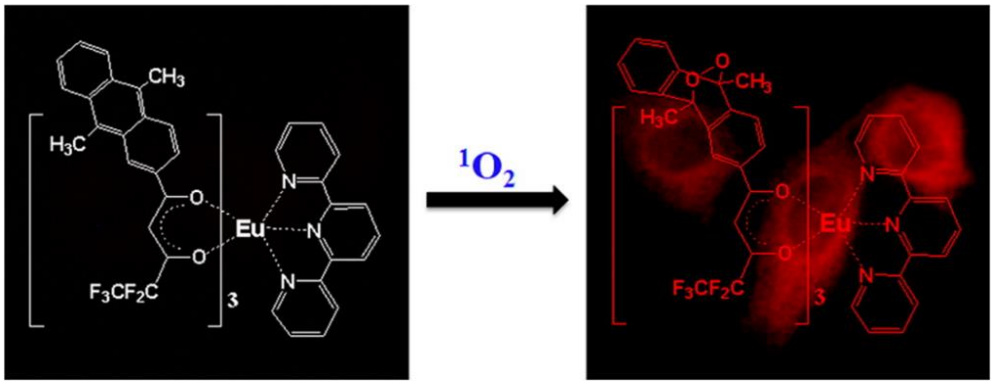

Figure 1.12. Eu(pfdap)$_3$(tpy) as a probe for the recognition and time-gated luminescence detection of $^1O_2$ in living cells.

1.2. Recent Developments on the Near Infrared (NIR) Luminescent Lanthanide β-Diketonate Complexes

Near infrared luminescence (NIR) is of interest because of its potential application in biological imaging and in telecommunications.[8e, 14, 34] Owing to their unique luminescent properties, in particular as NIR emitters, lanthanide cations such as Er, Nd and Yb complexes have been the subject of intense investigations over the last two decades.[35] Compared with the efficient NIR emission of lanthanide ions in inorganic systems, low luminescence quantum yields are commonly observed in organic lanthanide complexes.[36] This is due to the low-energy excited states of the NIR luminescent lanthanide ions, which are prone to quenching by multiphonon de-excitation caused by the coupling of high energy oscillators like O–H, N–H and C–H, present in the organic ligands or solvents. Strategies to overcome this problem include: (i) exploit the sterically demanding and/or multidentate ligands that can encapsulate the ion forming the hydrophobic shell around the metal ion[37] and (ii) replace the ubiquitous C–H bonds with C–D bonds or C–F bonds.[38] Among the NIR emitters, Yb^{3+} undoubtedly is one of the most efficient lanthanide ions, a result of the 'clear' excited and ground state levels, and the relatively larger energy gap between them (10,250 cm^{-1}).[39] To rationally optimize the ligands, the Yb^{3+} ion shows the highest NIR luminescence quantum yields in lanthanide complexes. Previously, various ligands have been designed for sensitizing the Yb^{3+} ion NIR luminescence, including macrocyclic porphyrins,[40] coronands,[41] cryptands,[42] cyclens,[43] calixarenes and

resorcinarenes;[44] acyclic beta-diketones,[45] quinolinates,[46] terphenyl,[47] and polyaminocarboxylates;[48] as well as other chelating agents such as some dye derivatives,[49] tropolonates,[50] imidophosphinates[51] and boron dipyrromethene (BODIPY).[52] Nevertheless, the luminescence quantum yields observed remain modest, typically in the range of 10^{-3} to 10^{-2}, due to the easy quenching by high energy oscillators present in ligands and solvents. Therefore, the design of ligands that can effectively supress nonradiative transitions is critical for synthesizing highly efficient organic lanthanide emitters. Among organic ligands, *β*-diketones are considered to be better candidates for sensitizing lanthanide ion luminescence, especially for visible light emitting Eu^{3+} and Tb^{3+} ions.[20e, 53] However, their ability with respect to populating lanthanide ion NIR luminescence seems to be limited, which is mainly due to the presence of solvents in the coordination sphere of the lanthanide *β*-diketone complexes.[54] To overcome this, the ancillary ligands are often employed to replace the solvents.[55]

A bis-*β*-diketone, bis(4,4,4-trifluoro-1,3-dioxobutyl)(2,2′-bithienyl) (BTT), which can be looked upon as coupling of two mono-*β*-diketones (2-thenoyltrifluoroacetone, TTA) at the 5,5′-position of thiophene ring, has been designed by Li and co-workers[36] for exploring the advantages of binuclear helical structure in sensitizing the lanthanide NIR luminescence. The Yb^{3+} ion was selected as the luminescent center, and its corresponding mono-*β*-diketone complex $Yb(TTA)_3(DMSO)$ and bis-*β*-diketone complex $Yb_2(BTT)_3(DMSO)$ were synthesized

and isolated. The photophysical properties related to the electronic transition are characterized by the absorbance spectra, the emission spectra, the emission quantum yields, the emission lifetimes, and the radiative (k_r) and nonradiative rate constants (k_{nr}). The luminescence quantum yield experiment reveals that the dinuclear complex has about 10 times luminescence enhancement compared with the mononuclear complex. (Figure 1.13.) This enhancement is attributed to several factors depending on the structure: (i) faster radiative rate constant; (ii) part-shielding the ion from the solvent molecules by encapsulation with the helicate to form a protective shell around the ion; and (iii) reducing the oscillator strength of absorption of the vibrational transition due to the tension caused by the helical twisting of ligands in helicate. Based on the above analysis, it has been concluded that the bright luminescence of the bis-*β*-diketone complex mainly results from efficiently restricting the nonradiative transition caused by the oscillators in ligands and solvents.

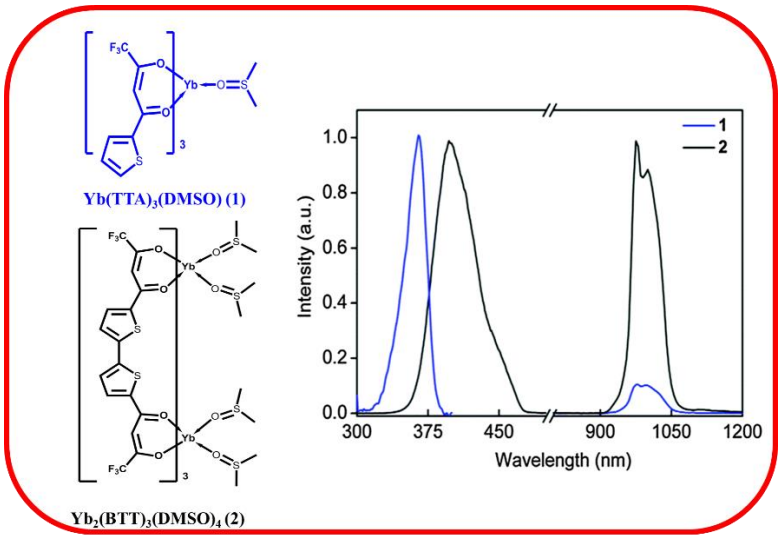

Figure 1.13. Molecular structures, excitation and emission spectra of $Yb(TTA)_3(DMSO)$ and $Yb_2(BTT)_3(DMSO)_4$.

A new antenna molecule containing four benzoyltrifluoroacetone (BTFA) moieties anchored to a single carbon atom and connected through four flexible methoxy groups, namely 1,10-(4,4′-(2,2-bis((4-(4,4,4-trifluoro-3-oxobutanoyl)phenoxy)methyl)propane-1,3-diyl)bis(oxy)bis(4,1-phenylene))bis(4,4,4-trifluorobutane-1,3-dione) [H_4L], has been designed and synthesized.[53a] Using this ligand, a series of homo- and hetero-metallic Ln^{3+} complexes of general formula [LnL]NBu_4 (where Ln = Er, Yb, $Er_{0.5}Yb_{0.5}$, $Er_{0.5}Gd_{0.5}$, $Yb_{0.5}Gd_{0.5}$ and NBu_4 = tetrabutyl ammonium) have been isolated. The developed complexes exhibit high molar absorption coefficients (>40 000 M^{-1} cm^{-1} around 330 nm in DMF) and display strong NIR (Er^{3+}, Yb^{3+}) luminescence in solid state and in DMF solution upon irradiation at the ligand-centred bands in the range 250–400 nm. Furthermore, these complexes have been doped into PMMA matrices yielding highly luminescent, photo-stable films and flexible resins made of fibres with average diameter 300–400 nm (Figure 1.14.). Photoluminescence studies show that the newly designed ligand is an adequate sensitizer for Yb^{3+} and Er^{3+} luminescence. The emission quantum yields and the luminescence lifetimes at room-temperature are and 2.6±0.4% and 12.1±0.1 μs for Yb^{3+} in solid state. Moreover, the overall quantum yields and lifetime measurements for the mixed metallic complex show that Yb^{3+}/Er^{3+} energy transfer occurs resulting in enhanced Er^{3+} emission.

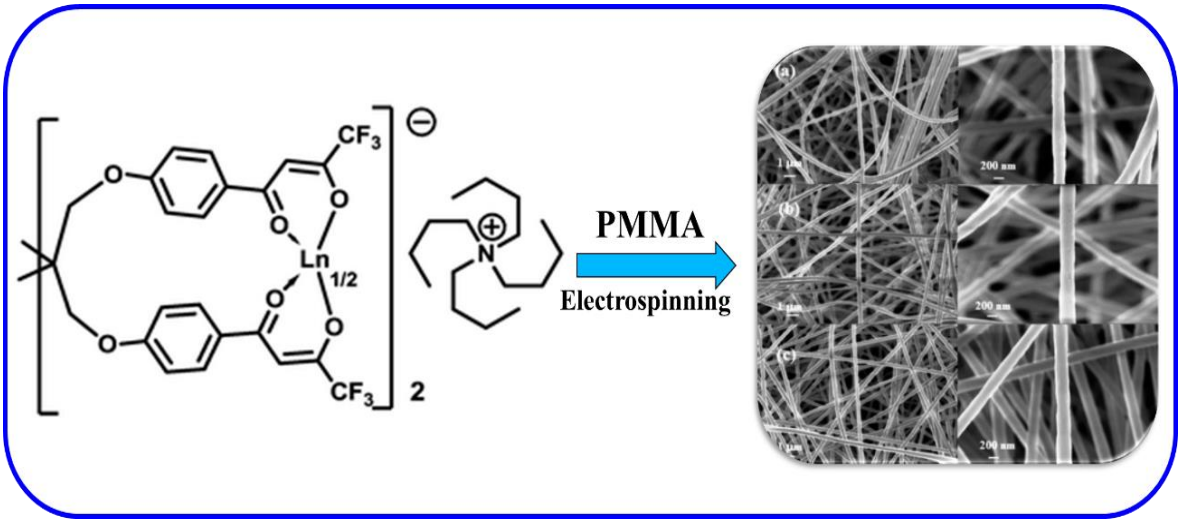

Figure 1.14. Molecular Structure of $[LnL]NBu_4$ (where Ln = Er, Yb, $Er_{0.5}Yb_{0.5}$, $Er_{0.5}Gd_{0.5}$, $Yb_{0.5}Gd_{0.5}$ and NBu_4 = tetrabutyl ammonium) and flexible fibers by doping $[LnL]NBu_4$ in PMMA.

Bünzli and co-workers[56] have demonstrated that 1,3-diketonato ligands containing push-pull chromophores are suitable for excitation of NIR emitting lanthanide ions. The new 1,3-diketonato ligand contains both an electron-donor [4-(dimethylamino)benzene] and an electron-acceptor (4-nitrobenzene) groups. These complexes display an intense intra-ligand charge-transfer absorption transition in the visible region of the spectrum at 400–550 nm which was utilized to achieve visible-light excitation of metal-centred infrared luminescence of Nd^{3+}, Er^{3+} and Yb^{3+} ions. For instance, the overall luminescence efficiency of the Yb^{3+} complex, ε X $Q^{Ln}{}_{L}$, is 26 $M^{-1}cm^{-1}$ at 428 nm (absorption maximum in the visible range), 5.2 M^{-1} cm^{-1} at 500 nm, and ca. 0.4 $M^{-1}cm^{-1}$ at 550 nm (Figure 1.15.).

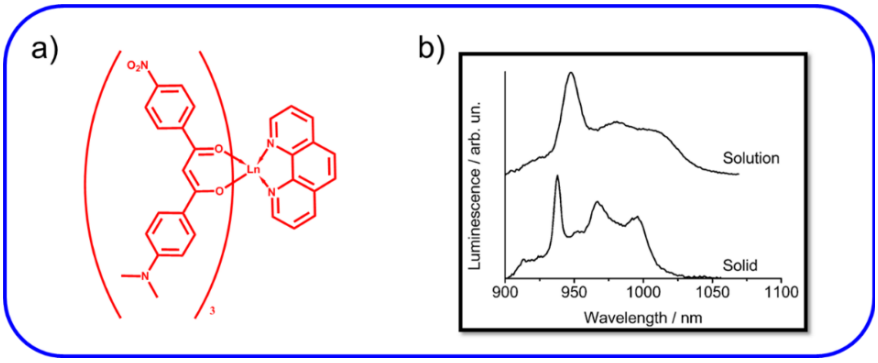

Figure 1.15. (a) Structure of [YbL$_3$phen] **(b)** Corrected and normalized luminescence spectra of [YbL$_3$phen] in DMSO solution (1.8 X 10^{-6} M) and in the solid state at room temperature under excitation at 430 nm.

In the subsequent studies, Bünzli and co-workers[57] have developed lanthanide complexes with two push-pull diketonate derivatives as sensitizers for NIR emitting materials. The ligand substituents consist of a carbazole moiety with hole-transport properties and an aromatic or heteroaromatic unit. The preferred cis-enol form contributes strongly to the binding of lanthanide ions (Ln = Nd and Er). The resulting tris(diketonate) ternary complexes with terpyridine (Ln = Nd and Er) display sizeable near-IR emission with long luminescence lifetimes.

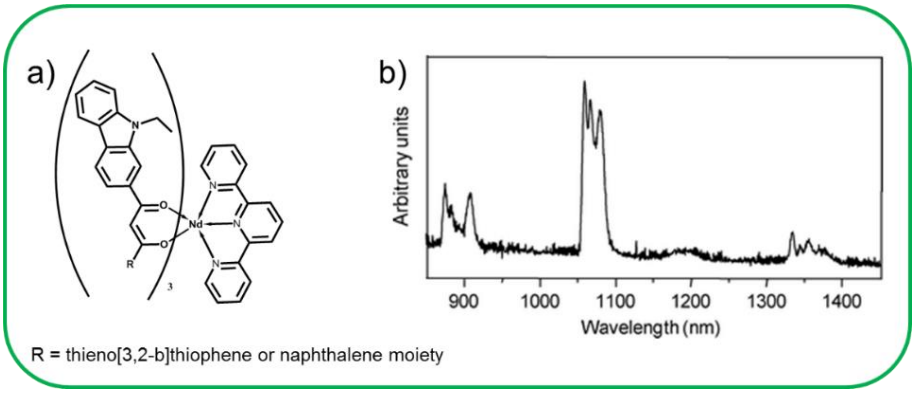

Figure 1.16. (a) Structure of Nd(CTPD)$_3$(tpy) **(b)** Normalized NIR emission spectrum of Nd(CTPD)$_3$(tpy) in solid state at 10 K (λ_{exc} = 400 nm).

1.3. Objectives of the Present Investigation

An ever growing attention is being given to the lanthanide ions Nd^{3+}, Er^{3+} and Yb^{3+} which display a long-lived metal-centred luminescence in the NIR range of the spectrum at 800 to 2000 nm.[6d, 39, 58] This interest is stirred by potential applications in telecommunications, bio-analyses, and medicine. The forbidden nature of f-f transitions in trivalent lanthanide ions results in a very weak intensity of the metal-centred absorption bands. As a result one has to coordinate a suitable chromophore to the lanthanide ion and to rely on energy transfer to achieve efficient excitation of the metal ion.[1b] Whereas enough energy transfer from the triplet state of the chromophore moiety is often a preferred pathway for the sensitization of the lanthanide ion luminescence. As a matter of fact, in comparison with the effective sensitization of visible luminescence of Eu^{3+} or Tb^{3+} ion with relatively high first excited state ($^5D_0$ for Eu^{3+}, 17250 cm^{-1} or $^5D_4$ for Tb^{3+}, 20500 cm^{-1}),[8a, 59] it remains a real challenge to synthesize suitable *β*-diketonate ligand with relatively lower triplet energy level matched well with the first excited state of NIR luminescent Ln^{3+} ions ($^4F_{3/2}$ for Nd^{3+}, 11257 cm^{-1}; $^2F_{5/2}$ for Yb^{3+}, 10400 cm^{-1}).[60] Therefore one of the primary objectives of the present investigation is to design and develop a novel *β*-diketonate type antenna molecule with suitable triplet energy level for the sensitization of NIR emitting lanthanide ions.

Recently, emissive europium complexes have emerged as a distinctive class of intracellular stains and probes.[2d, 6c, 8a] The europium based molecular materials offers

particular scope in this respect, as they possess several advantages over conventional fluorescent dyes.[61] In order to investigate intracellular and subcellular processes, luminescence stains are needed that can visualize particular cellular compartments with high spatial and temporal resolution. Thus, in live cell imaging process, the creation of selective stains-compounds that enter cells and localize preferentially to a particular organelle is recognized as a key challenge.[6c] This is a critical requirement not only for cell imaging but for any species being considered as a diagnostic or therapeutic agent. Thus, another objective of the present investigation is to develop a novel and selective europium based molecular probe for cellular imaging applications to visualize selected organelles, notably the MitoTracker or LysoTracker.

The use of lanthanide luminescent complexes as optical materials is still limited choice but to be applied as organic-inorganic hybrid materials.[62] Compared with the complication of trapping the lanthanide complexes into polymer matrices with covalent bonds for the formation of lanthanide containing metallopolymers,[63] one of the simple and effective solutions is through physical doping into a host polymer matrix where the obtained polymer supported doping hybrid materials are expected to have distinctively improved physical properties including good luminescence performance.[64] Therefore yet another objective of the current investigation is to develop efficient polymer supported hybrid materials doped with europium complexes and investigate their photophysical properties.

1.4. References

1. (a) A. Nadort, J. Zhao and E. M. Goldys, *Nanoscale*, 2016, **8**, 13099-13130; (b) J.-C. G. Bünzli and C. Piguet, *Chem. Soc. Rev.*, 2005, **34**, 1048-1077; (c) M. L. P. Reddy and S. Sivakumar, *Dalton Trans.*, 2013, **42**, 2663-2678; (d) L. Armelao, S. Quici, F. Barigelletti, G. Accorsi, G. Bottaro, M. Cavazzini and E. Tondello, *Coord. Chem. Rev.*, 2010, **254**, 487-505; (e) E. G. Moore, A. P. S. Samuel and K. N. Raymond, *Acc. Chem. Res.*, 2009, **42**, 542-552; (f) A. Døssing, *Eur. J. Inorg. Chem.*, 2005, **2005**, 1425-1434.

2. (a) J. M. Stanley and B. J. Holliday, *Coord. Chem. Rev.*, 2012, **256**, 1520-1530; (b) A. de Bettencourt-Dias, *Dalton Trans.*, 2007, **22**, 2229-2241; (c) J.-C. G. Bünzli, *Coord. Chem. Rev.*, 2015, **293-294**, 19-47; (d) S. V. Eliseeva and J.-C. G. Bünzli, *Chem. Soc. Rev.*, 2010, **39**, 189-227; (e) J. Kido and Y. Okamoto, *Chem. Rev.*, 2002, **102**, 2357-2368; (f) K. Kohtaro, in *Phosphor Handbook*, CRC Press, 2006.

3. (a) K. Takehiro and H. Takayuki, in *Phosphor Handbook*, CRC Press, 2006; (b) L. Ozawa and M. Itoh, *Chem. Rev.*, 2003, **103**, 3835-3856; (c) H. Xu, R. Chen, Q. Sun, W. Lai, Q. Su, W. Huang and X. Liu, *Chem. Soc. Rev.*, 2014, **43**, 3259-3302.

4. (a) K. Kuriki, Y. Koike and Y. Okamoto, *Chem. Rev.*, 2002, **102**, 2347-2356; (b) L. D. Carlos, R. A. S. Ferreira, V. de Bermudez and S. J. L. Ribeiro, *Adv. Mater.*, 2009, **21**, 509-534.

5. S. V. Eliseeva and J.-C. G. Bünzli, *New J. Chem.*, 2011, **35**, 1165-1176.

6. (a) A. J. Amoroso and S. J. A. Pope, *Chem. Soc. Rev.*, 2015, **44**, 4723-4742; (b) J.-C. G. Bünzli, *J. Lumin.*, 2016, **170**, 866-878; (c) S. J. Butler, L. Lamarque, R. Pal and D. Parker, *Chem. Sci.*, 2014, **5**, 1750; (d) S. Faulkner, S. J. A. Pope and B. P. Burton-Pye, *Appl. Spectrosc. Rev.*, 2005, **40**, 1-31; (e) R. C. Leif, L. M. Vallarino, M. C. Becker and S. Yang, *Cytometry A*, 2006, **69**, 767-778; (f) C. P. Montgomery, B. S. Murray, E. J. New, R. Pal and D. Parker, *Acc. Chem. Res.*, 2009, **42**, 925-937; (g) K. H. Thompson and C. Orvig, *Chem. Soc. Rev.*, 2006, **35**, 499-499; (h) X. Wang, H. Chang, J. Xie, B.

Zhao, B. Liu, S. Xu, W. Pei, N. Ren, L. Huang and W. Huang, *Coord. Chem. Rev.*, 0530, **273–274**.

7. R. D. Teo, J. Termini and H. B. Gray, *J. Med. Chem.*, 2016, **59**, 6012-6024.

8. (a) M. L. P. Reddy, V. Divya and R. Pavithran, *Dalton Trans.*, 2013, **42**, 15249-15262; (b) J.-C. G. Bünzli, *Interface Focus*, 2013, **3**, 20130032; (c) J.-C. G. Bünzli, *Chem. Lett.*, 2009, **38**, 104-109; (d) M. C. Heffern, L. M. Matosziuk and T. J. Meade, *Chem. Rev.*, 2014, **114**, 4496-4539; (e) M. Sy, A. Nonat, N. Hildebrandt and L. J. Charbonniere, *Chem. Commun.*, 2016, **52**, 5080-5095.

9. (a) J.-C. G. Bünzli and S. V. Eliseeva, in *Lanthanide Luminescence: Photophysical, Analytical and Biological Aspects*, eds. P. Hänninen and H. Härmä, Springer Berlin Heidelberg, Berlin, Heidelberg, 2011, DOI: 10.1007/4243_2010_3, pp. 1-45; (b) M. H. V. Werts, *Sci. Prog.*, 2005, **88**, 101-131.

10. J. M. González-Pérez and A. Matilla-Hernández, *Coord. Chem. Rev.*, 2013, **257**, 2623-2624.

11. K. Binnemans, *Coord. Chem. Rev.*, 2015, **295**, 1-45.

12. (a) S. I. Weissman, *J. Chem. Phys.*, 1942, **10**, 214-217; (b) C. Piguet and J.-C. G. Bünzli, *Chem. Soc. Rev.*, 1999, **28**, 347-358; (c) B. Alpha, J.-M. Lehn and G. Mathis, *Angew. Chem.*, 1987, **99**, 259-261; (d) N. Sabbatini, M. Guardigli and J.-M. Lehn, *Coord. Chem. Rev.*, 1993, **123**, 201-228.

13. J.-C. G. Bünzli, *Acc. Chem. Res.*, 2006, **39**, 53-61.

14. J.-C. G. Bünzli, *Chem. Rev.*, 2010, **110**, 2729-2755.

15. A. Thibon and V. C. Pierre, *Anal. Bioanal. Chem.*, 2009, **394**, 107-120.

16. W. D. Horrocks and D. R. Sudnick, *J. Am. Chem. Soc.*, 1979, **101**, 334-340.

17. (a) R. M. Supkowski and W. D. Horrocks Jr, *Inorg. Chim. Acta*, 2002, **340**, 44-48; (b) A. Beeby, I. M. Clarkson, R. S. Dickins, S. Faulkner, D. Parker, L. Royle, A. S. de Sousa, J. A. Gareth Williams and M. Woods, *J. Chem. Soc., Perkin Trans. 2*, 1999, **3**, 493-504.

18. T. Kimura and Y. Kato, *J. Alloys Compd.*, 1998, **275–277**, 806-810.

19. (a) C. Bischof, J. Wahsner, J. Scholten, S. Trosien and M. Seitz, *J. Am. Chem. Soc.*, 2010, **132**, 14334-14335; (b) A. Beeby, B. P. Burton-Pye, S. Faulkner, G. R. Motson, J. C. Jeffery, J. A. McCleverty and M. D. Ward, *Dalton Trans.*, 2002, **9**, 1923-1928.

20. (a) K. Binnemans, in *Handbook on the Physics and Chemistry of Rare Earths*, eds. J.-C. G. B. Karl A. Gschneidner and K. P. Vitalij, Elsevier, 2005, vol. Volume 35, pp. 107-272; (b) S. Lis, M. Elbanowski, B. Mąkowska and Z. Hnatejko, *J. Photochem. Photobiol. A*, 2002, **150**, 233-247; (c) J.-C. G. Bünzli and S. V. Eliseeva, *Chem. Sci.*, 2013, **4**, 1939-1949; (d) A. de Bettencourt-Dias, *Dalton transactions (Cambridge, England : 2003)*, 2007, **0**, 2229-2241; (e) J. Feng and H. Zhang, *Chem. Soc. Rev.*, 2013, **42**, 387-410.

21. (a) D. B. Nie, Z. Q. Chen, Z. Q. Bian, J. Q. Zhou, Z. W. Liu, F. F. Chen, Y. L. Zhao and C. H. Huang, *New J. Chem.*, 2007, **31**, 1639-1646; (b) Y. X. Zheng, F. Cardinali, N. Armaroli and G. Accorsi, *Eur. J. Inorg. Chem.*, 2008, **12**, 2075-2080; (c) P. He, H. H. Wang, H. G. Yan, W. Hu, J. X. Shi and M. L. Gong, *Dalton Trans.*, 2010, **39**, 8919-8924; (d) D. B. A. Raj, B. Francis, M. L. P. Reddy, R. R. Butorac, V. M. Lynch and A. H. Cowley, *Inorg. Chem.*, 2010, **49**, 9055-9063.

22. N. S. Baek, Y. H. Kim, Y. K. Eom, J. H. Oh, H. K. Kim, A. Aebischer, F. Gumy, A. S. Chauvin and J. C. G. Bünzli, *Dalton Trans.*, 2010, **39**, 1532-1538.

23. P. He, H. H. Wang, S. G. Liu, J. X. Shi, G. Wang and M. L. Gong, *Inorg. Chem.*, 2009, **48**, 11382-11387.

24. (a) P. He, H. H. Wang, S. G. Liu, W. Hu, J. X. Shi, G. Wang and M. L. Gong, *J. Electrochem. Soc.*, 2009, **156**, E46-E49; (b) P. He, H. H. Wang, S. G. Liu, J. X. Shi, G. Wang and M. L. Gong, *Electrochem. Solid-State Lett.*, 2009, **12**, B61-B64.

25. S.-g. Liu, W.-y. Su, R.-k. Pan and X.-p. Zhou, *Chin. J. Chem. Phys.*, 2012, **25**, 697-702.

26. B. Francis, C. Heering, R. O. Freire, M. L. P. Reddy and C. Janiak, *RSC Adv.*, 2015, **5**, 90720-90730.

27. V. Divya, V. Sankar, K. G. Raghu and M. L. P. Reddy, *Dalton Trans.*, 2013, **42**, 12317-12323.

28. T. V. U. Gangan and M. L. P. Reddy, *Dalton Trans.*, 2015, **44**, 15924-15937.

29. T. V. U. Gangan, S. Sreenadh and M. L. P. Reddy, *J. Photochem. Photobiol. A*, 2016, **328**, 171-181.

30. (a) S. Wang, B. S. Gaylord and G. C. Bazan, *J. Am. Chem. Soc.*, 2004, **126**, 5446-5451; (b) M. H. V. Werts, S. Gmouh, O. Mongin, T. Pons and M. Blanchard-Desce, *J. Am. Chem. Soc.*, 2004, **126**, 16294-16295; (c) P. N. Day, K. A. Nguyen and R. Pachter, *J. Phys. Chem. B*, 2005, **109**, 1803-1814.

31. D. B. Ambili Raj, S. Biju and M. L. P. Reddy, *Dalton Trans.*, 2009, **36**, 7519-7528.

32. V. Divya, R. O. Freire and M. L. P. Reddy, *Dalton Trans.*, 2011, **40**, 3257-3268.

33. J. Sun, B. Song, Z. Ye and J. Yuan, *Inorg. Chem.*, 2015, **54**, 11660-11668.

34. (a) J.-C. G. Bünzli and S. V. Eliseeva, *J. Rare Earths*, 2010, **28**, 824-842; (b) F.-F. Chen, Z.-Q. Chen, Z.-Q. Bian and C.-H. Huang, *Coord. Chem. Rev.*, 2010, **254**, 991-1010; (c) M. D. Ward, *Coord. Chem. Rev.*, 2007, **251**, 1663-1677; (d) C. Andraud and O. Maury, *Eur. J. Inorg. Chem.*, 2009, **29-30**, 4357-4371; (e) G. A. Hebbink, J. W. Stouwdam, D. N. Reinhoudt and F. van Veggel, *Adv. Mater.*, 2002, **14**, 1147-1150; (f)

M. P. O. Wolbers, F. van Veggel, B. H. M. Snellink-Ruel, J. W. Hofstraat, F. A. J. Geurts and D. N. Reinhoudt, *J. Chem. Soc., Perkin Trans. 2*, 1998, **10**, 2141-2150; (g) J. Zhang and S. Petoud, *Chem. Eur. J.*, 2008, **14**, 1264-1272; (h) V. Bulach, F. Sguerra and M. W. Hosseini, *Coord. Chem. Rev.*, 2012, **256**, 1468-1478.

35. (a) J. Chakraborty, A. Ray, G. Pilet, G. Chastanet, D. Luneau, R. F. Ziessel, L. J. Charbonniere, L. Carrella, E. Rentschler, M. S. El Fallah and S. Mitra, *Dalton Trans.*, 2009, DOI: 10.1039/b908910a, 10263-10272; (b) W. Huang, D. Wu, D. Guo, X. Zhu, C. He, Q. Meng and C. Duan, *Dalton Trans.*, 2009, **12**, 2081-2084; (c) X. Zhu, W.-K. Wong, W.-Y. Wong and X. Yang, *Eur. J. Inorg. Chem.*, 2011, **30**, 4651-4674; (d) X.-Y. Chen, X. Yang and B. J. Holliday, *Inorg. Chem.*, 2010, **49**, 2583-2585; (e) A. Kornienko, B. F. Moore, G. A. Kumar, M.-C. Tan, R. E. Riman, M. G. Brik, T. J. Emge and J. G. Brennan, *Inorg. Chem.*, 2011, **50**, 9184-9190; (f) M. Mato-Iglesias, T. Rodriguez-Blas, C. Platas-Iglesias, M. Starck, P. Kadjane, R. Ziessel and L. Charbonniere, *Inorg. Chem.*, 2009, **48**, 1507-1518; (g) B. F. Moore, G. A. Kumar, M.-C. Tan, J. Kohl, R. E. Riman, M. G. Brik, T. J. Emge and J. G. Brennan, *J. Am. Chem. Soc.*, 2011, **133**, 373-378; (h) T. Zhang, X. Zhu, C. C. W. Cheng, W.-M. Kwok, H.-L. Tam, J. Hao, D. W. J. Kwong, W.-K. Wong and K.-L. Wong, *J. Am. Chem. Soc.*, 2011, **133**, 20120-20122.

36. B. Li, H. Li, P. Chen, W. Sun, C. Wang, T. Gao and P. Yan, *Phys. Chem. Chem. Phys.*, 2015, **17**, 30510-30517.

37. (a) B. L. Reid, S. Stagni, J. M. Malicka, M. Cocchi, G. S. Hanan, M. I. Ogden and M. Massi, *Chem. Commun.*, 2014, **50**, 11580-11582; (b) S. W. Magennis, S. Parsons and Z. Pikramenou, *Chem. Eur. J.*, 2002, **8**, 5761-5771; (c) P. E. Ryan, L. Guenee, G. Canard, F. Gumy, J.-C. G. Buenzli and C. Piguet, *Inorg. Chem.*, 2009, **48**, 2549-2560; (d) E. R. Trivedi, S. V. Eliseeva, J. Jankolovits, M. M. Olmstead, S. Petoud and V. L. Pecoraro, *J. Am. Chem. Soc.*, 2014, **136**, 1526-1534.

38. (a) G. R. Desiraju, *Chem. Commun.*, 2005, **24**, 2995-3001; (b) H. Q. Ye, Y. Peng, Z. Li, C. C. Wang, Y. X. Zheng, M. Motevalli, P. B. Wyatt, W. P. Gillin and I. Hernandez,

J. Phys. Chem. C, 2013, **117**, 23970-23975; (c) Y. Peng, H. Ye, Z. Li, M. Motevalli, I. Hernandez, W. P. Gillin and P. B. Wyatt, *Journal of Physical Chemistry Letters*, 2014, **5**, 1560-1563; (d) G. Mancino, A. J. Ferguson, A. Beeby, N. J. Long and T. S. Jones, *J. Am. Chem. Soc.*, 2005, **127**, 524-525.

39. S. Comby and J.-C. G. Bünzli, in *Handbook on the Physics and Chemistry of Rare Earths*, eds. J.-C. G. Karl A. Gschneidner, Bünzli and K. P. Vitalij, Elsevier, 2007, vol. Volume 37, pp. 217-470.

40. (a) X.-S. Ke, B.-Y. Yang, X. Cheng, S. L.-F. Chan and J.-L. Zhang, *Chem. Eur. J.*, 2014, **20**, 4324-4333; (b) T. Zhang, C.-F. Chan, R. Lan, H. Li, N.-K. Mak, W.-K. Wong and K.-L. Wong, *Chem. Commun.*, 2013, **49**, 7252-7254.

41. (a) M. Vazquez Lopez, S. V. Eliseeva, J. M. Blanco, G. Rama, M. R. Bermejo, M. Eugenio Vazquez and J.-C. G. Bünzli, *Eur. J. Inorg. Chem.*, 2010, **28**, 4532-4545; (b) M. Andrews, J. E. Jones, L. P. Harding and S. J. A. Pope, *Chem. Commun.*, 2011, **47**, 206-208.

42. (a) C. Doffek and M. Seitz, *Angew. Chem.*, 2015, **54**, 9719-9721; (b) J. E. Jones and S. J. A. Pope, *Dalton Trans.*, 2009, **39**, 8421-8425.

43. M. Paluch, J. Lisowski and T. Lis, *Dalton Trans.*, 2006, **2**, 381-388.

44. L. R. MacGillivray, J. L. Reid and J. A. Ripmeester, *Chem. Commun.*, 2001, **11**, 1034-1035.

45. X. Guo, H. Guo, L. Fu, L. D. Carlos, R. A. S. Ferreira, L. Sun, R. Deng and H. Zhang, *J. Phys. Chem. C*, 2009, **113**, 12538-12545.

46. M. Albrecht, O. Osetska, R. Froehlich, J.-C. G. Buenzli, A. Aebischer, F. Gumy and J. Hamacek, *J. Am. Chem. Soc.*, 2007, **129**, 14178-+.

47. S. I. Klink, L. Grave, D. N. Reinhoudt, F. van Veggel, M. H. V. Werts, F. A. J. Geurts and J. W. Hofstraat, *J. Phys. Chem. A*, 2000, **104**, 5457-5468.

48. S. Quici, M. Cavazzini, G. Marzanni, G. Accorsi, N. Armaroli, B. Ventura and F. Barigelletti, *Inorg. Chem.*, 2005, **44**, 529-537.

49. G. A. Hebbink, S. I. Klink, L. Grave, P. Alink and F. van Veggel, *ChemPhysChem*, 2002, **3**, 1014-1018.

50. J. Zhang, P. D. Badger, S. J. Geib and S. Petoud, *Angew. Chem.*, 2005, **44**, 2508-2512.

51. P. B. Glover, A. P. Bassett, P. Nockemann, B. M. Kariuki, R. Van Deun and Z. Pikramenou, *Chem. Eur. J.*, 2007, **13**, 6308-6320.

52. (a) J. H. Ryu, Y. K. Eom, J.-C. G. Buenzli and H. K. Kim, *New J. Chem.*, 2012, **36**, 723-731; (b) R. F. Ziessel, G. Ulrich, L. Charbonniere, D. Imbert, R. Scopelliti and J. C. G. Bünzli, *Chem. Eur. J.*, 2006, **12**, 5060-5067.

53. (a) S. Biju, Y. K. Eom, J.-C. G. Bünzli and H. K. Kim, *J. Mater. Chem. C*, 2013, **1**, 6935-6944; (b) Z. Ahmed and K. Iftikhar, *J. Phys. Chem. A*, 2013, **117**, 11183-11201.

54. (a) Z. Ahmed and K. Iftikhar, *Polyhedron*, 2015, **85**, 570-592; (b) P. Martin-Ramos, P. S. Pereira da Silva, V. Lavin, I. R. Martin, F. Lahoz, P. Chamorro-Posada, M. R. Silva and J. Martin-Gil, *Dalton Trans.*, 2013, **42**, 13516-13526; (c) J. Feng, J.-B. Yu, S.-Y. Song, L.-N. Sun, W.-Q. Fan, X.-M. Guo, S. Dang and H.-J. Zhang, *Dalton Trans.*, 2009, **13**, 2406-2414.

55. J. Li, H. Li, P. Yan, P. Chen, G. Hou and G. Li, *Inorg. Chem.*, 2012, **51**, 5050-5057.

56. N. M. Shavaleev, R. Scopelliti, F. Gumy and J. C. G. Bünzli, *Eur. J. Inorg. Chem.*, 2008, **9**, 1523-1529.

57. N. S. Baek, Y. H. Kim, Y. K. Eom, J. H. Oh, H. K. Kim, A. Aebischer, F. Gumy, A.-S. Chauvin and J.-C. G. Bünzli, *Dalton Trans.*, 2010, **39**, 1532-1538.

58. T. Gunnlaugsson and F. Stomeo, *Org. Biomol. Chem.*, 2007, **5**, 1999-2009.

59. P. A. Vigato, V. Peruzzo and S. Tamburini, *Coord. Chem. Rev.*, 2009, **253**, 1099-1201.

60. (a) S. Dang, J. B. Yu, X. F. Wang, Z. Y. Guo, L. N. Sun, R. P. Deng, J. Feng, W. Q. Fan and H. J. Zhang, *J. Photochem. Photobiol. A*, 2010, **214**, 152-160; (b) C. Yu, Z. Zhang, L. Liu, W. Feng, X. Lü, W.-K. Wong and R. A. Jones, *Inorg. Chem. Commun.*, 2014, **49**, 30-33.

61. (a) C. P. Montgomery, B. S. Murray, E. J. New, R. Pal and D. Parker, *Accounts of Chemical Research*, 2009, **42**, 925-937; (b) E. J. New and D. Parker, *Org. Biomol. Chem.*, 2009, **7**, 851-855; (c) J. W. Walton, A. Bourdolle, S. J. Butler, M. Soulie, M. Delbianco, B. K. McMahon, R. Pal, H. Puschmann, J. M. Zwier, L. Lamarque, O. Maury, C. Andraud and D. Parker, *Chem. Commun.*, 2013, **49**, 1600-1602; (d) J. W. Walton, L. Di Bari, D. Parker, G. Pescitelli, H. Puschmann and D. S. Yufit, *Chem. Commun.*, 2011, **47**, 12289-12291; (e) J. H. Yu, D. Parker, R. Pal, R. A. Poole and M. J. Cann, *J. Am. Chem. Soc.*, 2006, **128**, 2294-2299.

62. B. Yan, *RSC Adv.*, 2012, **2**, 9304.

63. (a) Z. Zhang, W. Feng, P. Su, L. Liu, X. Lü, J. Song, D. Fan, W.-K. Wong, R. A. Jones and C. Su, *Synth. Met.*, 2015, **199**, 128-138; (b) T.-Z. Miao, W.-X. Feng, Z. Zhang, P.-Y. Su, X.-Q. Lü, J.-R. Song, D.-D. Fan, W.-K. Wong, R. A. Jones and C.-Y. Su, *Eur. J. Inorg. Chem.*, 2014, **17**, 2839-2848.

64. Z. Zhang, W. Feng, P. Su, X. Lü, J. Song, D. Fan, W. K. Wong, R. A. Jones and C. Su, *Inorg. Chem.*, 2014, **53**, 5950-5960.

Chapter 2

Near-infrared Luminescence of Nd^{3+} and Yb^{3+} Complexes Using a Polyfluorinated Pyrene-Based β-Diketonate Ligand

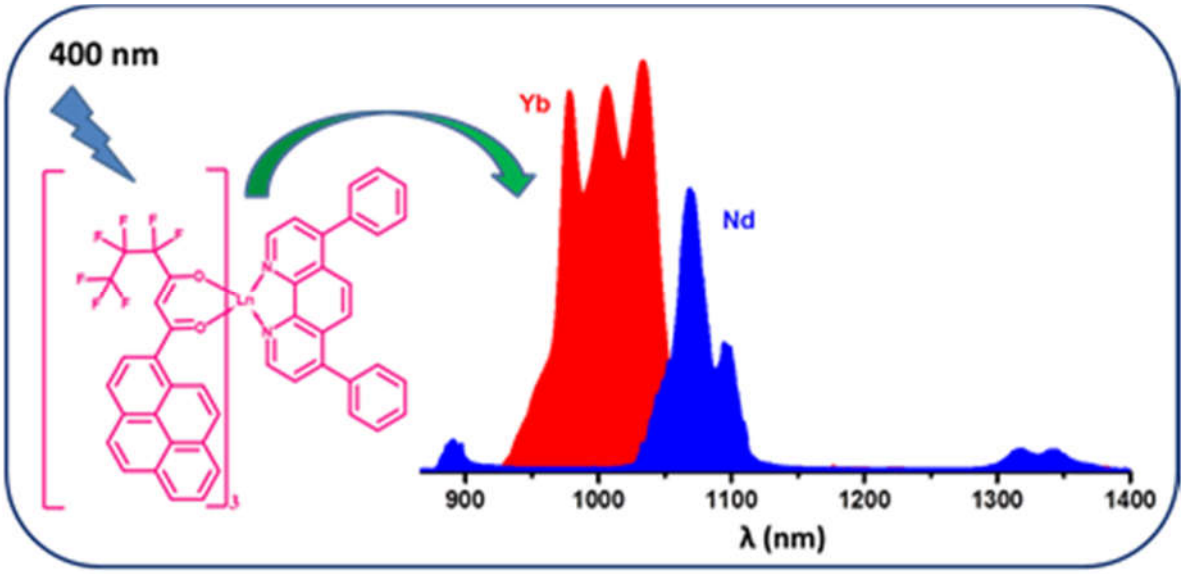

2.1. Abstract

*A new polyfluorinated β-diketonate ligand containing a pyrene chromophore, namely, 4,4,5,5,6,6,6-heptafluoro-3-hydroxy-1-(pyren-1-yl)hex-2-en-1-one (Hhfpyr) has been designed and employed for the development of a series of near-infrared (NIR) emitting lanthanide complexes (Nd^{3+} and Yb^{3+}) in the absence and presence of an ancillary ligand, 4,7-diphenyl-1,10-phenanthroline (bath). The isolated NIR emitting lanthanide complexes [$Nd(hfpyr)_3(H_2O)$ **1**, $Nd(hfpyr)_3(bath)$ **2**, $Yb(hfpyr)_3(H_2O)$ **3** and $Yb(hfpyr)_3(bath)$ **4**] have been characterized by various spectroscopic techniques and evaluated their photoluminescence properties. The photophysical properties disclosed that the developed pyrene-based β-diketonate ligand is well suited for the sensitization of Nd^{3+} as well as Yb^{3+} emissions, thanks to the favorable position of the triplet state (T_1) of the ligand ($\Delta E = T_1 - {}^4F_{3/2} = 4700\ cm^{-1}$ for Nd^{3+} and $\Delta E = T_1 - {}^2F_{5/2} = 6200\ cm^{-1}$*

*for Yb^{3+}), as evidenced from the phosphorescence spectra of the corresponding Gd^{3+} complexes. Most importantly, the displacement of solvent molecules from the coordination sphere of the NIR emitting lanthanide binary complexes (**1** and **3**) with an ancillary ligand markedly enhances the quantum yields ($\Phi_{overall}$ = 0.45 for **1** to 1.07% for **2** and from 1.69 for **3** to 3.08% for **4**) and excited state lifetime values (τ = 2.80 for **1** to 6.16 μs for **2** and from 6.88 for **3** to 13.45 μs for **4**). Notably, Yb^{3+} ternary compound **4** with promising NIR luminescence properties was embedded into PMMA matrices, giving rise to a series of PMMA-supported hybrid materials (PMMA@**4**), where the thermal stability and the film-forming properties were significantly enhanced.*

T. M. George, S. Varughese and M. L. P. Reddy; *RSC Adv.*, **2016**, 6, 69509–69520.

2.2. Introduction

Near-infrared (NIR) luminescence, especially from lanthanide complexes such as Nd^{3+} and Yb^{3+} has emerged as an area of paramount interest due to its pioneering technological applications in fields ranging from bioimaging to optical communications.[1] However, since f–f transitions are parity forbidden, unligated Ln^{3+} ions have strikingly low molar absorption coefficients and hence direct excitation of lanthanide ions always leads to modest luminescence intensities.[2] As a consequence, many efforts have been made in order to enhance the absorption coefficients of Ln^{3+} ions and thereby achieved efficient photoluminescence.[3] Fortunately, this objective can be easily realized by prudent selection of new antenna chromophores with suitable conjugated motifs.[4] In this context, β-diketonates are particularly important because such ligands can efficiently absorb ultraviolet light and transfer the absorbed energy to the central Ln^{3+} ions in an appropriately effective manner.[4c, 5] Indeed, there exists an

absolute challenge to design and develop a novel *β*-diketonate ligand with relatively low triplet energy level, which matches well with the first excited state of NIR luminescent Ln^{3+} ions[1a, 6] ($^4F_{3/2}$ for Nd^{3+} = 11,257 cm^{-1} or $^2F_{5/2}$ for Yb^{3+} = 10,400 cm^{-1}) as compared with visible luminescent Ln^{3+} ions having relatively high first excited state energy levels ($^5D_0$ for Eu^{3+} = 17,286 cm^{-1} or $^5D_4$ for Tb^{3+} = 20,545 cm^{-1}). Recently, some feasible strategies have been proposed by many researchers to improve the NIR luminescence of Ln^{3+} ions.[7] For example, the fluorination of the *β*-diketonate ligand for minimizing the non-radiative decay pathways or molecular engineering of the *β*-diketonate ligand with appended suitable extended π-conjugated chromophore moieties to achieve efficient sensitization of the NIR luminescence of Ln^{3+} ions.[8] Also, the replacement of coordinated solvent molecules around the central Ln^{3+} ion with an appropriate ancillary ligand, avoids the quenching effects due to the presence of high-frequency oscillators.[9] Bünzli and co-workers has reported a new antenna molecule containing four benzoyltrifluoroacetone moieties anchored to single carbon atom and connected through four flexible methoxy groups as a sensitizer for NIR emitting lanthanides.[10] New bis-*β*-diketonate ligand by coupling two mono-diketonate ligands (2-theonyltrifluoroacetone) has also been proposed for the sensitization of Yb^{3+} ions with higher quantum yields as compared with the mononuclear analogue.[11]

Pyrene, a well-known organic hydrocarbon was extensively employed as a fluorophore of choice in the field of photochemistry and photophysics.[12] In addition, some of the pyrene derivatives have been used in Organic Light Emitting Diodes

intending to improve the hole transporting ability because of its electron-rich property.[13] There are also a few reported examples that use pyrene as a sensitizer for lanthanide emission. The 'antenna effect' in europium complexes involving a pyrene-based triacid ligand was first disclosed by Fages *et al*.[14] Later, near-IR emission was noted in ytterbium and neodymium complexes containing a pyrene chromophore linked to a macrocycle via different tether lengths.[15] In the later studies, Pope reported Yb^{3+}, Nd^{3+} and Er^{3+} complexes with two pyrene chromophores tethered by a diethylene triaminepentaacetic acid chelate.[16] These investigations have inspired us to develop a new antenna ligand for the sensitization of Nd^{3+} and Yb^{3+} ions by anchoring a pyrene chromophore to the *β*-diketonate ligand (Figure 2.1).

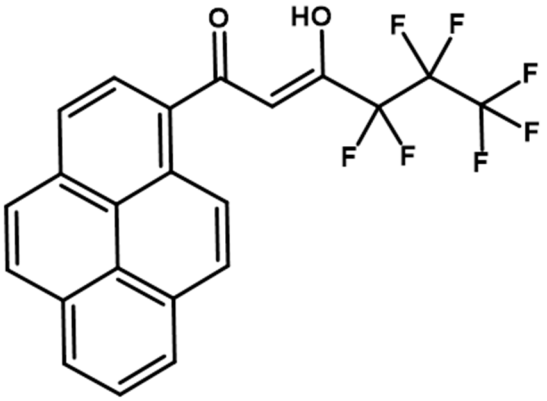

Figure 2.1. Structure of the ligand Hhfpyr.

It is well documented that the NIR-emitting Ln^{3+} ions are especially inclined to vibrational deactivation.[9] Organic chromophores containing high-energy oscillators, such as C–H and O–H bonds are able to quench the Ln^{3+} excited states nonradiatively, thus exhibiting weak luminescence intensities and shorter excited-state lifetimes. The

replacement of C–H bonds with C–F bonds is an important strategy for the design and development of novel Ln^{3+} complexes with efficient photophysical properties.[7h, 17] As per the earlier literature reports, the replacement of C–H bonds in a β-diketonate ligand with low energy C–F oscillators is able to lower the vibrational energy of the ligand and thereby enhances the emission intensity of the Ln^{3+} ion.[18] In addition, due to heavy atom effect, which facilitate the intersystem crossing and as a result the lanthanide-centered luminescent properties are improved.[19] Therefore in the present work, a new β-diketonate molecule, namely, 4,4,5,5,6,6,6-heptafluoro-3-hydroxy-1-(pyren-1-yl)hex-2-en-1-one (Hhfpyr) has been designed by simultaneously incorporating pyrene moiety as well as heptafluorinated alkyl chain. The developed β-diketonate ligand has been utilized for the construction of a series of lanthanide complexes (Ln^{3+} = Nd, Yb and Gd) in the absence and presence of an ancillary ligand, 4,7-diphenyl-1,10-phenanthroline. The synthesized lanthanide complexes were characterized by various spectroscopic techniques and evaluated their photophysical properties.

Nevertheless, NIR emitting Ln^{3+}-β-diketonate complexes typically exhibit low thermal-stability, limited photostability and poor mechanical properties. These inherent limitations hinder the practical application of NIR emitters in many of the optoelectronic technologies. It is well-known that the blending of luminescent near-IR emitting Ln^{3+} compounds in polymeric materials renders a series of advantages for the development of molecular materials, for instance, thermal, chemical and mechanical

stability, biocompatibility and the photoluminescence properties.[6a, 7e, 20] To the best of our knowledge, there are only few examples in the literature dealing with the incorporation of NIR emitting ternary-β-diketonate complexes into the PMMA materials.[6c, 21] Hence in the present study the newly developed luminescent NIR emitting Yb^{3+} complex has been incorporated into a host polymer matrix, such as poly(methyl methacrylate) films and investigated their photoluminescence behaviour.

2.3. Experimental Section

2.3.1. Materials and characterization

Ytterbium(III) nitrate hexahydrate (99.99%), neodymium(III) nitrate hexahydrate (99.99%), gadolinium(III) nitrate hexahydrate (99.99%), lanthanum(III) nitrate hexahydrate (99.99%), 1-acetylpyrene (97%), ethyl perfluorobutyrate (97%), sodium hydride (60% dispersion in mineral oil), poly(methyl methacrylate) (98%) and bathophenanthroline (97%) were purchased from Sigma-Aldrich and used without further purification. All the other chemicals employed were of analytical reagent grade.

Single-crystal XRD data for complex **3** were collected with a Rigaku Saturn 724+ diffractometer using graphite-monochromated Mo Kα radiation, and the data were processed using Rigaku Crystal Clear software. The molecular structure of the complex was solved and refined by the SHELXTL suite of programs.[22]

Elemental analyses were carried out on Elementar – vario MICRO cube elemental analyzer. A Perkin-Elmer Spectrum two FT-IR spectrometer was used to

record the infra-red spectral data and a Bruker Avance II 500 MHz NMR spectrometer was used to record the ^{1}H NMR (500 MHz) and ^{13}C NMR (125.7 MHz) spectra with tetramethylsilane as the internal standard. The electrospray ionization (ESI) mass spectra were measured with a Thermo Scientific Exactive Benchtop LC/MS Orbitrap Mass Spectrometer. The thermogravimetric analyses were performed on a TG/DTA-6200 (SII Nano Technology Inc., Japan). The optical spectra of the synthesized ligand and its corresponding metal complexes were recorded with a Shimadzu UV-3600 UV-vis spectrophotometer.

Photophysical measurements were carried out in the solid state at room temperature. Emission spectra were obtained with an Edinburgh FLS 980 spectrofluorometer equipped with a 450 W xenon arc lamp. Emission spectra were corrected for source intensity (lamp and grating) and emission spectral response (detector and grating) by standard correction curves. The absolute fluorescence quantum yields were measured on an Edinburgh FLS 980 steady state spectrometer using an integrating sphere. Luminescent excited state lifetimes in the range from 0.5 ns to 50 μs were measured by an Edinburgh FLS 980 spectrofluorometer equipped with a digital oscilloscope (Tektronix) for data acquisition in time-correlated single-photon counting experiments with a pulsed microsecond xenon flashlamp. The estimated experimental errors are 2 nm on the photoluminescence bands maxima, 5% on the luminescence quantum yield.

The lifetime measurements carried out at low temperature using a Spex 1040D phosphorimeter.

2.3.2. Synthesis of the ligand 4,4,5,5,6,6,6-heptafluoro-3-hydroxy-1-(pyren-2-yl)hex-2-en-1-one (Hhfpyr)

The new β-diketonate ligand (Hhfpyr) was prepared according to a modified Claisen condensation method as detailed in Scheme 2.1. 1-Acetylpyrene (1.0 mmol) and ethyl perfluorobutyrate (1.0 mmol) were dissolved in dry tetrahydrofuran (25 mL) and the resultant mixture was stirred for 15 min in an ice bath at 0 °C. To this reaction mixture, sodium hydride (2.0 mmol) was added dropwise in nitrogen atmosphere and stirred for 20 min, followed by further stirring for 12 h at 70 °C. To the above reaction mixture, 40 mL of 2M HCl was added and extracted twice into dichloromethane (2×30 mL). Then the organic layer was collected and dried over Na_2SO_4, and the solvent was removed by evaporation. The product obtained was then purified by column chromatography on silica gel with a solvent mixture consisting of hexane and ethyl acetate (10:1) as an eluent. Yield: 80%. Elemental analysis (%): calculated for $C_{22}H_{11}F_7O_2$ (440.06): C 60.01, H 2.52; found: C 60.23, H 2.63. ^{1}H NMR ($CDC1_3$, 500 MHz) δ (ppm): 15.53 (broad, enol–OH), 8.78 (d, 1H, J = 9 Hz), 8.23 (m, 6H), 8.05 (m, 2H), 6.62 (s, 1H). ^{13}C NMR(125.7 MHz, $CDCl_3$) δ (ppm): 190.58, 176.78, 134.71, 131.14, 130.51, 130.21, 129.90, 128.09, 127.05, 126.78, 126.70, 126.64, 126.55, 125.01, 124.38, 125.01, 124.38, 124.26, 124.11, 99.48, 77.16–76.05

($CDCl_3$). FT-IR (KBr) ν_{max} (cm^{-1}): 3427 (O–H), 1596, 1508, 1346, 1226, 1069, 962, 898, 763, 680, 539. *m/z* = 463.05 $(M+Na)^+$.

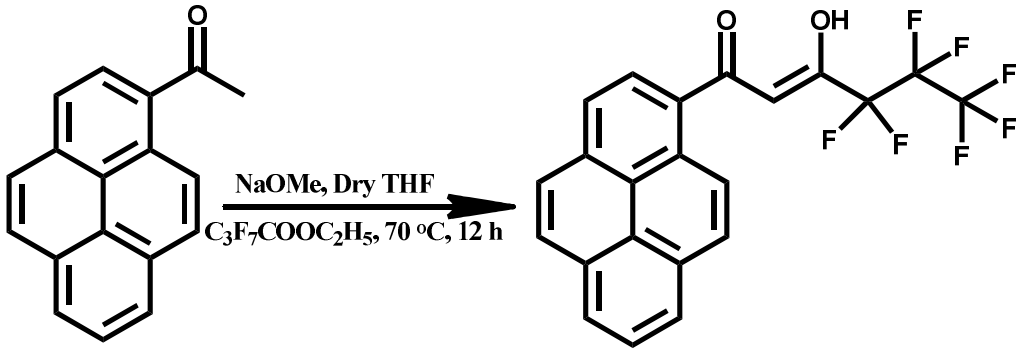

Scheme 2.1. Synthetic procedure for the ligand Hhfpyr.

2.3.3. Synthesis of complexes $Ln(hfpyr)_3(H_2O)$ [Ln = Nd (1), Yb (3) Gd (5) and La (6)]

To a methanolic solution of Hhfpyr (12 mmol), 12 mmol of NaOH in water was added and stirred for 5 min. $Ln(NO_3)_3{\cdot}6(H_2O)$ in 3 mL of water (4 mmol) was added drop-wise to the above reaction mixture and stirred for 24 h at 298K (Scheme 2.2). The resultant crude precipitate was filtered, washed with water and dried. The obtained metal complex was recrystallized from chloroform solution.

$Nd(hfpyr)_3(H_2O)$ (1). Elemental analysis (%): calculated for $C_{66}H_{32}F_{21}O_8Nd$ (1480.16): C 53.56, H 2.18; Found: C 53.35, H 2.27. FT-IR (KBr) ν_{max} (cm^{-1}): 3434, 1609, 1514, 1344, 1226, 1153, 1068, 1028, 968, 846, 742, 681, 536. *m/z* = 1462.09 $[Nd(hfpyr)_3+1]^+$.

$Yb(hfpyr)_3(H_2O)$ (3). Elemental analysis (%): calculated for $C_{66}H_{32}F_{21}O_8Yb$ (1508.98): C 52.53, H 2.14; Found: C 52.39, H 2.28. FT-IR (KBr) ν_{max} (cm^{-1}):

3435, 1610, 1514, 1345, 1233, 1179, 1032, 971, 849, 746, 685, 540. *m/z* = 1492.11 $[Yb(hfpyr)_3+1]^+$.

$Gd(hfpyr)_3(H_2O)$ (5). Elemental analysis (%): calculated for $C_{66}H_{32}F_{21}O_8Gd$ (1493.19): C 53.09, H 2.16; Found: C 53.29, H 2.28. FT-IR (KBr) ν_{max} (cm^{-1}): 3436, 1607, 1516, 1345, 1232, 1179, 1031, 970, 850, 745, 682, 539. *m/z* = 1494.11 $[Gd(hfpyr)_3(H_2O)]^+$.

$La(hfpyr)_3(H_2O)$ (6). Elemental analysis (%): calculated for $C_{66}H_{32}F_{21}O_8La$ (1474.83): C 53.75, H 2.19; Found: C 53.68, H 2.28. ^1H NMR ($CDC1_3$, 500 MHz) δ (ppm): 8.49 (s, 3H), 8.02 (d, 18H), 7.40 (s, 3H), 7.02 (s, 3H), 6.51 (s, 3H). FT-IR (KBr) ν_{max} (cm^{-1}): 3424, 1611, 1512, 1345, 1229, 1153, 1066, 1033, 966, 847, 750, 667, 536. *m/z* = 1457.09 $[La(hfpyr)_3+1]^+$.

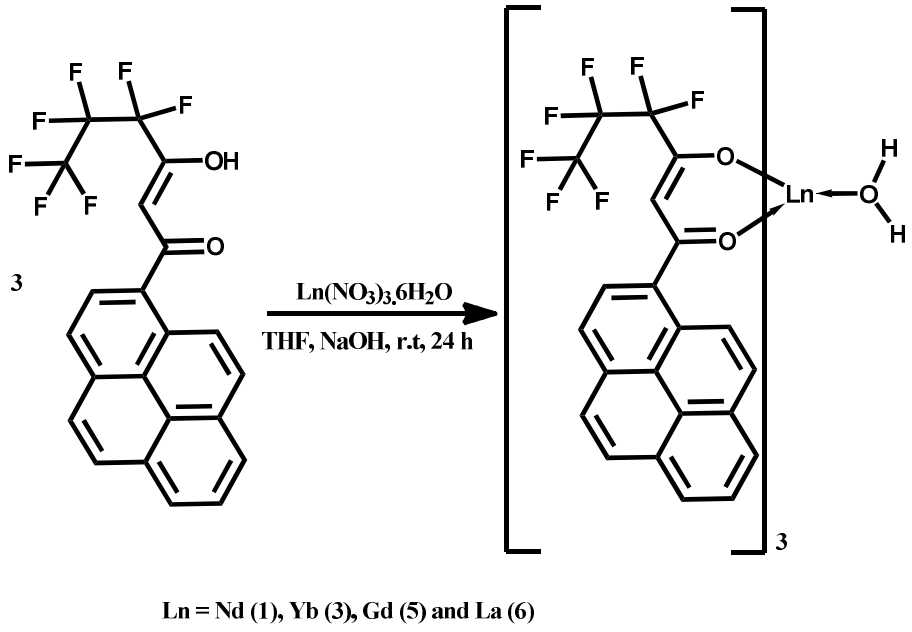

Scheme 2.2. Synthesis of the Ln^{3+} (Ln = Nd, Yb, Gd and La) binary complexes.

2.3.4. Synthesis of Ln^{3+} ternary complexes $Ln(hfpyr)_3(bath)$ [Ln = Nd (2), Yb (4) and La (7)]

The ternary Ln^{3+} compounds were synthesized by mixing equimolar solutions of the corresponding binary complexes and an ancillary ligand; bathophenanthroline (bath) in $CHCl_3$ solution and the resultant mixture was stirred for 12 h at 70°C. The metal complexes were then isolated after the removal of solvent by evaporation process. Finally, the ternary lanthanide complexes were obtained by recrystallization from chloroform solution (as described in scheme 2.3).

$Nd(hfpyr)_3(bath)$ (2). Elemental analysis (%): calculated for $C_{90}H_{46}F_{21}N_2O_8Nd$ (1794.55): C 60.24, H 2.58, N 1.56; Found: C 60.35, H 2.39 N 1.52. FT-IR (KBr) ν_{max} (cm^{-1}): 3028, 1608, 1538 1513, 1477, 1342, 1225, 1152, 1032, 970, 846, 792, 624, 540. *m/z* = 1794.22 $[Nd(hfpyr)_3(bath)]^+$.

$Yb(hfpyr)_3(bath)$ (4). Elemental analysis (%): calculated for $C_{90}H_{46}F_{21}N_2O_8Yb$ (1823.36): C 59.28, H 2.54, N 1.54; Found: C 59.37, H 2.39 N 1.56. FT-IR (KBr) ν_{max} (cm^{-1}): 3047, 1609, 1541 1515, 1477, 1344, 1224, 1156, 1031, 963, 848, 789, 630, 536. *m/z* = 1384.18 $[Yb(hfpyr)_2(bath)]^+$.

$La(hfpyr)_3(bath)$ (7). Elemental analysis (%): calculated for $C_{90}H_{46}F_{21}N_2O_8La$ (1788.21): C 60.42, H 2.59, N 1.57; Found: C 60.53, H 2.66 N 1.48. ^1H NMR ($CDC1_3$, 500 MHz) δ (ppm): 9.57 (s, 2H), 8.72 (m, 3H), 8.13 (m, 4H), 8.08 (m, 3H), 7.99 (m,

5H), 7.84 (m, 6H) 7.48-7.37 (m, 17H), 6.99 (m, 3H) 6.49 (s, 3H). FT-IR (KBr) ν_{max} (cm^{-1}): 3037, 1608, 1541, 1511, 1464, 1343, 1262, 1227, 1029, 969, 849, 762, 668, 595. *m/z* = 1788.53 $[La(hfpyr)_3(bath)]^+$.

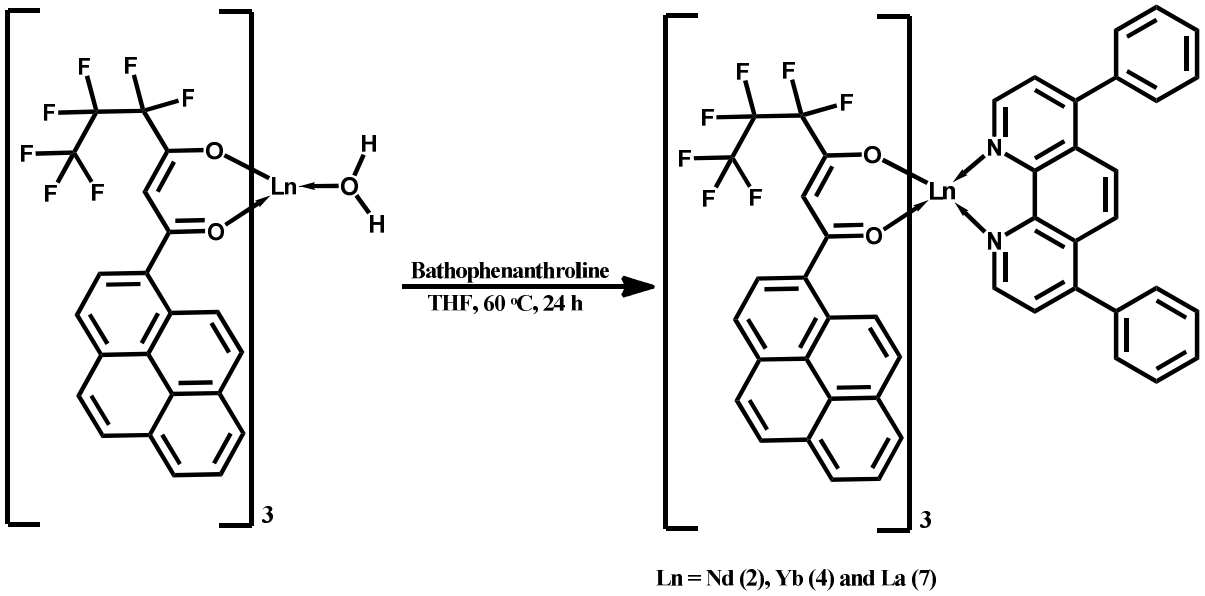

Scheme 2.3. Synthesis of the Ln^{3+} (Ln = Nd, Yb and La) ternary complexes.

2.3.5. Synthesis of Yb^{3+} complex doped PMMA polymer films

The PMMA polymer was doped with the Yb^{3+} complex **4** in the proportions 1, 3, 5, 7 and 9 % (w/w). The PMMA powder was dissolved in chloroform, followed by addition of the required amount of complex **4** in chloroform solution, and the respective mixture was heated at 40 °C for 35 min. The polymer films were then obtained after evaporation of excess solvent at 60°C.

2.4. Results and Discussion

2.4.1. Synthesis and characterization of the Hhfpyr ligand and Ln^{3+} complexes 1–5

The β-diketonate ligand 4,4,5,5,6,6,6-heptafluoro-3-hydroxy-1-(pyren-1-yl)hex-2-en-1-one (Hhfpyr) was synthesized in 80% yield by a modified claisen condensation reaction of 1-acetylpyrene with the ethyl perfluorobutyrate ester in the presence of sodium hydride in THF medium. The corresponding one pot synthesis of the ligand is described in scheme 2.1. The developed ligand has been characterized by the ^{1}H NMR, ^{13}C NMR, FT-IR and electrospray ionisation mass spectroscopic (ESI-MS) methods as well as by elemental analysis. The developed β-diketonate ligand mainly exists as enol form in $CDCl_3$ solution, as evident from the ^{1}H NMR spectrum of the compound. In the ^{1}H NMR spectrum of Hhfpyr, a broad peak at δ 15.64 ppm corresponding to enolic –OH has been noted. Further, the absence of methyne protons at δ 3.70 ppm confirms the existence of the ligand in enolic form. The synthesis routines for Ln^{3+} binary and ternary complexes are detailed in schemes 2.2 and 2.3, respectively. The elemental analyses and ESI-MS studies of Ln^{3+} complexes (**1-5**) revealed that the central lanthanide ion is coordinating to three β-diketonate ligands. On the other hand, in the case of Ln^{3+} ternary complexes (**2, 4** and **7**), one molecule of the bidentate nitrogen donor, 4,7-diphenyl-1,10-phenanthroline (bath), is also present in the coordination sphere. The FT-IR spectra of the binary Ln^{3+} complexes (**1**, **3, 5 and 6**) display a

broad absorption in the 3000−3500 cm^{-1} region, thereby illustrating the presence of water molecule in the coordination sphere of the metal ions. The absence of this broad band in the case of ternary Nd^{3+} Yb^{3+} and La^{3+} complexes (**2**, **4 and 7**) inferred that the water molecule is successfully displaced by the bidentate bathophenanthroline ligand. The carbonyl stretching frequency (>C=O) of free ligand Hhfpyr (1596 cm^{-1}) was shifted to higher wave numbers in complexes **1-5** (1609 cm^{-1} for **1**; 1610 cm^{-1} for **2**; 1607 cm^{-1} for **3**; 1608 cm^{-1} for **4**; 1609 cm^{-1} for **5**) demonstrating the involvement of carbonyl oxygen in the complex formation with the Ln^{3+} ion. The bands assigned to bathophenanthroline ring stretching modes C=N and C=C can be observed in the 1540–1500 cm^{-1} range and in the 1030–1000 cm^{-1} range, respectively. These bands are shifted in comparison with that of free ancillary ligand, suggesting that bathophenanthroline is coordinating to Ln^{3+} ion.

To further understand the coordination behaviour of the ligands with the lanthanide ions, in the current study, anti-paramagnetic lanthanum complexes have been synthesized and characterized by various spectroscopic techniques. The ^1H NMR spectrum of the lanthanum binary β-diketonate complex, $La(hfpyr)_3(H_2O)$ is consistent with the presence of three Hhfpyr units coordinated to the lanthanide ion. The signal for methine proton (-CH) of Hhfpyr appears at 6.51 ppm (δ) and the aromatic protons of the pyrene moiety resonates in the range 8.49 to 7.02 ppm (δ). The upfield shift of the β-diketonate

resonances, in the complex, substantiates coordination of ligands with the lanthanide ion. The proton signals of the coordinated water molecule with the metal ion can be noted at 2.59 ppm (δ). In the ternary lanthanum complex, $La(hfpyr)_3(bath)$, the methine proton appears at 6.48 ppm (δ). The signals due to aromatic protons of pyrene and bathophenanthroline moiety appear in the range 9.57 to 6.78 ppm (δ). The proton signals appeared in the ternary complex indicates the presence of three Hhfpyr units and one bathophenanthroline moiety in the coordinated complex. Further, no signals for coordinated water molecule noted in the $La(hfpyr)_3(bath)$, which indicates the displacement of a coordinated water molecule with the ancillary ligand in the corresponding ternary complex.

The thermal behaviour of Nd^{3+} and Yb^{3+} β-diketonate complexes (**1-5**) was evaluated by means of thermogravimetric analysis (TGA) under nitrogen atmosphere and the results are given in Figures 2.2 and 2.3. It is clear from the TGA data that the complexes **1** and **3** undergo mass loss approximately 1.19 % (Calcd: 1.20 %) in the first step upto 160 °C, corresponding to the elimination of coordinated water molecule. On the other hand, in the case of ternary Ln^{3+} complexes (**2** and **4**), no weight loss was noted in the range of 120-160 °C, which indicates that these complexes exist as anhydrous in nature. The above results are in accordance with the FT-IR spectral data. The weight loss noted in the thermal analysis of these complexes is found to be much lower than the calculated value for the non-volatile lanthanide oxide, indicating the partial sublimation of these compounds under

atmospheric pressure which is well documented in many of the lanthanide fluorinated complexes.[5b, 23]

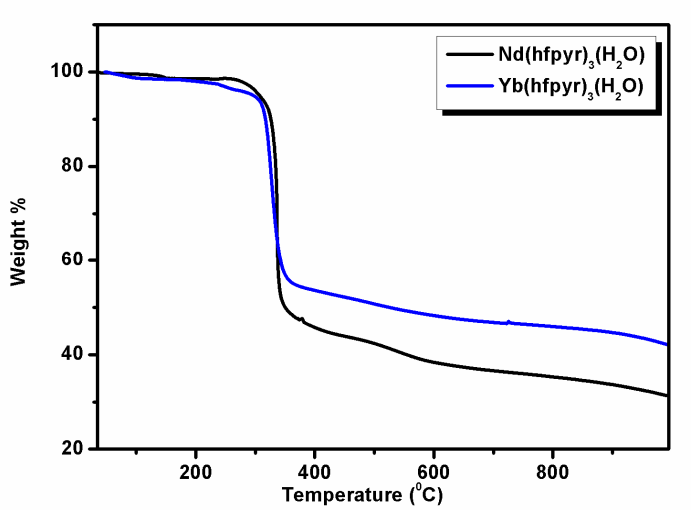

Figure 2.2. Thermogravimetric curves for complexes $Nd(hfpyr)_3(H_2O)$ **1** and $Yb(hfpyr)_3(H_2O)$ **3**.

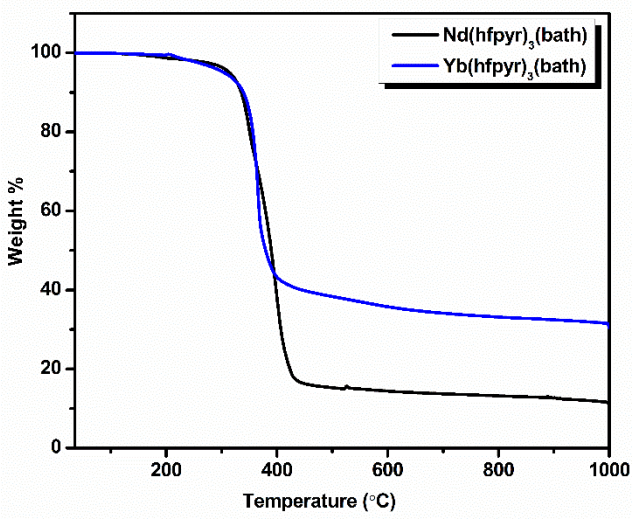

Figure 2.3. Thermogravimetric curves for complexes $Nd(hfpyr)_3(bath)$ **1** and $Yb(hfpyr)_3(bath)$ **3**.

2.4.2. X-ray Single Crystal Structure of 3

Slow diffusion of hexane into a solution of the Yb^{3+} binary β-diketonate complex in methanol resulted in the growth of single crystals of **3**. However, our efforts

to grow single-crystals of the other Ln^{3+} complexes were not fruitful. The molecular structure of the Yb^{3+}-pyrene anchored β-diketonate complex (**3**) obtained by X-ray single-crystal diffraction technique is shown in Figure 2.4. The pertinent data collection parameters and a list of significant bond distances and angles are presented in Table 2.1 and 2.2, respectively. Yb^{3+} binary β-diketonate complex was found to crystallize in the triclinic crystal system with a $P\bar{1}$ space group. The structure reveals that the Yb^{3+} center adopts a distorted-trigonal prismatic coordination geometry, comprising of three β-diketonate ligands and one solvent water molecule. These results are in good agreement with the crystal structure of tris(acetylacetonato)aquoytterbium reported elsewhere.[24]

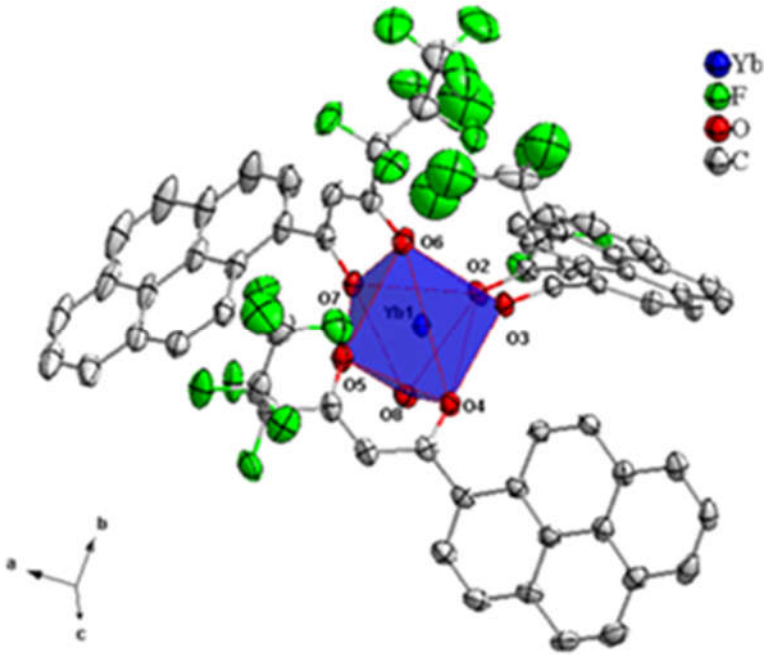

Figure. 2.4 ORTEP diagram of $[Yb(hfpyr)_3(H_2O)]$ **3** with the thermal ellipsoids drawn at 30% probability level and the hydrogen atoms removed for clarity.

Table 2.1 Crystallographic and refinement data for **3.**

formula	C_{66} H_{32} F_{21} O_7 Yb
formula weight	1508.96
crystal system	triclinic
space group	$P\bar{1}$
crystallite size (mm^3)	0.20 × 0.20 × 0.15
temperature (K)	123 K
a (Å)	14.204(3)
b (Å)	15.184(3)
c (Å)	17.459(4)
α (deg)	113.56(1)
β (deg)	108.085(15)
γ (deg)	94.308(12)
V ($Å^3$)	3194.2(12)
Z	2
D_{calcd} (g cm^{-1})	1.569
μ(Mo Kα) (mm^{-1})	1.577
F(000)	1486.0
R1 [$I > 2\sigma(I)$]	0.0606
wR2 [$I > 2\sigma(I)$]	0.1638
R1 (all data)	0.0677
wR2 (all data)	0.1696
GOF	1.178
CCDC	1473942

Table 2.2 Selected bond lengths (A˚) and angles (°) for complex **3**

Bond lengths (Å)		**Bond angles (°)**	
Yb1-O2	2.2685	O5-Yb1-O4	75.928
Yb1-O3	2.2352	O3-Yb1-O2	75.222
Yb1-O4	2.2209	O3 -Yb1-O7	139.825
Yb1-O5	2.2130	O2-Yb1-O8	80.475
Yb1-O6	2.2335	O6-Yb1-O8	153.723
Yb1-O7	2.2980	O5-Yb1-O6	88.143
Yb1-O8	2.2980	O4-Yb1-O3	73.531

In general, most of the lanthanide-β-diketonate complexes are eight-coordinated and the coordination sphere features three bidentate β-diketonate ligands and two solvent molecules.[5a] Unusually in the present study, the binary Yb-β-diketonate complex is seven-coordinated and the coordination sphere consisting of three bidentate β-diketonate ligands and one water molecule. This can be attributed to the presence of three bulky conjugated pyrene appended β-diketonate ligands in the coordination sphere of the metal ion, which may sterically hinders the presence of water molecule. The average metal-oxygen distance (2.245 Å) of the β-diketonate ligands is found to be shorter than of the coordinated water molecule (2.298 Å). This observation could be attributed to the presence of a formal negative charge on the β-diketonate oxygen atoms which could enhance the binding to the Yb^{3+} cation due to electrostatic effects.[5a,25] Further, it is interesting to note that one of the metal-oxygen distance of the β-diketonate ligand is surprisingly larger (Yb1-O(7) = 2.298 Å) as compared to the remaining metal-oxygen distances of the β-diketonates [Yb1-O(2) = 2.269 Å; Yb1-O(3) = 2.235 Å; Yb1-O(4) = 2.221 Å; Yb1-O(5) = 2.213 Å; Yb1-O(6) = 2.233 Å]. This may be due to the strong intermolecular hydrogen bonding formation between the coordinated water molecule of Yb1 and one of the β-diketonate oxygen atom coordinated to the neighbouring metal centre as shown in Figure 2.5 [the O–H···O (H···O distance = 2.10 Å with an angle of 133.0° falls within the typical

range hydrogen bonding interactions].[25] In addition, there also exists a strong intermolecular hydrogen bonding interaction between the coordinated water molecule and the fluorine atom of the β-diketonate ligand coordinated to the adjacent Yb1 centre [O–H···F (H···F = 2.18 Å) with an angle of 143.0°]. These intermolecular interactions combine to form an interesting dimeric unit between the two coordinated metal centres.

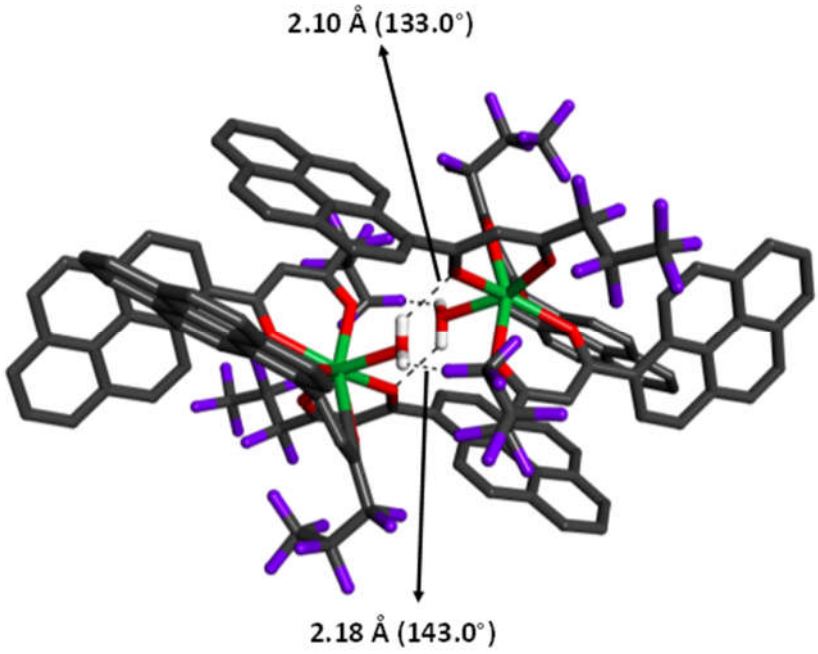

Figure 2.5 Intermolecular hydrogen bond present in **3** between water oxygen atoms and β-diketonate oxygen and fluorine atoms of Hhfpyr (shown with broken lines).

2.4.3. Electronic Spectroscopy

The room-temperature absorption spectra of the ligands and the corresponding Nd^{3+} and Yb^{3+} complexes (**1-4**) recorded in THF solution ($c = 1 \times 10^{-5}$ M) are shown in Figures 2.6 and 2.7 respectively. The spectral shapes of the complexes

are similar to that of the free Hhfpyr, indicating that the coordination of Ln^{3+} ion does not have significant influence on the energy of the singlet state of the *β*-diketonate. The ligand displays a composite broad band in the wavelength region 325-475 nm (λ_{max} = 370 nm), which can be assigned to the singlet-singlet *n*-*π** enolic transition of the *β*-diketonate. In addition, a high energy absorption band noted in the region 275-325 nm can be attributed to the *π*-*π** transition of the aromatic moiety of the *β*-diketonate. The molar absorption coefficient (*ε*) of the developed *β*-diketonate ligand was found to be 15,800 $Lmol^{-1}cm^{-1}$ at λ_{max} = 370 nm, which highlights that the*β*-diketonate ligand has an ability to absorb light.

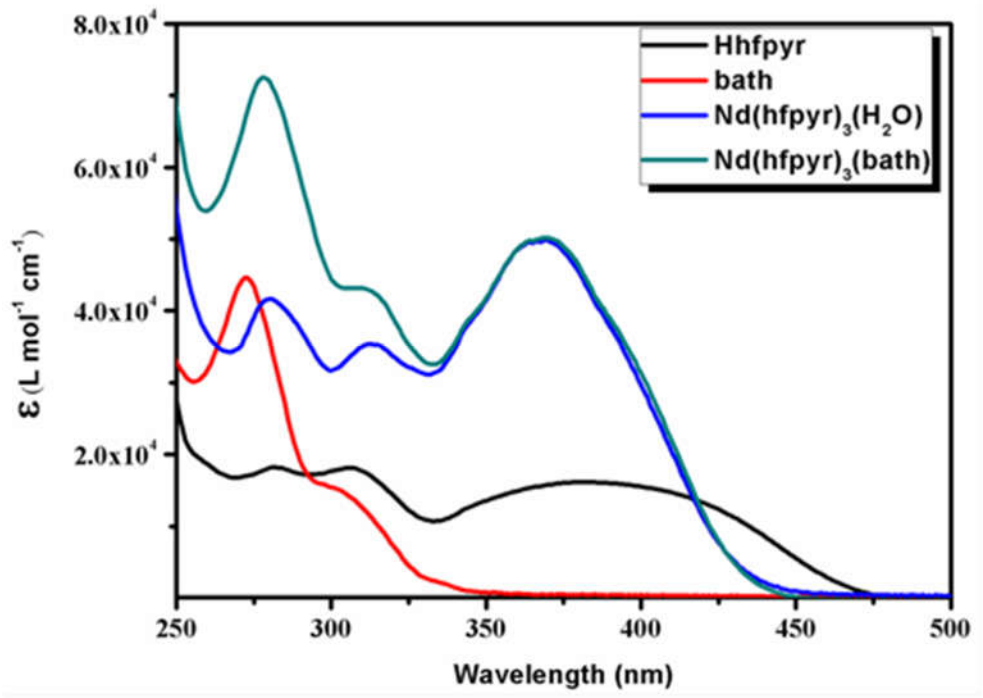

Figure 2.6. UV–vis absorption spectra of the ligands Hhfpyr, bath and complexes **1** and **2** in THF (*c* = 1 x 10^{-5} M) solution at 298K.

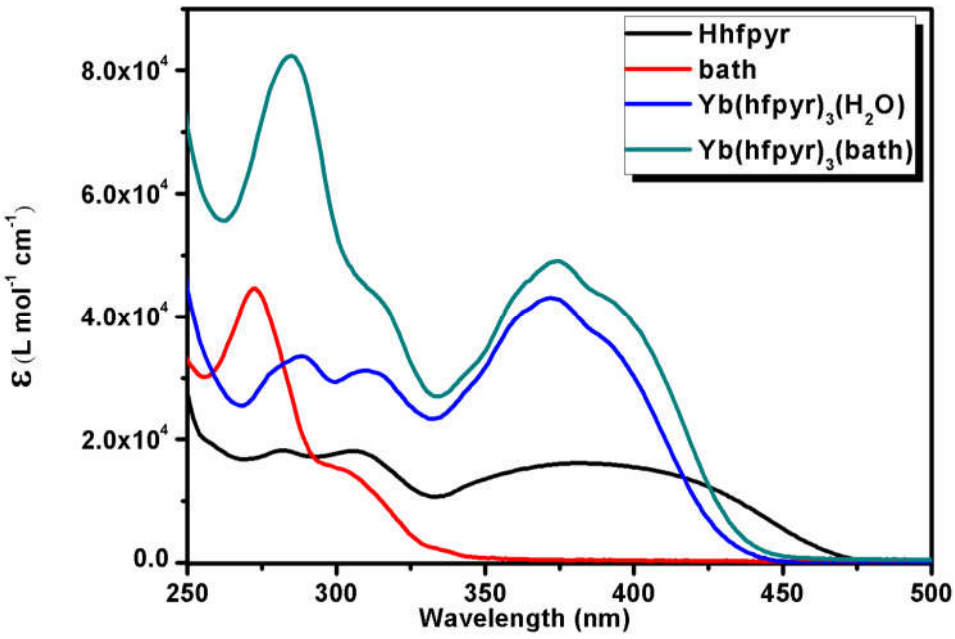

Figure 2.7. UV–vis absorption spectra of the ligands Hhfpyr, bath and complexes **3** and **4** in THF (c = 1 x 10^{-5} M) solution at 298K.

The magnitudes of the molar absorption coefficient values of Nd^{3+} complexes **1** (ε = 49,800 $Lmol^{-1}cm^{-1}$ at λ_{max} = 370 nm) and **2** (ε = 50,200 $Lmol^{-1}cm^{-1}$ at λ_{max} = 370 nm) were found to be approximately three-fold higher than that of the β-diketonate ligand. This is in consistent with the presence of three β-diketonate ligands in the respective complexes as observed from the elemental analysis data. Similar trends have been noticed in the case of Yb^{3+} complexes **3** (ε = 49,500 $Lmol^{-1}cm^{-1}$ at λ_{max} = 370 nm) and **4** (ε = 49,300 $Lmol^{-1}cm^{-1}$).

2.4.4. Photophysical properties

NIR luminescent Nd^{3+} and Yb^{3+} complexes possess considerable promise for practical applications, as their photophysical properties have several distinct

advantages over organic fluorophores and semiconductor nanoparticles.[1c] For near-infrared Ln^{3+}, their lowest excited states, and their ground states are primarily close in their energy, and hence, the emission often occurs in the infrared region and their intensities are weaker by several orders of magnitude, compared to that of visible light emitting Ln^{3+} ions.[8c] Moreover, their deactivation process often occurs easily through a non-radiative transition. Therefore, a fundamental challenge is to develop an appropriate antenna molecule for the sensitization of the near-infrared lanthanide ions. Thus, in the current study, a new *β*-diketonate molecule has been developed by anchoring pyrene as a chromophore group.

To understand the energy transfer processes in the newly isolated NIR emitting Nd^{3+} and Yb^{3+} *β*-diketonate complexes, it is necessary to determine the singlet (S_1) and triplet (T_1) energy levels of the synthesized new *β*-diketonate ligand. The singlet energy level of the ligand was determined by reference to the UV-vis upper absorption edge of the $Gd(hfpyr)_3(H_2O)$ **5** (Figure 2.8), and the value was found to be 22935 cm^{-1} (436 nm).[26] The triplet energy level of the *β*-diketonate ligand was determined by referring to the lower wavelength emission edge from the low-temperature phosphorescence spectrum of (Figure 2.8) the $Gd(hfpyr)_3(H_2O)$ **5**.[27] The efficient ligand-to-metal energy transfer requires a good intersystem-crossing efficiency, which is maximized when the energy difference between singlet and triplet states, ΔE (S_1-T_1), is closed to 5000 cm^{-1}

as coined by Reinhoudt's empirical rule.[28] In the present system, it amounts to 6728 cm^{-1}, and therefore the newly developed β-diketonate ligand exhibits a good intersystem-crossing efficiency. It is well recognized that the Gd^{3+} complexes are a popular choice for elucidating the triplet energy level of a newly developed antenna molecule due to the following reason: i) the first excited state energy levels of Gd^{3+} are situated at high energies (^5I_J = 36,900 cm^{-1}), and hence there is no Gd^{3+} emission in the visible region and all the emissions noted is due to the ligand part of the complex. Therefore, the lower emission edge of the 77 K phosphorescence spectrum of the Gd^{3+} complex designates the triplet energy level of the ligand.[27] Thus the triplet energy level of the developed β-diketonate ligand (T^1 = 16,207 cm^{-1}; 617 nm) lie well above the energy of the main emitting level of $^4F_{3/2}$ for Nd^{3+} (11,257 cm^{-1}) or $^2F_{5/2}$ for Yb^{3+} (10,400 cm^{-1}), implying that the developed β-diketonate ligand can act as an efficient antenna molecule for the sensitization of both trivalent Nd^{3+} or Yb^{3+} ions. The room-temperature lifetime experiment of $Gd(hfpyr)_3(H_2O)$ shows that the decay curve can be fitted to a bi-exponential decay with τ_1 = 1.58 ns and τ_2 = 6.66 ns (Figure 2.9). This indicates that the main energy transfer in the present complexes may be through the triplet state of the ligand.[29] The long lifetime value (typically 522 μs) measured for $Gd(hfpyr)_3(H_2O)$ at 77K is consistent with the emission from characteristic triplet state (Figure 2.9).[30]

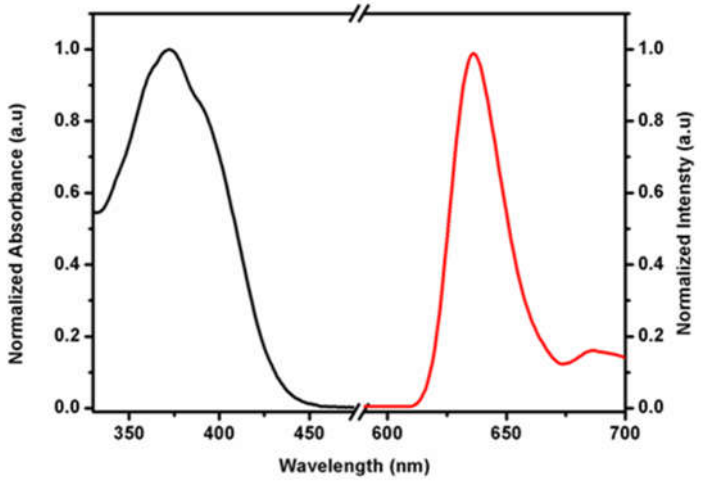

Figure 2.8. UV–vis absorption spectrum at 298 K (black) and 77 K phosphorescence spectra (red) of the $Gd(hfpyr)_3(H_2O)$ complex.

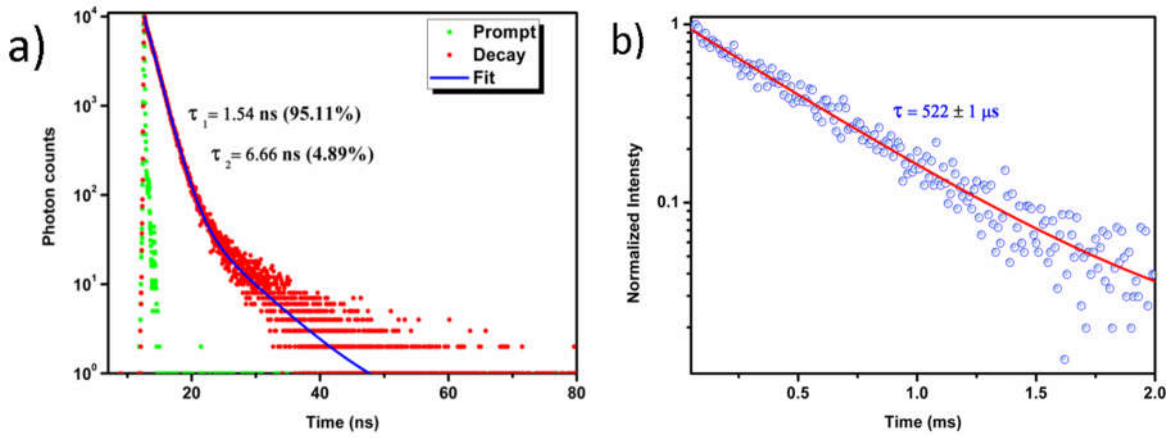

Figure 2.9. a) Life time decay profile for complex $Gd(hfpyr)_3(H_2O)$ **5** in THF solution (c = 1 x 10^{-5} M) monitored at approximately 514 nm (λ_{exc} = 375 nm) at 298 K. b) Life time decay profile for complex $Gd(hfpyr)_3(H_2O)$ **5** monitored at approximately 637 nm (λ_{exc} = 375 nm) at 77 K.

The excitation and emission profiles for the Nd^{3+} complexes (**1** and **2**) in the solid state at room temperature are depicted in figure 2.10. The excitation spectra of these complexes monitored around the intense $^4F_{3/2} \rightarrow {}^4I_{11/2}$ transition

(1068 nm) of the Nd^{3+} ion consist of a broad band in the region 250-500 nm (λ_{exc} = 400 nm) and several weak intra-configurational f-f transitions. The broad band is due to the excitation of the organic chromophores (Hhfpyr and bath) and the weak intra-configurational f-f transitions originating from the ground state of the Nd^{3+} ion. The f-f transitions could be assigned to $^4I_{9/2} \rightarrow {}^2K_{15/2}$, $^4G_{9/2}$, $^2(D,P)_{3/2}$,$^4G_{11/2}$ (509 nm), $^4I_{9/2} \rightarrow {}^4G_{9/2}$, $^4G_{7/2}$, $^2K_{13/2}$ (528 nm), and $^4I_{9/2} \rightarrow {}^4G_{5/2}$, $^2G_{7/2}$ (584 nm).[8g] However, these f-f transitions are weaker than the absorption of the organic ligands, which proves that the luminescence sensitization *via* excitation of the pyrene-based polyfluorinated-*β*-diketonate ligand is efficient. Moreover, the excitation spectra of these complexes show a good overlap with ligand-centred *π*-*π** absorption band of the complex which reflects that energy transfer takes place from ligands to Nd^{3+} ion (antenna effect).

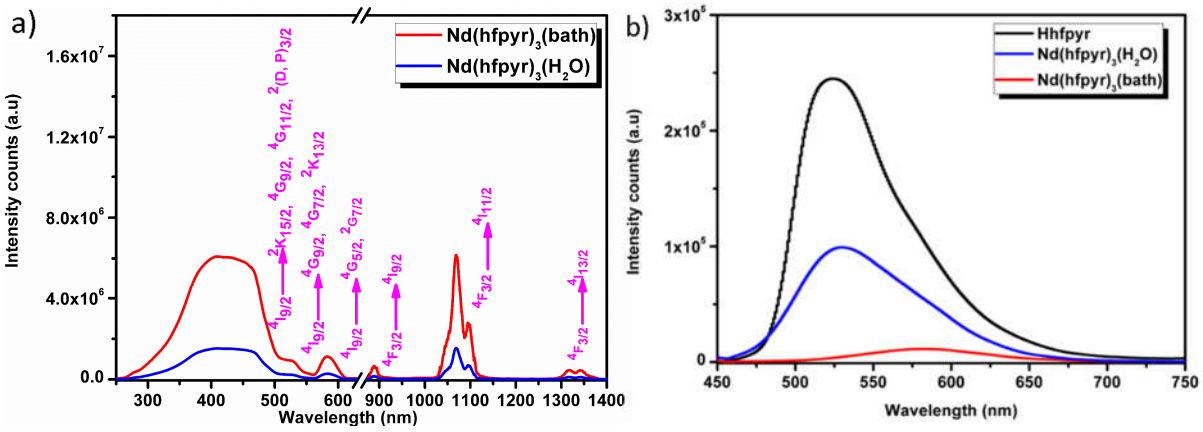

Figure 2.10. a) Room temperature excitation and emission spectra of complexes **1** and **2** in the solid-state. b) Emission spectra for the free ligand Hhfpyr, **1** and **2** in the visible range (λ_{exc} = 400 nm) at 298 K.

Under the ligand excitation (λ_{exc} = 400 nm), the emission spectra of the Nd^{3+} complexes (**1** and **2**) exhibit characteristic sharp bands of the Nd^{3+} ion in the range 850-1400 nm spectral range (Figure 2.10). The emission spectra essentially display three emission peaks that are assigned to $^4F_{3/2}\rightarrow{}^4I_{9/2}$ (891 nm), $^4F_{3/2}\rightarrow{}^4I_{11/2}$ (1068 nm) and $^4F_{3/2}\rightarrow{}^4I_{13/2}$ (1331 nm).[31] It is interesting to note that some crystal field fine structure can be observed from the emission profiles of these complexes, which illustrates that the Nd^{3+} ion occupies well-defined transitions, the intensity of the $^4F_{3/2}\rightarrow{}^4I_{11/2}$ transition is strongest, which has potential application in laser systems.[1a] On the other hand, the longer emission wavelength line of Nd^{3+} ($^4F_{3/2}\rightarrow{}^4I_{13/2}$) at 1331 nm may find applications in the development of new optical amplification materials for telecommunications.[1a] Further, a moderate residual ligand emission has been observed in Nd^{3+} binary complex (Figure 2.10). On the other hand, negligible residual ligand emission can be noted from ternary Nd^{3+} compound. The results demonstrated that the displacement of a water molecule in the coordination sphere of the Nd^{3+} in $Nd(hfpyr)_3(H_2O)$ by an ancillary ligand, 4,7- diphenyl-1,10-phenanthroline remarkably enhances (4-fold) the emission intensity of the transition $^4F_{3/2}\rightarrow{}^4I_{11/2}$.

The solid-state room temperature (298 K) excitation spectra of Yb^{3+} complexes (**3** and **4**) obtained by monitoring the characteristic emission of the Yb^{3+} ion at 979 nm are given in figure 2.11. The excitation profiles are dominated

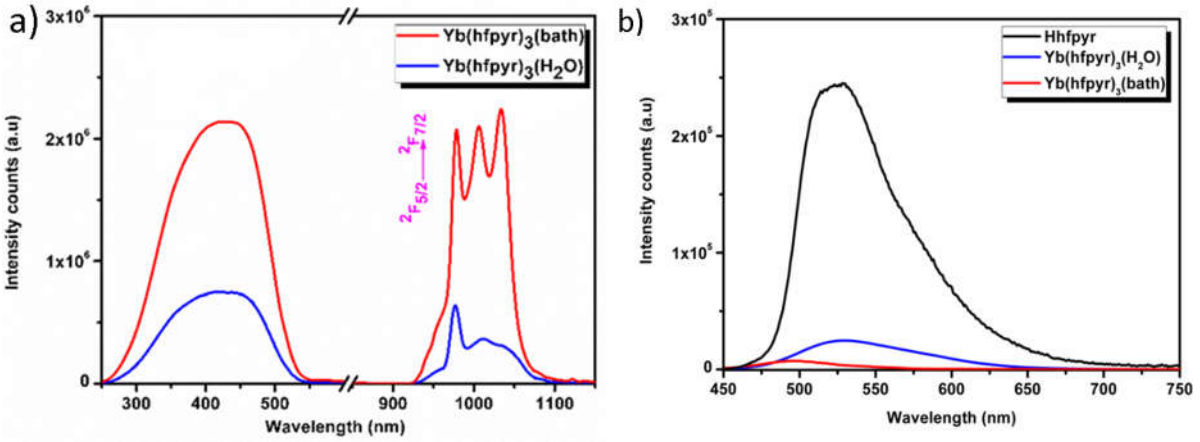

Figure 2.11. a) Room temperature excitation and emission spectra of complexes **3** and **4** in the solid state. b) Emission spectra for the free ligand Hhfpyr, **3** and **4** in the visible range (λ_{exc} = 400 nm) at 298 K.

by a broad band ranging from 250-550 nm for both the binary and ternary complexes. This broad band can be accredited to the absorption of the organic chromophores (Hhfpyr and bath) employed for the synthesis of the Yb^{3+} ion complexes. The emission spectra of the Yb^{3+} complexes derived from pyrene-based β-diketonate ligand (**3** and **4**), upon ligand-mediated excitation at 400 nm, clearly shows the characteristic emission bands for Yb^{3+} ion at 979 nm, which are assigned to $^2F_{5/2} \rightarrow {}^2F_{7/2}$ transition.[31d, 31e] Further, it can be noted that the primary emission band of Yb^{3+} ion has been split into an envelope of bands arising at the lower energy side (1006 nm and 1033 nm). These spectral features can be attributed to the splitting of the emitting levels as a consequence of ligand field effects.[32] The emission intensity at 979 nm of Yb^{3+} ternary complex (**4**) has been significantly enhanced (about three fold) as compared to Yb^{3+} binary

complex (**2**). Accordingly, negligible residual ligand emission has been noted in Yb^{3+} ternary complex as compared to binary counterpart (Figure 2.11).

Thus, the Yb^{3+} ion emission in the NIR region is important because in these regions biological tissues and fluids are relatively transparent, and the development of new Yb^{3+} ion complexes may find as bioprobes in fluoroimmunoassay and in vivo applications.[1a, 33]

The excited state $^4F_{3/2}$ (Nd^{3+}) and $^2F_{5/2}$ (Yb^{3+}) lifetime values (τ_{obs}) of the Ln^{3+} complexes **1-4** were determined at ambient temperature (298 K), by monitoring within the intense lines of the $^4F_{3/2} \rightarrow {}^4I_{11/2}$ and $^2F_{5/2} \rightarrow {}^2F_{7/2}$ transitions, respectively (Figures 2.12 and 2.13), and the pertinent values are given in Table 2.3. The observed luminescent decay profiles correspond to mono-exponential functions, highlighting the presence of single emissive Ln^{3+} center. The shorter lifetime values noted in the case of binary lanthanide complexes (**1** and **3**) may be due to the dominant non-radiative decay channels associated with the vibronic coupling due to the presence of solvent molecules in the coordination sphere of these respective complexes.[17b] On the other hand, a two-fold enhancement in the excited state lifetime values have been observed in the case of ternary Ln^{3+} complexes as compared to corresponding binary complexes.

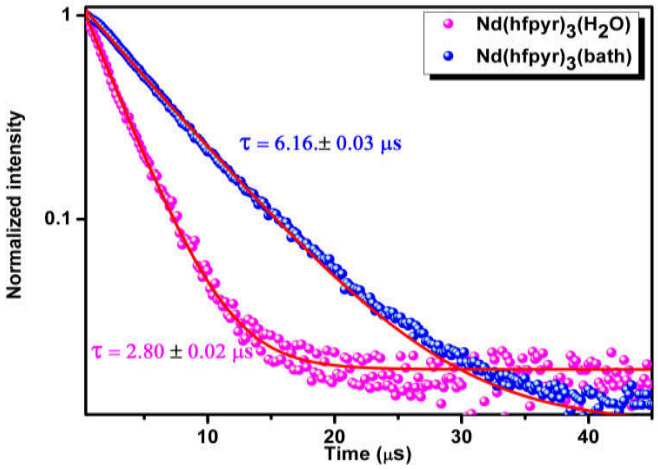

Figure 2.12. Experimental luminescence decay profiles for complexes **1** and **2** in solid state monitored at approximately 1069 nm and excited 400 nm.

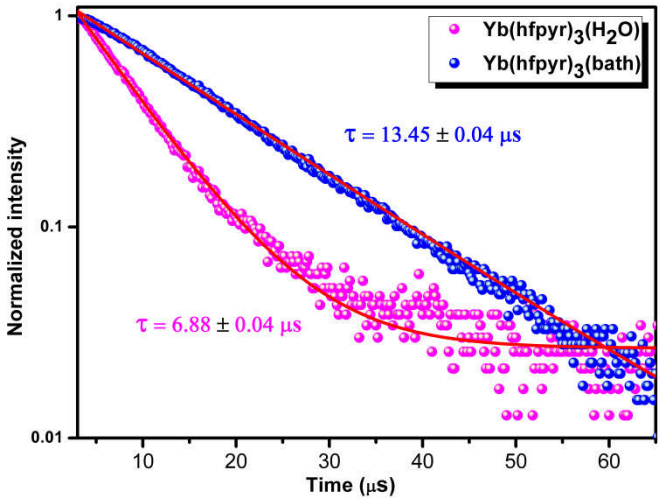

Figure 2.13. Experimental luminescence decay profiles for complexes **3** and **4** in solid state monitored at approximately 1069 nm and excited 400 nm.

The overall quantum yields ($\Phi_{overall}$) of the developed NIR emitting Nd^{3+} and Yb^{3+} complexes (**1-4**) have been calculated intending to understand more about the photophysical properties. Therefore, it is appropriate to analyse the NIR emission behaviour of the Ln^{3+} complexes in terms of overall quantum yields

($\Phi_{overall}$). As it is well-known that, the overall quantum yield is generally regulated by the sensitization efficiency of the antenna molecule (Φ_{sens}) as well as the intrinsic luminescent quantum yield (Φ_{Ln}) of the Ln^{3+} ion [$\Phi_{overall} = \Phi_{sens}$ Φ_{Ln}]. The Φ_{Ln} of the complexes was determined by using the following eq. 1.[2b, 34]

$$\Phi_{Ln} = (\tau_{obs} / \tau_{rad}) \quad \text{eq.1}$$

Where τ_{obs} is the observed lifetime and τ_{rad} is 'natural' lifetime of Ln^{3+}. Table 2.3 summarizes the various photophysical properties of the Ln^{3+} complexes, such as $\Phi_{overall,}$ $\Phi_{Ln,}$ and radiative (A_{RAD}) and non-radiative (A_{NR}) decay rates. The solid-state quantum yields ($\Phi_{overall}$) noted for the Nd^{3+} and Yb^{3+} ternary complexes (1.07 ± 0.05 % for **2** and 3.08 ± 0.15 % for **4**) are found to be significantly higher (2-fold) than that of the corresponding binary counterparts (0.45 ± 0.02 % for **1** and 1.69 ± 0.08 % for **3**). This can be explained on the basis of displacement of potentially quenching O-H oscillators present in the coordination sphere of the metal ions by the ancillary ligand, 4,7-diphenyl-1,10-phenanthroline. Similar trends have been noted earlier.[4a, 6b] These results are also in good agreement with the decrease of non-radiative decay rates in the corresponding ternary Ln^{3+} complexes. The luminescent lifetimes and quantum yields values observed in the present study are in line with, or moderately higher than the recently published results on NIR luminescent lanthanide β-diketonate complexes.[8g, 8h, 10, 35]

Table 2.3. Luminescence Parameters radiative (A_{RAD}, s^{-1}) and non-radiative (A_{NR}, s^{-1}) rates, lifetime (τ_{obs}, μs), intrinsic quantum yield (Φ_{Ln}, %) and overall quantum yield ($\Phi_{overall}$, %) for complexes **1-4.**

Complex	A_{RAD} (s^{-1})	A_{NR} (s^{-1})	τ_{obs} (μs)	Φ_{Ln} (%)	$\Phi_{overall}$ (%)
$Nd(hfpyr)_3(H_2O)$ **1**	1607	3.65×10^5	2.80±0.02	1.04	0.45
$Nd(hfpyr)_3$(bath) **2**	1737	1.61×10^5	6.16±0.03	2.28	1.07
$Yb(hfpyr)_3(H_2O)$ **3**	2456	1.43×10^5	6.88±0.04	0.34	1.69
$Yb(hfpyr)_3$(bath) **4**	2389	7.20×10^4	13.45±0.04	0.67	3.08

To calculate the efficiency of the sensitization process, it is necessary to know the radiative lifetime values (τ_{rad}), which are not easy to determine experimentally. It is clear from the literature that the τ_{rad} values for Nd^{3+} and Yb^{3+} vary widely and depend heavily on the solvent or the physical state of the sample. Taking into account 0.27 ms for Nd^{3+} as and a value of 2.0 ms commonly assumed for Yb^{3+}, the data for sensitization $\Phi_{sens} = 0.45$ for Nd^{3+}, while a value >1 is noted for Yb^{3+}, meaning that the actual radiative lifetime is larger than 2 ms in our system. Similar kind of results has also been reported by Bünzli and co-workers.[7c]

2.4.5. Synthesis, characterization and photophysical properties of PMMA doped hybrid materials

In view of the low cost, low optical absorbance and good mechanical properties,[10] in the present study PMMA has been blended with the developed NIR emitting Yb^{3+} ternary complex (**4**) in proportions of 1, 3, 5, 7 and 9 % (w/w) and

corresponding polymeric films [PMMA@ 1% Yb, PMMA@ 3% Yb, PMMA@ 5%, Yb PMMA@ 7% Yb and PMMA@ 9% Yb] were isolated, characterized and evaluated their photophysical properties. The FT-IR spectra of precursor metal complex $Yb(hfpyr)_3(bath)$ **4** and the corresponding embedded Yb^{3+} complex in PMMA film (PMMA@7% Yb) were recorded in the 400–4000 cm^{-1} region and the results are shown in figure 2.14. The characteristic absorptions of the $–O–CH_2$ asymmetric stretch, the $–CH_3$ asymmetric stretch, the –C=O stretch, the $–O–CH_3$ deformation and the –C–O–C– symmetric stretch of pure PMMA was observed at 3000-3002, 2947-2950, 1730-1732, 1380-1385 and 989-993 cm^{-1} region, respectively.[36] On the other hand, the weakening of vibrations of the ternary complex along with PMMA absorptions noted in the hybrid film indicate that the metal complex is embedded into PMMA matrix.

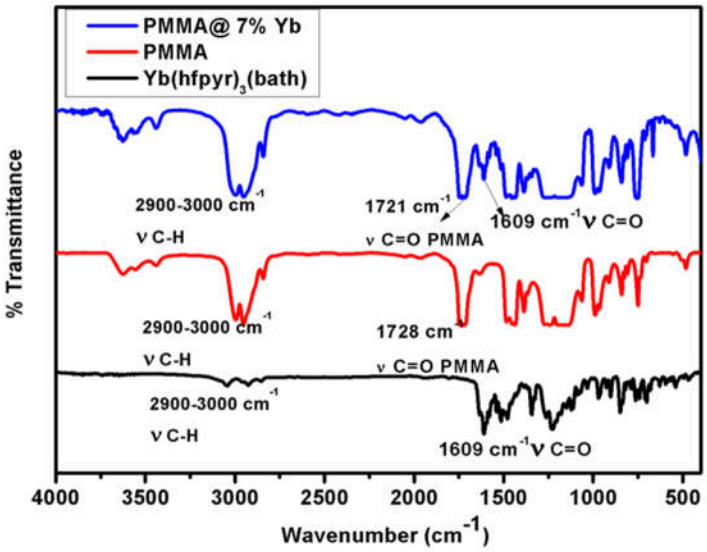

Figure 2.14. FT-IR Spectra of the complex $Yb(hfpyr)_3(bath)$, PMMA and PMMA film doped with complex **4.**

The thermal stabilities of the precursor complex Yb(hfpyr)$_3$(bath) **4** as well as the typical metal complex embedded into polymer film (PMMA@ 7% Yb) have been assessed by TGA analyses and the results are depicted in figures 2.3 and 2.15 respectively. As can be clearly seen from the results that the thermal stability of the parent Yb^{3+} ternary complex (366°C decomposition temperature) was significantly improved after doping into the PMMA matrix (416 °C decomposition temperature). The TGA curve of PMMA@7%Yb film indicates that the decomposition starts at 290 °C. The polymer has been completely departed from the hybrid material when the temperature reaches at 427 °C.

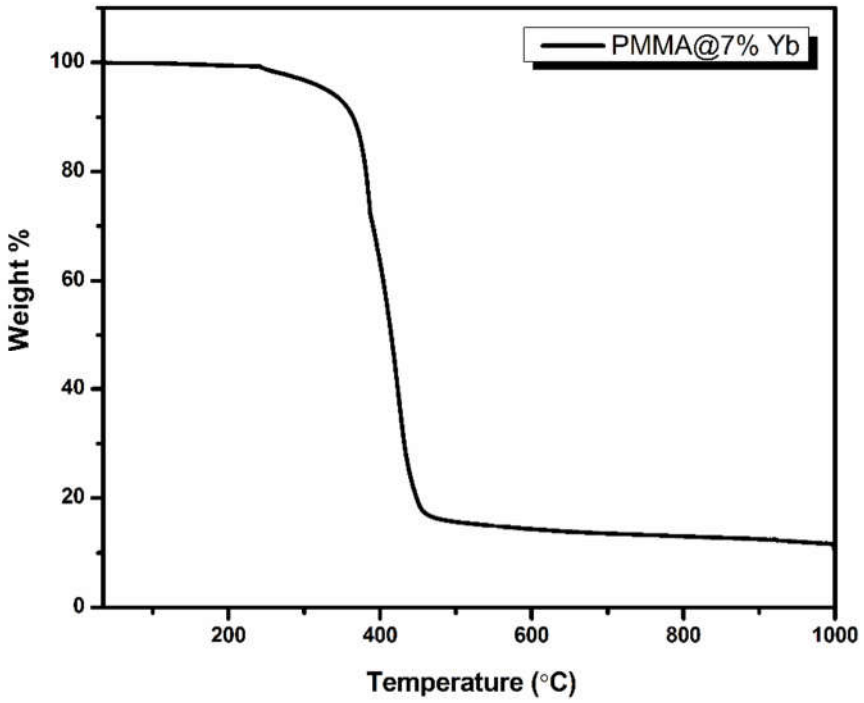

Figure 2.15. Thermogravimetric curve for the PMMA film doped with Yb(hfpyr)$_3$(bath) **4.**

The solid-state excitation and the emission profiles of a series of PMMA embedded Yb ternary metal complex [PMMA@ 1% Yb, PMMA@ 3% Yb,

PMMA@ 5%, Yb PMMA@ 7% Yb and PMMA@ 9% Yb] polymeric films recorded at room temperature (298 K) are displayed in figure 2.16. A broad band noted in the wavelength region 250–500 nm of the excitation spectra can be attributed to the absorptions of the ligand systems. The emission spectra (λ_{exc} = 400 nm) clearly illustrates the presence of characteristic emission band of Yb^{3+} ion at 979 nm, which can be assigned to $^2F_{5/2} \rightarrow {}^2F_{7/2}$ transition.[6c,34] Further, the luminescence intensity of the Yb^{3+} ion at 979 nm increases initially with the increase of dopant metal complex concentration in the polymer film to a maximum (PMMA@ 7% Yb) and thereafter decreases at higher concentration (PMMA@ 9% Yb). The energy transfer between the Yb^{3+} ions themselves is a non-radiative process, which accounts for the observed decrease in the Yb^{3+} emission, especially at high dopant metal complex concentration. It is noteworthy to mention that the emission intensity of the 7% Yb complex doped PMMA film at 979 nm has been markedly improved (about 1.4 fold) as compared to the precursor ternary Yb^{3+} complex. As a consequence, the overall quantum yields of the hybrid materials (3.40-3.62%) have also been moderately enhanced (Table 2.4). In conclusion, the above results disclose that Yb^{3+} ternary complex retains its original photophysical properties even after doping into the PMMA matrix. Further, the thermal stability and film forming properties have been significantly improved as compared to precursor complex.

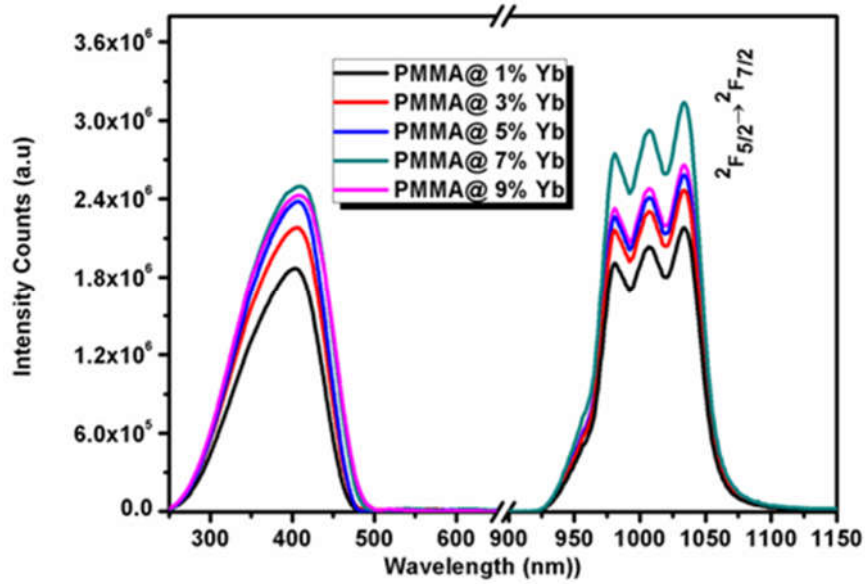

Figure 2.16. Excitation and emission spectra of PMMA films doped with 1, 3, 5, 7 and 9% (w/w) of $Yb(hfpyr)_3(bath)$. The data were recorded at 298 K.

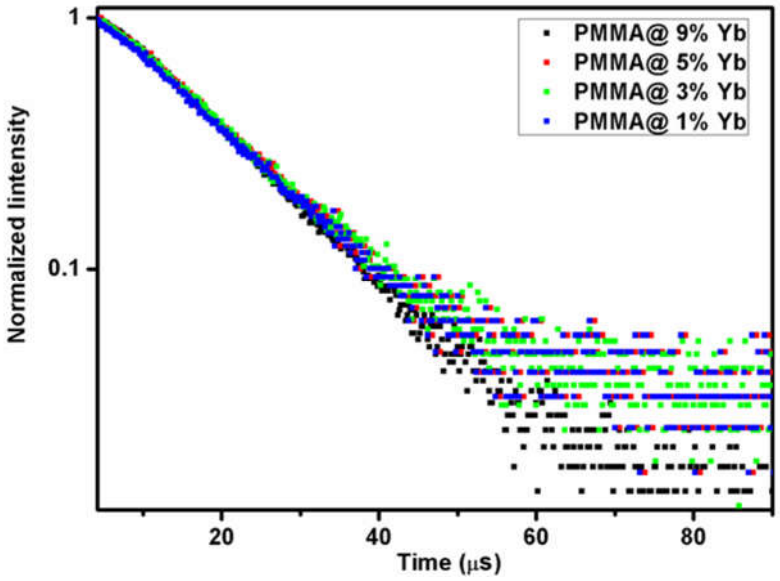

Figure 2.17. Life time decay profiles for $Yb(hfpyr)_3(bath)$ **4**, doped into PMMA polymer where emission monitored around 979 nm. The straight lines are the best fits considering single-exponential behaviour.

Table 2.4. Luminescence Parameters for complex **4** and PMMA films doped with various amounts of the complex **4**, at 298 K

Complex/ Film	A_{RAD} (s^{-1})	A_{NR} (s^{-1})	τ_{obs} (μs)	Φ_{Ln} (%)	$\Phi_{Overall}$ (%)
$Yb(hfpyr)_3(bath)$	2289	7.20×10^4	13.45±0.02	0.743	3.08
PMMA@ 1% Yb	2259	6.50×10^4	14.87±0.02	0.738	3.36
PMMA@ 3% Yb	2317	6.54×10^4	14.76±0.02	0.728	3.42
PMMA@ 5% Yb	2443	6.61×10^4	14.57±0.02	0.744	3.56
PMMA@ 7% Yb	2432	6.47×10^4	14.88±0.02	0.741	3.62
PMMA@ 9% Yb	2388	6.50×10^4	14.82±0.02	0.743	3.54

The luminescent decay profiles of the polymeric hybrid films were obtained by monitoring the emission at 979 nm corresponding to $^2F_{5/2} \rightarrow {}^2F_{7/2}$ transition and excited at 400 nm and the results are given in figure 2.17. The lifetime values of the isolated hybrid films are listed in Table 2.4. All the τ values of the hybrid polymer films (14-15 μs) are found to be moderately higher than the precursor Yb^{3+} ternary complex **4** (13.45 μs), thus highlighting the radiative process are operative in the doped films due to the absence of multiphonon relaxation by coupling with the –OH oscillators.[9] Furthermore, the excited state lifetime values are not influenced by the doping process into the PMMA matrix.

2.5. Conclusions

- In summary, a novel β-diketonate ligand, 4,4,5,5,6,6,6-heptafluoro-3-hydroxy-1-(pyren-1-yl)hex-2-en-1-one has been successfully synthesized by incorporating highly conjugated pyrene moiety as a sensitizing unit and polyfluorinated alkyl group with low energy C-F oscillators, with an aim to develop near-infrared (NIR) emitting lanthanide complexes.
- The designed β-diketonate ligand has a triplet energy level of 16,207 cm^{-1}, which lies well above the energy of the main emitting level of Nd^{3+} ($^4F_{3/2}$ =11,257 cm^{-1}) or Yb^{3+} ($^2F_{5/2}$ = 10,400 cm^{-1}), implying that it can act as an efficient antenna molecule for the sensitization of NIR emitting lanthanide ions.
- The developed NIR emitting lanthanide complexes possess markedly high molar absorption coefficient values (about ε = 49,000 to 50,000 $Lmol^{-1}cm^{-1}$), indicating the adequate light-harvesting capacity of these compounds.
- The luminescent lifetimes and quantum yields values observed in the present study are found be significantly higher than many of the existing NIR emitting lanthanide β-diketonate complexes.
- Thus, the currently derived new Nd^{3+} and Yb^{3+} compounds may find potential applications as bioprobes in fluoroimmunoassay and new optical amplification materials for telecommunications.
- The thermal stability of the Yb^{3+} ternary complex incorporated PMMA film has been greatly enhanced as compared to parent compound, apart from exhibiting good film forming capacity.

2.6. References

1. (a) S. Comby and J.-C. G. Bünzli, in *Handbook on the Physics and Chemistry of Rare Earths*, eds. J.-C. G. B. Karl A. Gschneidner and K. P. Vitalij, Elsevier, 2007, vol. Volume 37, pp. 217-470; (b) J.-C. G. Bünzli and S. V. Eliseeva, *Chem. Sci.*, 2013, **4**, 1939; (c) S. V. Eliseeva and J.-C. G. Bünzli, *Chem. Soc. Rev.*, 2010, **39**, 189-227; (d) A. J. Amoroso and S. J. A. Pope, *Chem. Soc. Rev.*, 2015, **44**, 4723-4742; (e) J. C. G. Bünzli and S. V. Eliseeva, *J. Rare Earths*, 2010, **28**, 824-842; (f) L. Prodi, E. Rampazzo, F. Rastrelli, A. Speghini and N. Zaccheroni, *Chem. Soc. Rev.*, 2015, **44**, 4922-4952.

2. (a) P. A. Tanner and C.-K. Duan, *Coord. Chem. Rev.*, 2010, **254**, 3026-3029; (b) J. Feng and H. Zhang, *Chem. Soc. Rev.*, 2013, **42**, 387-410; (c) L. Armelao, S. Quici, F. Barigelletti, G. Accorsi, G. Bottaro, M. Cavazzini and E. Tondello, *Coord. Chem. Rev.*, 2010, **254**, 487-505; (d) J.-C. G. Bünzli and C. Piguet, *Chem. Soc. Rev.*, 2005, **34**, 1048-1077.

3. (a) X. Wang, H. Chang, J. Xie, B. Zhao, B. Liu, S. Xu, W. Pei, N. Ren, L. Huang and W. Huang, *Coord. Chem. Rev.*, 2014, **273–274**, 201-212; (b) J.-C. G. Bünzli, *Acc. Chem. Res.*, 2006, **39**, 53-61; (c) M. L. P. Reddy and S. Sivakumar, *Dalton Trans.*, 2013, **42**, 2663-2678; (d) E. G. Moore, A. P. S. Samuel and K. N. Raymond, *Acc. Chem. Res.*, 2009, **42**, 542-552.

4. (a) A. D. Bettencourt-dias, P. S. Barber and S. Viswanathan, *Coord. Chem. Rev.*, 2014, **273-274**, 165-200; (b) D. V. Kazakov and F. E. Safarov, *Photochem. Photobiol. Sci.*, 2014, **13**, 1646-1649; (c) M. L. P. Reddy, V. Divya and R. Pavithran, *Dalton Trans.*, 2013, **42**, 15249-15262; (d) Y. Ma and Y. Wang, *Coord. Chem. Rev.*, 2010, **254**, 972-990.

5. (a) K. Binnemans, in *Handbook on the Physics and Chemistry of Rare Earths*, eds. J.-C. G. B. Karl A. Gschneidner and K. P. Vitalij, Elsevier, 2005, vol. Volume 35, pp. 107-272; (b) D. B. A. Raj, B. Francis, M. L. P. Reddy, R. R. Butorac, V. M. Lynch and

A. H. Cowley, *Inorg. Chem.*, 2010, **49**, 9055-9063; (c) T. M. George, M. J. Sajan, N. Gopakumar and M. L. P. Reddy, *J. Photochem. Photobiol., A*, 2016, **317**, 88-99; (d) J. Sun, B. Song, Z. Ye and J. Yuan, *Inorg. Chem.*, 2015, **54**, 11660-11668; (e) T. V. Usha Gangan and M. L. P. Reddy, *Dalton Trans.*, 2015, **44**, 15924-15937; (f) F. Cao, Z. Yuan, J. Liu and J. Ling, *RSC Adv.*, 2015, **5**, 102535-102541; (g) P. N. Remya, S. Biju, M. L. Reddy, A. H. Cowley and M. Findlater, *Inorg. Chem.*, 2008, **47**, 7396-7404; (h) S. Biju, D. B. A. Raj, M. L. P. Reddy and B. M. Kariuki, *Inorg. Chem.*, 2006, **45**, 10651-10660; (i) B. Francis, C. Heering, R. O. Freire, M. L. P. Reddy and C. Janiak, *RSC Adv.*, 2015, **5**, 90720-90730; (j) K. Miyata, Y. Konno, T. Nakanishi, A. Kobayashi, M. Kato, K. Fushimi and Y. Hasegawa, *Angew. Chem. Int. Ed.* , 2013, **52**, 6413-6416; (k) J. Yuasa, T. Ohno, H. Tsumatori, R. Shiba, H. Kamikubo, M. Kataoka, Y. Hasegawa and T. Kawai, *Chem. Commun.*, 2013, **49**, 4604-4606; (l) Y. Hirai, T. Nakanishi, Y. Kitagawa, K. Fushimi, T. Seki, H. Ito, H. Fueno, K. Tanaka, T. Satoh and Y. Hasegawa, *Inorg. Chem.*, 2015, **54**, 4364-4370; (m) V. Divya, R. O. Freire and M. L. Reddy, *Dalton Trans.*, 2011, **40**, 3257-3268; (n) V. Divya, V. Sankar, K. G. Raghu and M. L. P. Reddy, *Dalton Trans.*, 2013, **42**, 12317-12323.

6. (a) C. Yu, Z. Zhang, L. Liu, H. Li, Y. He, X. Lu, W.-K. Wong and R. A. Jones, *New J. Chem.*, 2015, **39**, 3698-3707; (b) Y. Hou, J. Shi, W. Chu and Z. Sun, *Eur. J. Inorg. Chem.*, 2013, **7**, 3063-3069; (c) Z. Zhang, C. Yu, L. Liu, H. Li, Y. He, X. Lü, W. K. Wong and R. A. Jones, *J. Photochem. Photobiol., A*, 2016, **314**, 104-113.

7. (a) S. Comby, D. Imbert, C. Vandevyver and J. C. Bünzli, *Chemistry*, 2007, **13**, 936-944; (b) N. M. Shavaleev, R. Scopelliti, F. Gumy and J. C. Bünzli, *Inorg. Chem.*, 2008, **47**, 9055-9068; (c) S. Comby, D. Imbert, A. S. Chauvin and J. C. G. Bünzli, *Inorg. Chem.*, 2006, **45**, 732-743; (d) E. R. Trivedi, S. V. Eliseeva, J. Jankolovits, M. M. Olmstead, S. Petoud and V. L. Pecoraro, *J. Am. Chem. Soc.*, 2014, **136**, 1526-1534; (e) A. Sanguineti, A. Monguzzi, G. Vaccaro, F. Meinardi, E. Ronchi, M. Moret, U. Cosentino, G. Moro, R. Simonutti, M. Mauri, R. Tubino and L. Beverina, *Phys. Chem. Chem. Phys.*, 2012, **14**, 6452; (f) S. Dang, J. B. Yu, X. F. Wang, Z. Y. Guo, L. N. Sun, R. P. Deng, J. Feng, W. Q. Fan and H. J. Zhang, *J. Photochem. Photobiol., A*, 2010, **214**, 152-160; (g) X. S. Ke, B. Y. Yang, X. Cheng, S. L. F. Chan and J. L. Zhang,

Chem. Eur. J., 2014, **20**, 4324-4333; (h) P. B. Glover, A. P. Bassett, P. Nockemann, B. M. Kariuki, R. Van Deun and Z. Pikramenou, *Chem. Eur. J.*, 2007, **13**, 6308-6320.

8. (a) A. W. Woodward, A. Frazer, A. R. Morales, J. Yu, A. F. Moore, A. D. Campiglia, E. V. Jucov, T. V Timofeeva and K. D. Belfield, *Dalton Trans.*, 2014, **43**, 16626-16639; (b) P. Martín-Ramos, P. S. Pereira da Silva, V. Lavín, I. R. Martín, F. Lahoz, P. Chamorro-Posada, M. Ramos Silva and J. Martín-Gil, *Dalton Trans.*, 2013, **42**, 13516-13526; (c) L. Yang, Z. Gong, D. Nie, B. Lou, Z. Bian, M. Guan, C. Huang, H. J. Lee and W. P. Baik, *New J. Chem.*, 2006, **30**, 791-796; (d) A. Monguzzi, R. Tubino, F. Meinardi, A. O. Biroli, M. Pizzotti, F. Demartin, F. Quochi, F. Cordella and M. A. Loi, *Chem. Mater.*, 2009, **21**, 128-135; (e) X. Guo, H. Guo, L. Fu, L. D. Carlos, R. A. S. Ferreira, L. Sun, R. Deng and H. Zhang, *J. Phys. Chem. C*, 2009, **113**, 12538-12545; (f) T. S. Kang, B. S. Harrison, M. Bouguettaya, T. J. Foley, J. M. Boncella, K. S. Schanze and J. R. Reynolds, *Adv. Funct. Mater.*, 2003, **13**, 205-210; (g) Z. Ahmed and K. Iftikhar, *J. Phys. Chem. A*, 2013, **117**, 11183-11201; (h) N. M. Shavaleev, R. Scopelliti, F. Gumy and J. C. G. Bünzli, *Eur. J. Inorg. Chem.*, 2008, **9**, 1523-1529; (i) B. L. Reid, S. Stagni, J. M. Malicka, M. Cocchi, A. N. Sobolev, B. W. Skelton, E. G. Moore, G. S. Hanan, M. I. Ogden and M. Massi, *Chem. Eur. J.*, 2015, **21**, 18354-18363.

9. (a) G. M. Davies, R. J. Aarons, G. R. Motson, J. C. Jeffery, H. Adams, S. Faulkner and M. D. Ward, *Dalton Trans.*, 2004, **8**, 1136-1144; (b) J. Feng, J. B. Yu, S. Y. Song, L. N. Sun, W. Q. Fan, X. M. Guo, S. Dang and H. J. Zhang, *Dalton Trans.*, 2009, **13**, 2406-2414; (c) N. M. Shavaleev, S. J. A. Pope, Z. R. Bell, S. Faulkner and M. D. Ward, *Dalton Trans.*, 2003, **5**, 808-814.

10. S. Biju, Y. K. Eom, J.-C. G. Bünzli and H. K. Kim, *J. Mater. Chem. C*, 2013, **1**, 6935-6944.

11. B. Li, H. Li, P. Chen, W. Sun, C. Wang, T. Gao and P. Yan, *Phys. Chem. Chem. Phys.*, 2015, **17**, 30510-30517.

12. (a) A. J. Howarth, M. B. Majewski and M. O. Wolf, *Coord. Chem. Rev.*, 2015, **282-283**, 139-149; (b) A. G. Crawford, A. D. Dwyer, Z. Q. Liu, A. Steffen, A. Beeby, L. O. Palsson, D. J. Tozer and T. B. Marder, *J. Am. Chem. Soc.*, 2011, **133**, 13349-13362.

13. (a) R. Haldar, K. Prasad, P. K. Samanta, S. Pati and T. K. Maji, *Cryst. Growth Des.*, 2016, **16**, 82-91; (b) F. Liu, C. Tang, Q. Q. Chen, F. F. Shi, H. B. Wu, L. H. Xie, B. Peng, W. Wei, Y. Cao and W. Huang, *J. Phys. Chem. C*, 2009, **113**, 4641-4647; (c) C. Tang, F. Liu, Y.-J. Xia, L.-H. Xie, A. Wei, S.-B. Li, Q.-L. Fan and W. Huang, *J. Mater. Chem.*, 2006, **16**, 4074.

14. J. E. Sohna Sohna and F. Fages, *Tetrahedron Lett.*, 1997, **38**, 1381-1384.

15. S. Faulkner, M. C. Carrie, S. J. A. Pope, J. Squire, A. Beeby and P. G. Sammes, *Dalton Trans.*, 2004, **9**, 1405-1409.

16. S. J. A. Pope, *Polyhedron*, 2007, **26**, 4818-4824.

17. (a) Y. Hasegawa, T. Ohkubo, K. Sogabe, Y. Kawamura, Y. Wada, N. Nakashima and S. Yanagida, *Angew. Chem. Int. Ed.* , 2000, **39**, 357-360; (b) A. Døssing, *Eur. J. Inorg. Chem.*, 2005, **2005**, 1425-1434; (c) A. Beeby, I. M. Clarkson, R. S. Dickins, S. Faulkner, D. Parker, L. Royle, A. S. de Sousa, J. A. Gareth Williams and M. Woods, *J. Chem. Soc., Perkin Trans. 2*, 1999, **3**, 493-504.

18. (a) J. Li, H. Li, P. Yan, P. Chen, G. Hou and G. Li, *Inorg. Chem.*, 2012, **51**, 5050-5057; (b) D. B. Ambili Raj, S. Biju and M. L. Reddy, *Dalton Trans.*, 2009, **36**, 7519-7528.

19. (a) V. Divya and M. L. P. Reddy, *J. Mater. Chem. C*, 2013, **1**, 160-170; (b) D. B. A. Raj, S. Biju and M. L. P. Reddy, *Inorg. Chem.*, 2008, **47**, 8091-8100.

20. (a) W. Fan, J. Feng, S. Song, Y. Lei, L. Zhou, G. Zheng, S. Dang, S. Wang and H. Zhang, *Nanoscale*, 2010, **2**, 2096-2103; (b) Z. Zhang, W. Feng, P. Su, X. Lü, J. Song, D. Fan, W. K. Wong, R. A. Jones and C. Su, *Inorg. Chem.*, 2014, **53**, 5950-5960.

21. W. Li, P. Yan, G. Hou, H. Li and G. Li, *RSC Adv.*, 2013, **3**, 18173-18180.

22. (a) K. S. Bejoymohandas, A. Kumar, S. Sreenadh, E. Varathan, S. Varughese, V. Subramanian and M. L. P. Reddy, *Inorg. Chem.*, 2016, **55**, 3448-3461; (b) K. S. Bejoymohandas, A. Kumar, S. Varughese, E. Varathan, V. Subramanian and M. L. P. Reddy, *J. Mater. Chem. C*, 2015, **3**, 7405-7420.

23. S. V. Eliseeva, D. N. Pleshkov, K. A. Lyssenko, L. S. Lepnev, J. C. Bünzli and N. P. Kuzmina, *Inorg. Chem.*, 2010, **49**, 9300-9311.

24. J. A. Cunningham, D. E. Sands, W. F. Wagner and M. F. Richardson, *Inorg. Chem.*, 1969, **8**, 22-28.

25. S. Biju, M. L. P. Reddy, A. H. Cowley and K. V. Vasudevan, *Cryst. Growth Des.*, 2009, **9**, 3562-3569.

26. V. Divya, S. Biju, R. L. Varma and M. L. P. Reddy, *J. Mater. Chem.*, 2010, **20**, 5220-5227.

27. A. R. Ramya, D. Sharma, S. Natarajan and M. L. P. Reddy, *Inorg. Chem.*, 2012, **51**, 8818-8826.

28. F. J. Steemers, W. Verboom, D. N. Reinhoudt, E. B. van der Tol and J. W. Verhoeven, *J. Am. Chem. Soc.*, 1995, **117**, 9408-9414.

29. L. Yang, Z. Gong, D. Nie, B. Lou, Z. Bian, M. Guan, C. Huang, H. J. Lee and W. P. Baik, *New J. Chem.*, 2006, **30**, 791-796.

30. O. L. Malta, H. F. Brito, J. F. S. Menezes, F. R. Gonçalves e Silva, C. de Mello Donegá and S. Alves Jr, *Chem. Phys. Lett.*, 1998, **282**, 233-238.

31. (a) P. O. A. S. I. Klink, L. Grave, F. G. A. Peters, J. W. Hofstraat, F. Geurts, F. C. J. M. van Veggel, *J. Chem. Soc., Perkin Trans. 2*, 2001, DOI: 10.1039/B007704F, 363-372; (b) W.-T. W. W. P.-W. Lai, *New J. Chem.*, 2000, **24**, 943-944; (c) F. C. J. M. v. V. J. W. Stouwdam, *Nano Lett.*, 2002, **2**, 733-737; (d) L. N. Sun, J. B. Yu, G. L. Zheng, H. J. Zhang, Q. G. Meng, C. Y. Peng, L. S. Fu, F. Y. Liu and Y. N. Yu, *Eur. J. Inorg.*

Chem., 2006, **19**, 3962-3973; (e) J.-c. G. Bünzli and S. V. Eliseeva, *Springer Series on Fluorescence*, 2011, DOI: 10.1007/4243, 1-45.

32. O. L. M. F. R. G. e Silva, C. Reinhard, H.-U. Güdel, C. Piguet, J. E. Moser and J.-C. G. Bünzli, *J. Phys. Chem. A*, 2002, **106**, 1670-1677.

33. R. J. A. G. M. Davies, G. R. Motson, J. C. Jeffery, H. Adams, S. Faulkner and M. D. Ward, *Dalton Trans.*, 2004, **8**, 1136-1144.

34. (a) L. D. Carlos, R. A. S. Ferreira, V. D. Bermudez and S. J. L. Ribeiro, *Adv. Mater.*, 2009, **21**, 509-534; (b) A. de Bettencourt-Dias, *Dalton Trans.*, 2007, **22**, 2229-2241.

35. (a) L. N. Puntus, K. J. Schenk and J.-C. G. Bünzli, *Eur. J. Inorg. Chem.*, 2005, **2005**, 4739-4744; (b) Y. F. Yuan, T. Cardinaels, K. Lunstroot, K. Van Hecke, L. Van Meervelt, C. Görller-Walrand, K. Binnemans and P. Nockemann, *Inorg. Chem.*, 2007, **46**, 5302-5309.

36. P. Y. Weizuo Li, Guangfeng Hou, Hongfeng Li and Guangming Li, *Dalton Trans.*, 2013, **42**, 11537-11547.

Chapter 3

Lysosome Targetable Luminescent Bioprobe Based on a Europium β-Diketonate Complex for Cellular Imaging Applications

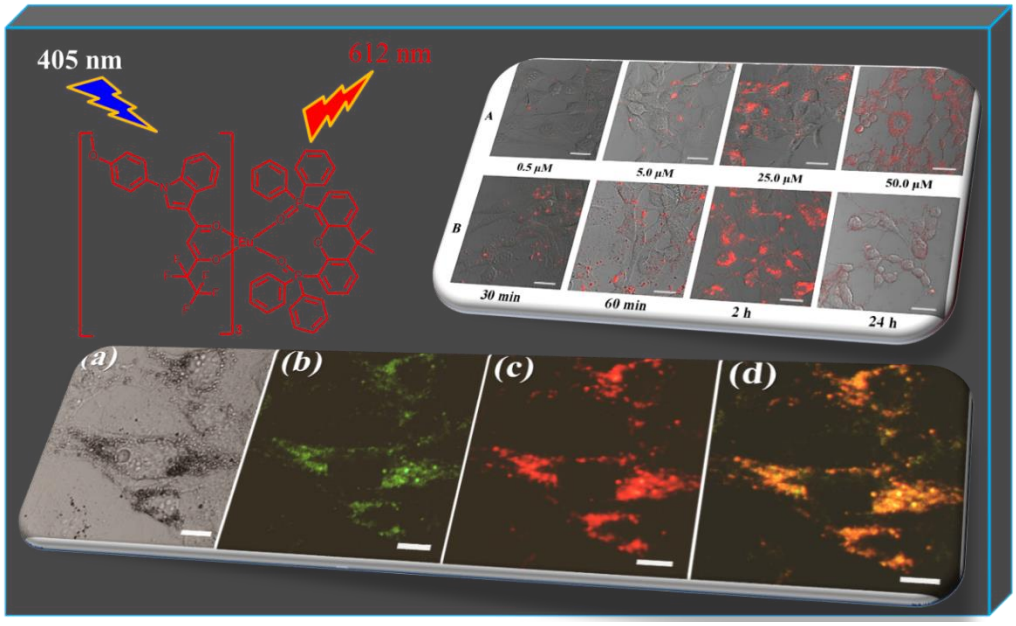

3.1. Abstract

Herein, we report a novel lysosome targetable luminescent bioprobe derived from a europium coordination compound, namely, Eu(pfphOCH$_3$IN)$_3$(DDXPO) ***4*** *[where HpfphOCH$_3$IN = 4,4,5,5,5-pentafluoro-3-hydroxy-1-(1-(4-methoxyphenyl)-1H-indol-3-yl)pent-2-en-1-one and DDXPO = 4,5-bis(diphenylphosphino)-9,9-dimethylxanthene oxide]. Notably, the newly designed europium complex exhibits significant quantum yield ($\Phi_{overall}$ = 25 ± 3%) and $^5D_0$ excited state lifetime (τ = 398 ± 3 μs) values under physiological pH (7.2) conditions when excited at 405 nm. Hence the developed europium complex has been evaluated for the live cell imaging application using mouse pre-adipocyte cell lines (3T3L1). Colocalization studies of the*

designed bio-probe with commercial Lysosome-GFP in 3T3L1 cells demonstrated the specific localization of the probe in the lysosome with a high colocalization coefficient (A = 0.83). Most importantly, the developed bioprobe exhibits good cell permeability, photostability and non-cytotoxicity.

T. M. George, Mahesh S. Krishna, and M. L. P. Reddy, *Dalton Transactions*, **2016,** 45**,** 18719-18729.

3.2. Introduction

In recent years, luminescent lanthanide bioprobes have been emerged as viable alternatives to existing organic fluorescent probes, due to their unique photophysical properties, and several distinct advantages such as less sensitive nature to photobleaching, long-lived excited state lifetimes and large Stokes' shifts upon ligand excitation.[1] The large Stokes' shifts benefit to avoid the self-absorption of ligand and reduce the background signals. The f−f transitions are formally forbidden by the spin and Laporte rule and hence feature long excited-state lifetimes in the milli to microsecond range. The long decay times offers an immense advantage for the time-gated detection of biological samples, wherein interfering short-lived autofluorescence and scattering is suppressed. Due to shielding of the 5s and 5p orbitals in lanthanides, the 4f orbitals do not directly participate in chemical bonding. Thus the emission wavelengths of lanthanides are minimally perturbed by the surrounding matrix and ligand field, resulting in sharp and line-like emission bands.[2] These properties confer luminescent Ln^{3+} complexes for time-gated or time-resolved live-cell or in vivo imaging. Such an

approach enhances signal-to-noise ratios through the elimination of interferences from scattering and short-lived autofluorescence of biological species.[3,4] Finally, the antenna effect has another advantage, while the excitation of the ligand has performed in the UV to blue spectral regions; emission is noted in the visible or NIR domains, and the pseudo-Stokes shift is large, decreasing the need for efficient filtering between the excitation and emission channels.[5] As a consequence, a large number of luminescent bioprobes have been developed for cellular imaging applications and these data are covered in pioneering review articles.[1, 3, 6] However, a major limitation of the existing lanthanide probes is that of excitation window is limited to UV region.[7] Another problem with the currently available lanthanide luminescent probes is photobleaching, especially when the sample is exposed to continuous intense excitation for monitoring the biological processes, typically, the luminescence imaging of cellular and histochemical processes.[8] Thus it is paramount important to extend the excitation window towards the visible region to minimize the effects of excitation phototoxicity on the biological samples.

Nevertheless, a major challenge in the live-cell imaging is the creation of selective stains-compounds that enter cells and localize preferentially to a particular organelle without perturbing cell homeostasis.[1b] Numerous luminescent lanthanide coordination compounds based on cryptates,[9] helicates,[10] polyaminocarboxylates,[11] aminophosphinates,[12] β-diketonates[13] and notably

based on 9-N_3 or 12-N_4 ligand frameworks[6a, 14] have been developed that are tackled to meet a set of stringent requirements for use as cellular stains.[15] To utilize the luminescent europium complex for live cell imaging applications, it must possess some certain biological properties. Importantly, the luminescent complex must readily cross the cell membrane and localize in a region of interest within the cell. These important biological properties have led to recent efforts by many investigators to characterize the subcellular behavior of a large number of sensitized lanthanide complexes.[1h, 13b, 13c] Typically, a pH sensor might best localized in lysosomes, in which acidity can signify endosome age or health.[1h, 16] Recently, cyclometalated iridium (III) complexes containing *β*-carboline (a kind of biologically active indole alkaloids) as ligands have been reported as pH responsive tumor/lysosome-targeted PDT agents.[17] The use of terpyridine as ancillary ligand in europium *β*-diketonate complexes exhibit selectivity towards mitochondria of living cells.[13b, 13c] On the basis of wide existence, and the important physiological activities of indole derivatives, especially its lysosome specificity in live cell imaging, in the current study, a new *β*-diketone ligand namely 4,4,5,5,5-pentafluoro-3-hydroxy-1-(1-(4-methoxyphenyl)-1H-indol-3-yl)pent-2-en-1-one (Fig. 1) has been synthesized and utilized for the development of a Eu^{3+} ternary complex in the presence of an ancillary ligand (DDXPO). The developed coordination compound has been characterized by various spectroscopic techniques and evaluated its photophysical properties in biologically relevant pH conditions with a view to develop a bioprobe for cellular imaging applications.

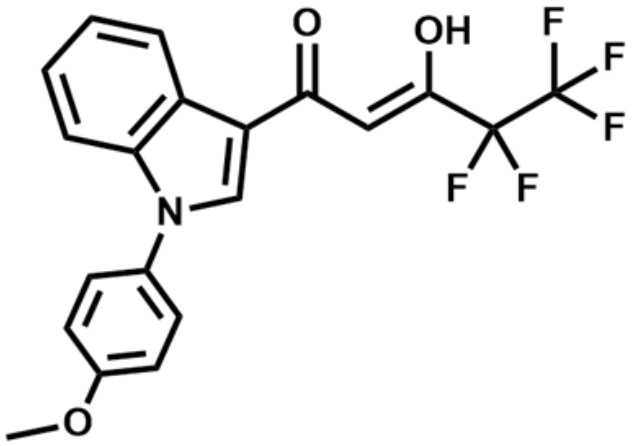

Figure 3.1. Structure of the ligand HpfphOCH$_3$IN.

3.3. Experimental Section

3.3.1. Materials and characterization

The chemicals were acquired from commercial sources and used as purchased: europium(III) nitrate hexahydrate, 99.99% (Alfa Aesar); gadolinium(III) nitrate hexahydrate, 99.999% (Sigma Aldrich); lanthanum(III) nitrate hexahydrate, 99.99% (Sigma Aldrich); sodium hydride 60% dispersion in mineral oil (Sigma Aldrich); ethyl pentafluoropropionate, 98% (Sigma Aldrich); 4,5-bis(diphenylphosphino)-9,9-dimethylxanthene, 97% (Sigma Aldrich); 3-acetylindole, 98% (Alfa Aesar); 4-methoxyphenylboronic acid, 98% (Alfa Aesar); diisopropylethylamine, 99% (Alfa Aesar) and copper(II) acetate, 97%

(Sigma Aldrich). All the other chemical materials purchased were of analytical reagent grade and used as supplied.

Elemental analyses were performed on a Elementar-vario MICRO cube elemental analyzer. The FT-IR spectral data were recorded using KBr pellets on a Perkin-Elmer Spectrum two FT-IR spectrometer. The NMR data of the ligands as well as designed lanthanide complexes were recorded using a Bruker 500 MHz NMR spectrometer [^{1}H NMR (500 MHz); ^{13}C NMR (125.7 MHz) and ^{31}P NMR (202.44 MHz)] in chloroform-d solution. The chemical shift values are expressed in parts per million relative to tetramethylsilane ($SiMe_4$) for ^{1}H NMR and ^{13}C NMR spectra, and with respect to 85% phosphoric acid for ^{31}P NMR spectra. Electrospray ionization (ESI) mass spectra were acquired by a Thermo Scientific Exactive Benchtop LC/MS Orbitrap Mass Spectrometer. The absorption spectra of the ligand and the complex were measured with a UV-vis spectrophotometer (Shimadzu, UV-2450). The solution state photoluminescence (PL) spectrum was recorded on a Spex-Fluorolog FL22 spectrofluorimeter equipped with a double grating 0.22 m Spex 1680 monochromator and a 450W Xe lamp as the excitation source. Lifetime measurement was recorded at room temperature using a Spex 1040D phosphorimeter. The overall quantum yield ($\Phi_{overall}$) was studied in a buffer solution of pH 7.2 (Hanks Balanced Salt Solution, HBSS) at 298 K using equation (1) and is measured relative to a quinine sulfate in 1 N H_2SO_4 solution (Φ_{ref} = 54.6%),[18]

$$\Phi_{overall} = \frac{n^2 A_{ref} I}{n_{ref}^2 A I_{ref}} \Phi_{ref} \qquad (1)$$

where *n*, *A*, and *I* denote the refractive index of the solvent, the absorbance at the excitation wavelength and the area of the emission spectrum, respectively, and Φ_{ref} represents the quantum yield of the standard quinine sulfate solution. The subscript ref denotes the reference, and the absence of a subscript implies an unknown sample. The refractive index is assumed to be equivalent to that of the pure solvent: 1.33 for water at room temperature. All data reported are averages of at least three independent measurements.[13b]

3.3.2. Synthesis of 1-(1-(4-methoxyphenyl)-1H-indol-3-yl)ethanone

A mixture of 3-acetylindole (1.0 mmol), 4-methoxyphenylboronic acid (2.5 mmol), anhydrous copper (II) acetate (2.5 mmol) and diisopropylethylamine (99%, 2.5 mmol) in 2mL dry dichloromethane (DCM) was taken in a sealed flask (25 mL) and stirred at room temperature for 24 h. From the resultant reaction mixture, DCM was removed under reduced pressure. Then 10 mL of water and 10 mL of chloroform were added. The corresponding aqueous layer was extracted with chloroform (2 x 10 mL). The concentrated organic layer was purified by column chromatography on silica gel using ethyl acetate and hexane (2:98) as the eluent. Yield: 80%. ^{1}H NMR ($CDCl_3$, 500 MHz) δ (ppm): 8.44 (d, 1H, J = 8.0 Hz), 7.88 (s, 1H), 7.35 (m, 5H), 7.06 (d, 2H, J = 9.0 Hz), 3.89 (s, 3H),

2.57 (s, 3H). ^{13}C NMR (125.7 MHz, $CDCl_3$) δ (ppm): 193.31, 159.29, 137.53, 135.01, 131.21, 126.46, 126.30, 123.79, 122.96, 122.67, 118.29, 114.97, 110.76, 55.67, 27.71. *m/z* = 266.11 $(M+H)^+$.

3.3.3. Synthesis of the ligand 4,4,5,5,5-pentafluoro-3-hydroxy-1-(1-(4-methoxyphenyl)-1H-indol-3-yl)pent-2-en-1-one. (HpfphOCH$_3$IN)

A modified Claisen condensation procedure is used for the synthesis of the new β-diketonate ligand as described in scheme 3.1. 1-(1-(4-methoxyphenyl)-1H-indol-3-yl)ethanone (1.0 mmol) and ethyl pentafluoropropionate (1.0 mmol) were added to 15 mL of dried tetrahydrofuran (THF) and stirred for 10 min at 0 °C in nitrogen atmosphere. Sodium hydride (2.0 mmol) was added to the above reaction mixture and stirred for 20 min followed by stirring at 60°C for 24 h. After cooling the reaction mixture to room temperature, 2M HCl (25 mL) was added and then the suspension extracted thrice with dichloromethane (3 × 20 mL). The organic layer was dried over Na_2SO_4, and the solvent was evaporated. The obtained crude product is then purified by silica gel column chromatography using the solvent mixture of ethyl acetate and hexane (1:99) as the eluent to get the product. Yield: 85%. Elemental analysis (%): Calculated for $C_{20}H_{14}F_5NO_3$ (412.09): C 58.43, H 3.43, N 3.41; Found: C 58.54, H 3.36, N 3.48. ^{1}H NMR ($CDCl_3$, 500 MHz) δ (ppm): 15.96 (broad, enol–OH), 8.30 (d, 1H, J = 7.5 Hz), 7.42-7.32 (m, 5H), 7.08 (s, 2H, J = 9.0 Hz), 6.48 (s, 1H), 3.90 (s, 3H). ^{13}C NMR (125.7 MHz, in $CDCl_3$) δ (ppm): 184.85, 172.77, 159.73, 138.07, 134.90, 130.52,

126.47, 125.75, 124.46, 123.68, 122.34, 119.29, 115.09, 113.50, 111.53, 94.53, 55.70. FT-IR (KBr) ν_{max} (cm^{-1}): 3425, 2944, 1616, 1515 1460, 1324, 1254, 1209, 1028, 832 741. m/z = 412.09 $(M+H)^+$.

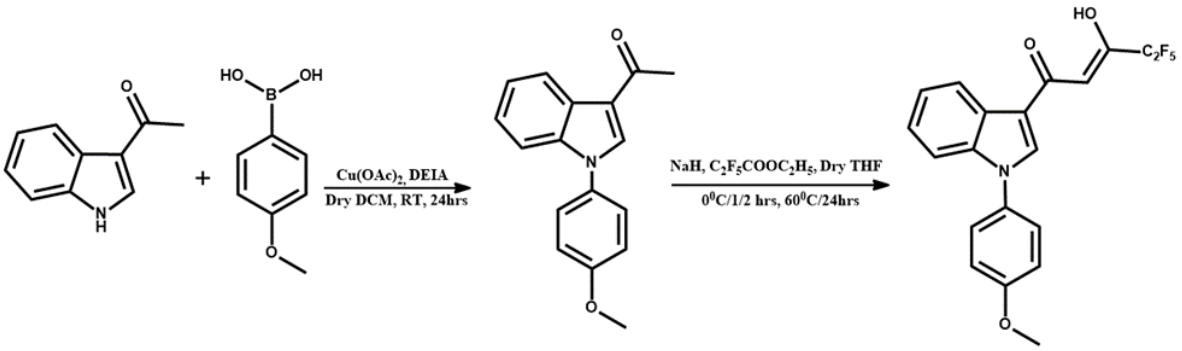

Scheme 3.1. Synthetic procedure for the ligand HpfphOCH$_3$IN.

3.3.4. Synthesis of the ligand 4,5-Bis(diphenylphosphino)-9,9-dimethylxanthene oxide (DDXPO)

The corresponding phosphine (5.0 mmol) was dissolved in 10 mL of 1,4-dioxane solution, to which 1.0 mL of 30% H_2O_2 (10.5 mmol) was added dropwise with vigorous stirring. The resultant mixture was then stirred for 2 h and then 10 mL of water was added to the reaction mixture to arrest the reaction. The mixture was extracted with 3 × 30 mL of dichloromethane. The oily phase was then washed with 2 × 30 mL of water to remove 1,4-dioxane. The dichloromethane layer was dried with Na_2SO_4. The solvent was removed in vacuo. The product was recrystallized from dichloromethane. Yield: 95%. Elemental analysis (%): calculated for $C_{39}H_{32}O_3P_2$ (610.18): C 76.71, H 5.28; Found: C 76.52, H 5.40. ^{1}H NMR ($CDCl_3$, 500 MHz) δ (ppm): 7.61 (d, 2 H, J = 7.5 Hz), 7.41 (m, 12 H), 7.30 (m, 8 H), 6.99 (t, 2 H), 6.80–6.76 (m, 2 H), 1.70 (s, 6 H). ^{31}P

NMR ($CDCl_3$, 202.44 MHz) δ (ppm): 30.97. FT-IR (KBr) ν_{max} (cm^{-1}): 1727, 1670, 1436, 1401, 1229, 1191, 1114, 875, 785, 746, 719, 694. m/z = 611.31 $(M+H)^+$.

3.3.5. Synthesis of complexes $Ln(pfphOCH_3IN)_3(H_2O)_2$ [Ln = Eu (1), Gd (2) La (3)]

To a methanolic solution of β-diketonate ligand ($HpfphOCH_3IN$, 3.0 mmol), NaOH (3.0 mmol) in water was added and stirred for 5 min. To this solution, $Ln(NO_3)_3{\cdot}6(H_2O)$ (where Ln = Eu^{3+}, Gd^{3+}, La^{3+}) (1.0 mmol) in 2 mL methanol was added dropwise and it was further stirred for 24 h at room temperature. The precipitate formed after the addition of water was filtered off and dried. The solid product was isolated by recrystallization from chloroform solution and used for analysis and photophysical properties. Attempts to grow single crystals of complexes were unsuccessful. The synthesis procedure is detailed in scheme 3.2.

$Eu(pfphOCH_3IN)_3(H_2O)_2$ (1). Elemental analysis (%): Calculated for $C_{60}H_{43}F_{15}N_3O_{11}Eu$ (1418.94): C 51.03, H 3.17, N 2.93; Found: C 51.21, H 3.25, N 2.91. IR (KBr) ν_{max} (cm^{-1}): 3425, 2916, 1598, 1518, 1453, 1333, 1249, 1203, 1036, 833, 740. *m/z* = 1384.17 $[Eu(pfphOCH_3IN)_3]^+$.

$Gd(pfphOCH_3IN)_3(H_2O)_2$ (2). Elemental analysis (%): Calculated for $C_{60}H_{43}F_{15}N_3O_{11}Gd$ (1424.22): C 50.60, H 3.04, N 2.95; Found: C 50.68, H 3.23, N 2.98. IR (KBr) ν_{max} (cm^{-1}): 3424, 2925, 1601, 1516, 1453, 1360, 1213, 1035, 834, 745. *m/z* = 1389.17 $[Gd(pfphOCH_3IN)_3+H]^+$.

La(pfphOCH$_3$IN)$_3$(H$_2$O)$_2$ (3). Elemental analysis (%): Calculated for $C_{60}H_{43}F_{15}N_3O_{11}La$ (1405.17): C 51.26, H 3.08, N 2.99; Found: C 51.37, H 3.05, N 3.11. ^{1}H NMR ($CDCl_3$, 500 MHz) δ (ppm): 8.38 (d, 3H), 7.79 (s, 3H), 7. 36 (s, 1H), 7.26 (m, 15H) 7.05-6.97 (m, 5H), 6.35 (s, 3H), 3.86 (s, 9H). IR (KBr) ν_{max} (cm^{-1}): 3428, 2926, 1599, 1460, 1213, 1182, 1036, 907, 750. *m/z* = 1411.29 [La(pfphOCH$_3$IN)$_3$(H$_2$O)+Na]$^+$.

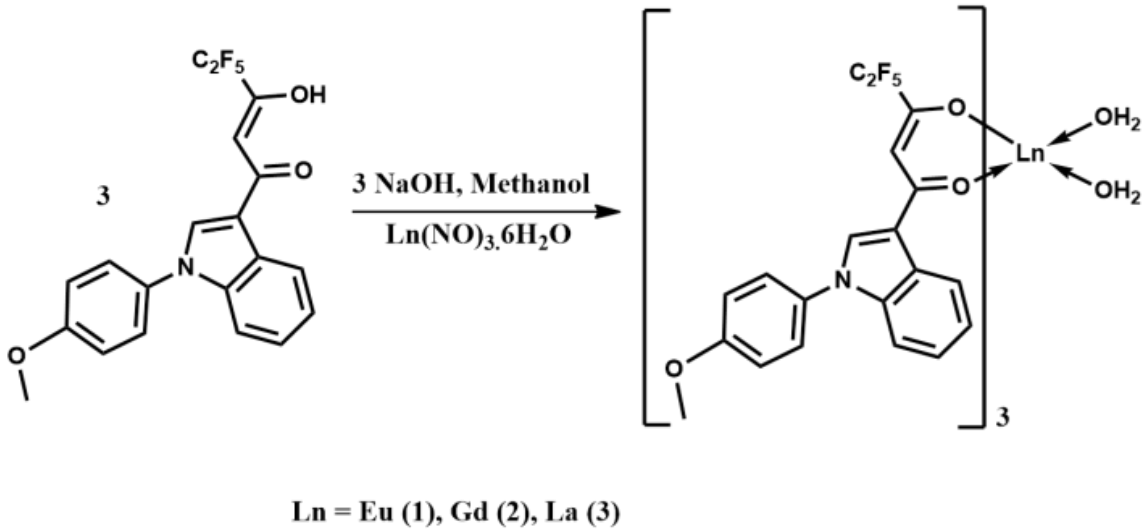

Scheme 3.2. Synthesis of the Ln^{3+} (Ln = Eu, Gd and La) binary complexes.

3.3.6. Synthesis of Ln^{3+} ternary complexes Ln(pfphOCH$_3$IN)$_3$(DDXPO) [Ln = Eu (4) and La (5)]

Ternary Ln^{3+} complexes were synthesized by stirring equimolar quantities of corresponding europium or lanthanum binary complexes and DDXPO in $CHCl_3$ solution for 12 h at 70°C. The products were isolated by solvent evaporation and purified by recrystallization from dichloromethane and hexane. The synthesis procedure is detailed in scheme 3.3.

Eu(pfphOCH$_3$IN)$_3$(DDXPO) (4). Elemental analysis (%): Calculated for $C_{99}H_{71}O_{12}F_{15}N_3P_2Eu$ (1993.52): C 59.65, H 3.59, N 2.11; Found: C 59.73, H 3.62, N 2.26. IR (KBr) ν_{max} (cm^{-1}): 3028, 1601, 1514, 1457, 1405, 1360, 1180, 1216, 1037, 904, 745. *m/z* = 1583.26 [Eu(pfphOCH$_3$IN)$_2$(DDXPO)]$^+$. ^{31}P NMR ($CDCl_3$, 202.44 MHz) δ (ppm): -80.86.

La(pfphOCH$_3$IN)$_3$(DDXPO) (5). Elemental analysis (%): Calculated for $C_{99}H_{71}O_{12}F_{15}N_3P_2La$(1979.33): C 60.04, H 3.61, N 2.12; Found: C 60.22, H 3.57, N 2.35. ^{1}H NMR ($CDCl_3$, 500MHz) δ (ppm): 8.57 (d, 3H), 7.57 (s, 3H), 7.41 (m, 8H), 7.36-7.35 (m, 4H),7.29-7.23 (m, 9H),7.10-7.07 (m, 4H), 7.04-7.01 (m, 3H),6.97-6.99 (m, 6H), 6.86 (s, 7H), 6.71 (t, 3H),6.04 (s, 3H), 6.53 (m, 2H),6.32 (s, 2H), 3.87 (s, 9H), 1.61 (s, 6H). IR (KBr) ν_{max} (cm^{-1}): 3064, 1600, 1515, 1452, 1325, 1182, 1098, 1036, 745. *m/z* = 1570.18 [La(pfphOCH$_3$IN)$_2$(DDXPO)]$^+$. ^{31}P NMR ($CDCl_3$, 202.44 MHz) δ (ppm): 31.85.

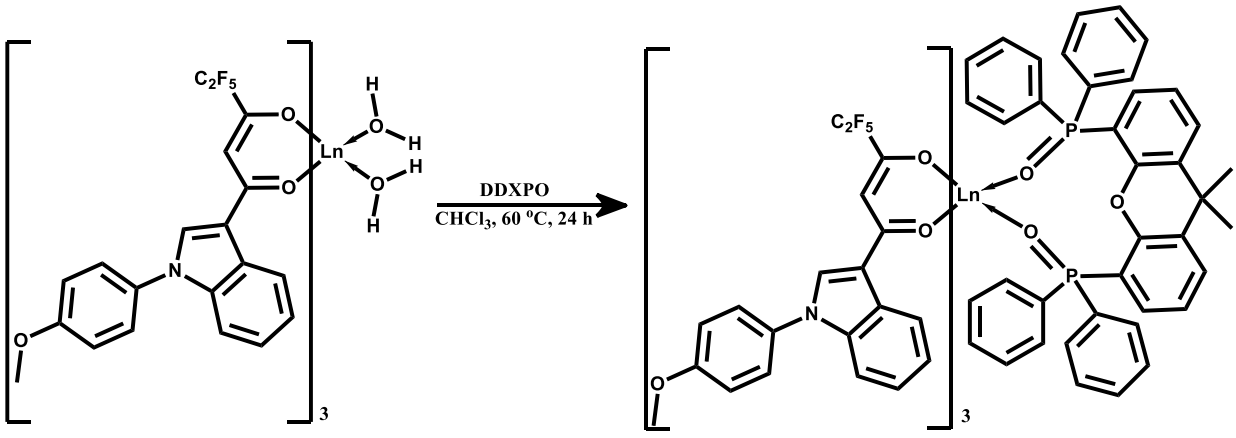

Scheme 3.3. Synthesis of the Ln^{3+} (Ln = Eu and La) ternary complexes.

3.3.7. Sample preparation for biological studies

The complex **4** was dissolved in DMSO at a concentration of 100 mg/mL. Sub stocks were prepared at desired concentrations in Dulbecco's Minimal Essential Medium (DMEM, Sigma-Aldrich) so that the final concentration of DMSO in cell culture should be less than 0.01%. All the biological studies using complex **4** were performed at a pH of 7.2 which is a critical factor for regular cellular function.

3.3.8. Cytotoxicity and cell imaging studies

Cytotoxicity measurement of the complex **4** on 3T3L1 cell lines (mouse pre-adipocyte cell lines, National Centre for Cell Science, Pune, India) was performed. Dulbecco's modified eagles medium (DMEM, Sigma-Aldrich), fetal bovine serum (FBS, Sigma-Aldrich), antibiotic (1% penicillin/streptomycin, Sigma-Aldrich) and MTT (3-[4,5-dimethylthiazol-2-yl]-2,5-diphenyl tetrazoliumbromide, Sigma-Aldrich) are the chemicals and reagents used.

3.3.9. Cell culture

The cells were cultured in DMEM supplemented with 10% fetal bovine serum (FBS) and an antibiotic (1% penicillin/streptomycin) in 5% CO_2 at 37 °C and 99% humidity. The cells from exponentially growing cultures were used for the experiments. The growth medium was changed every other day until the time of use of the cells.

3.3.10. MTT assay for cytotoxicity studies

Cytotoxicity of complex **4** was analysed by MTT assay as per the reference protocol (Wilson, 2000).[19] Briefly, 1 $\times 10^4$/mL cells were seeded at log phase in 96 well plates and incubated for 24 h. Growth media was removed and fresh media with complex **4** at different concentration (0.05, 5, 25, 50 and 125 μM) and DMSO as the control and incubated for 16 h. Next day, the sample containing media was removed and cells incubated with MTT (50 μg/mL) for 3-4 h. Crystals developed were solubilized by shaking in DMSO for 2 h and absorbance was measured at 570 nm using UV-Vis. spectrophotometer (UV-1700, Shimadzu, Japan). Percentage of cell viability was calculated and plotted against concentration.

3.3.11. Fluorescence imaging and co-localization studies of $Eu(pfphOCH_3IN)_3(DDXPO)$ with confocal microscopy

Cells were seeded (1×10^4/well) in 96 well black walled bio-imaging plate (BD Bioscience, USA) and incubated to approximately 70% confluence. Growth media was replaced with complex **4** containing media at 0.5, 5, 25 and 50 μM concentration and incubated for 24 h. Fluorescence of the compound was imaged using a confocal microscope (SP8 WLL, Leica, Gmbh) after three times wash using Hank's Balanced Salt Solution (HBSS). Fluorescence of complex **4** at different time intervals was also analyzed as part of standardization. Co-

localization studies of complex **4** was carried out after lysosome and mitochondrial staining using CellLight® Lysosome-GFP, BacMam 2.0 and CellLight mito-GFP, BacMam 2.0, respectively (Thermo Fisher Scientific, USA). Briefly, cells after reaching 70% confluent stage, were incubated with a viral particle load of 1×10^8/mL calculating an approximate value of 30 particles/cell (PPC) as per the manufacturer's instruction. Cells were incubated for 16-18 hours in the presence of CellLight solution. The images obtained from Lysosome-GFP/mitochondrial-GFP using an excitation source of 488 nm and monitoring the emission wavelength at 520 nm. These images were then merged/overlaid on the images acquired using the excitation signal of 405 nm and the emission wavelength of 612 nm.

3.4. Results and Discussion

3.4.1. Synthesis and characterization of HpfphOCH$_3$IN ligand and Ln^{3+} complexes 1–5

The β-diketonate ligand (HpfphOCH$_3$IN) was synthesized with an overall yield of 85% adapting the protocol as summarized in Scheme 3.1. The detailed characterization of the designed ligand has been carried out by ^{1}H NMR, ^{13}C NMR, FT-IR and electrospray ionization mass spectroscopic (ESI-MS) methods as well as by elemental analysis. The singlet peak observed in the ^{1}H NMR spectrum of the ligand at about 6.48 ppm (δ) is assigned to methine proton. The

active H^{enol} proton can be observed at 15.96 ppm (δ) reveals that the β-diketonate ligand exists as enol form in $CDCl_3$ solution. The other signals noted in the range of 7.07–8.30 ppm (δ) are attributed to the aromatic protons of the ligand. The ancillary ligand 4,5-bis(diphenylphosphino)-9,9-dimethylxanthene oxide (DDXPO) was prepared according to the literature procedure.[7d] The synthesis procedures for Ln^{3+} (Eu^{3+}, Gd^{3+} and La^{3+}) complexes are outlined in Schemes 3.2 and 3.3. The isolated lanthanide complexes were characterized by FT-IR, mass spectroscopy (ESI-MS) and elemental analyses. The elemental analyses and ESI-MS studies of Ln^{3+} complexes (**1–3**), indicates that the central Ln^{3+} ion is coordinated to three β-diketonate ligands. On the other hand, in the ternary Ln^{3+} complexes (**4** and **5**), one molecule of the bidentate oxygen donor, DDXPO also present in the coordination sphere of the metal ion. The IR carbonyl stretching frequency of the ligand $HpfphOCH_3IN$ (1616 cm^{-1}) is shifted to lower wavenumbers in **1–5** (1598 cm^{-1} for **1**; 1601 cm^{-1} for **2**; 1599 cm^{-1} for **3**; 1601 cm^{-1} for **4**; 1600 cm^{-1} for **5**), thus indicating the coordination of the carbonyl oxygen to the Ln^{3+} ion. In addition, the ($\nu_{P=O}$), stretching frequency of DDXPO (1190 cm^{-1}) has been shifted to lower wavenumbers in complex **4** (1180 cm^{-1}) and complex **5** (1182 cm^{-1}) which verifies the participation of phosphoryl oxygen of DDXPO in the complex formation with Ln^{3+} ions. This behaviour is further confirmed from the ^{31}P NMR spectral data (30.97 ppm in the DDXPO; -80.86 ppm in complex **4**).

In order to get more information about the coordination behaviour of the europium complexes, in the present study the corresponding lanthanum complexes have been isolated and characterized by various spectral techniques (the pertinent data is given in the experimental section). The ^{1}H NMR spectrum of the La(pfphOCH$_3$IN)$_3$(H$_2$O)$_2$ is in accordance with the presence of three β-diketonate moieties coordinated to the central lanthanide ion. The ^{1}H NMR signal for methine proton (–CH) of HpfphOCH$_3$IN resonates at 6.35 ppm (δ) and the aromatic protons resonates in the range 8.39 to 6.97 ppm (δ). The observed upfield shift in the β-diketonate resonances, in the complex, reveals the coordination of HpfphOCH$_3$IN ligands with the Ln^{3+} ion. The proton signals of the chelated water molecule with the Ln^{3+} ion can be seen at 1.88 ppm (δ). In the ternary lanthanum complex, La(pfphOCH$_3$IN)$_3$(DDXPO), the methine proton appears at 6.05 ppm (δ). The signals due to the aromatic protons of the β-diketonate ligand (HpfphOCH$_3$IN) and DDXPO moiety noted in the range 8.58 to 6.30 ppm (δ). The proton signals appeared in the ternary lanthanum complex indicates the existence of three HpfphOCH$_3$IN units and one DDXPO moiety in the coordinated complex. Moreover, no signals for the coordinated water molecule are noted in the La(pfphOCH$_3$IN)$_3$(DDXPO), which substantiates the replacement of coordinated water molecules by the chelating ligand in complex **5**.

3.4.2. The absorption spectra of the ligand and the Eu^{3+} complex

The absorption spectra of the ligand $HpfphOCH_3IN$ and the corresponding Eu^{3+} complex were investigated in aqueous media buffered to physiological pH 7.2 [% DMSO: % HBSS = 0.01: 99.99; c = 2.5 x 10^{-5} M] at 298 K (Figure 3.2). The maximum absorption bands are observed at 435 nm for *β*-diketonate ligand and at around 393 nm for europium complex, which is attributed to singlet-singlet n–π* enolic transition assigned to the *β*-diketonate moiety. Further, the higher energy absorption band detected in the range of 280-300 nm can be ascribed to the $^1\pi$–π* transition of the aromatic moiety of the *β*-diketonate ligand. In comparison with absorption maximum of the ligand, the absorption maximum of the complex is dramatically blue-shifted about 42 nm, which may be due to the perturbation induced by the coordination of Eu^{3+} ion. However, the spectral pattern of the complex is similar to that of the free ligand, suggesting that the coordination of Eu^{3+} ion has no significant influence on the $^1\pi$–π* state energy. The determined molar absorption coefficient value of Eu^{3+} complex at 393 nm, 3.58×10^4 L mol^{-1} cm^{-1}, is about three times higher than that of the ligand (393 nm, 1.26×10^4 L mol^{-1} cm^{-1}), indicating the presence of three *β*-diketonate ligands in the corresponding complex. The high molar absorption coefficient value noted clearly illustrates the good light absorption ability of the newly developed ligand.[20]

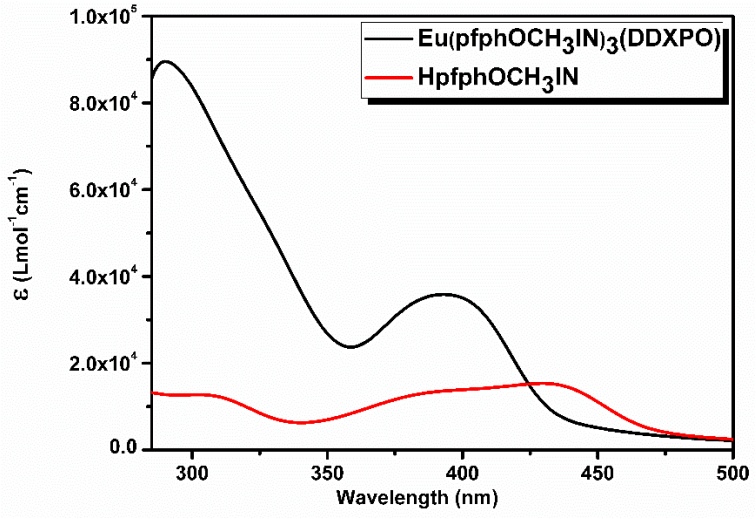

Figure 3.2. UV-vis absorption spectra of the ligand $HpfphOCH_3IN$ and complex **4** in in a buffer solution of pH 7.2 [% DMSO: % HBSS =0.01: 99.99; c = 2.5 x 10^{-5} M].

3.4.3. Photophysical properties

To evaluate triplet energy (T_1) of the newly developed *β*-diketonate ligand, low-temperature phosphorescence spectrum of the corresponding gadolinium complex was measured and the results are shown in figure 3.3. In this work gadolinium chelate was used to estimate the triplet energy level of the ligand due to the following reasons: i) Strong spin-orbital coupling or heavy atom effect of Gd^{3+} ion increases the probability of intersystem crossing from singlet to triplet excited state and ii) the energy level of Gd^{3+} ion is too high to accept the energy from the triplet state of the antenna chromophore ligand, so that only ligand-based emission can be observed. As a consequence the triplet energy level of the ligand can be estimated from the lower emission edge of the phosphorescent spectrum.[5,21] The singlet energy level (S_1) of the ligand was determined from the upper absorption edge of the electronic spectrum of the

Gd^{3+} complex (Figure 3.3).[5] Thus the singlet and triplet energy levels of the *β*-diketonate ligand are found to be 25,000 cm^{-1} (400 nm) and 21,881 cm^{-1} (457 nm), respectively. As per the Dexter theory, the intramolecular energy transfer from the triplet state (T_1) of the ligand to the emitting resonance level of the lanthanide ion has a significant influence on europium luminescence. It is interesting to note that the energy gap between the triplet state of the newly designed *β*-diketonate ligand and $^5D_0$ excited state of Eu^{3+} ion (17,250 cm^{-1}) is found to be ΔE = 4631 cm^{-1}, which is considered to be an ideal situation for sensitization of Eu^{3+} luminescence.[5] The energy gap between the S_1 and T_1 states of the HpfphOCH$_3$IN, $\Delta E = (S_1\text{-}T_1)$ 3119 cm^{-1}, which is again considered as optimum for intersystem crossing in visible-light excited europium complexes.[5k]

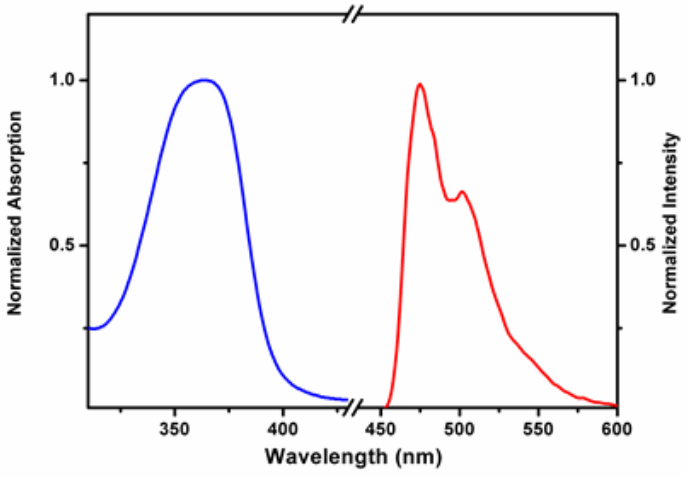

Figure 3.3. UV-vis absorption spectra at 298 K (blue) and 77 K phosphorescence spectra (red) of complex **2** in THF.

The excitation and emission profiles of the developed europium complex recorded in a buffer solution of pH 7.2 [% DMSO: % HBSS = 0.01: 99.99; c = 2.5 x 10^{-5} M] at 298 K are shown in Fig. 3.4. The excitation spectrum was recorded by monitoring the $^5D_0 \rightarrow {}^7F_2$ (612 nm) transition of the Eu^{3+}. The excitation spectrum displays a broad band between 280 to 425 nm, which can be designated to the π–π* electronic transition of the *β*-diketonate ligand. The absence of any absorption bands due to the f-f transitions of the Eu^{3+} ion clearly attests that luminescence sensitization *via* the excitation of the ligand is effective. The room temperature (298 K) emission spectrum of the europium complex was recorded in a buffer solution of pH = 7.2 by exciting at 405 nm and the pertinent results are depicted in figure 3.4.

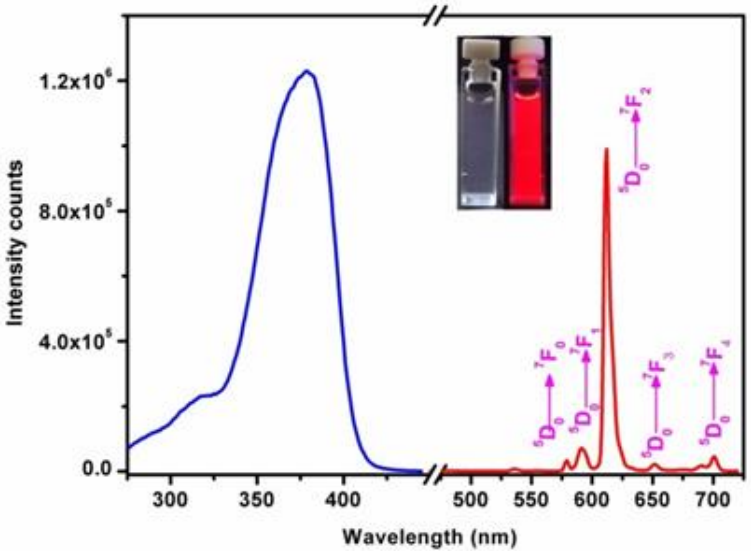

Figure 3.4. Solution-state excitation emission spectra $Eu(pfphOCH_3IN)_3(DDXPO)$ in a buffer solution of pH 7.2 [% DMSO : % HBSS =0.01: 99.99; c = 2.5 x 10^{-5} M] at 298 K, emission monitored at around 612 nm (λ_{exc} = 405 nm). Inset: photograph of the complex **4** in buffer solution under day light and UV light with 365 nm excitation).

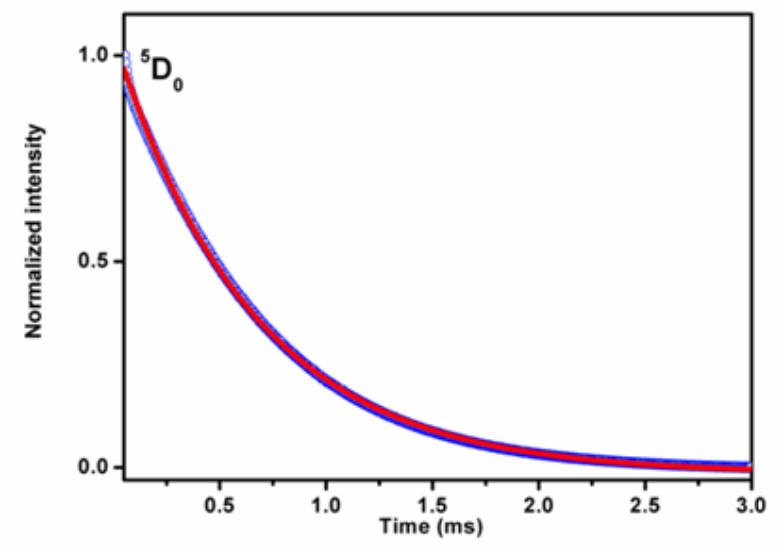

Figure 3.5. The $^5D_0$ decay profile for the complex **4** in a buffer solution of pH 7.2 [% DMSO: % HBSS =0.01: 99.99; c = 2.5 x 10^{-5} M] at 298 K, excited at 405 nm. The emission was monitored at 612 nm.

The emission bands of the europium complex are observed at 580, 593, 612, 652 and 697 nm, and are attributed to the f-f transitions of $^5D_0 \rightarrow {}^7F_J$ with J = 0, 1, 2, 3 and 4, respectively.[22] The transition of highest intensity is dominated by the hypersensitive $^5D_0 \rightarrow {}^7F_2$ transition which occurs around 612 nm, indicating that the Eu^{3+} is not located in a site with inversion center symmetry. Moreover, the presence of only one sharp peak in the region of the $^5D_0 \rightarrow {}^7F_0$ transition at 580 nm suggests the existence of single chemical environment around the Eu^{3+}. No broad emission band resulting from the organic ligand molecule in the blue region can be observed, which indicate that the ligand transfers the absorbed energy effectively to the emitting level of metal ion. The luminescence lifetime of the designed europium complex was measured at room temperature from the luminescent decay profile by fitting with monoexponential decay

curve (Fig. 3.5) and the lifetime data is shown in Table 1. This data indicate the existence of single chemical environment around the Eu^{3+}.To gain a better understanding of the luminescence efficiency of the designed Eu^{3+} compound, it was appropriate to analyse the emission profile of the complex in terms of eqn (2),[4d,23]

$$\Phi_{overall} = \Phi_{sens} \times \Phi_{Ln} = \Phi_{sens} \times (\tau_{obs}/\tau_{rad}) \qquad (2)$$

Where $\Phi_{overall}$ and Φ_{Ln} represent the overall and intrinsic luminescence quantum yields of Eu^{3+}; Φ_{sens} represents the efficiency of the ligand-to-metal energy transfer, τ_{obs} and τ_{rad} are the observed and the radiative lifetimes of Eu^{3+} ($^5D_0$). Due to the low absorption intensities of direct f-f excitation, the intrinsic luminescence quantum yields of Eu^{3+} could not be determined experimentally. The intrinsic quantum yield of Eu^{3+} could not be determined experimentally upon direct f-f excitation because of very low absorption intensity. Hence, the radiative lifetime of Eu^{3+} ($^5D_0$) has been calculated from eqn. (3),

$$1/\tau_{rad} = A_{MD,0} \times n^3 \times (I_{tot}/I_{MD}) \qquad (3)$$

where n represents the refractive index (1.33) of the medium. $A_{MD,0}$ is the spontaneous emission probability for the $^5D_0 \rightarrow {}^7F_1$ transition in *vacuo* (14.65 s^{-1}), and I_{tot}/I_{MD} signifies the ratio of the total integrated intensity of the corrected Eu^{3+} emission spectrum to the integrated intensity of the magnetic dipole $^5D_0 \rightarrow {}^7F_1$ transition. The intrinsic quantum yield for the synthesized Eu^{3+}-β-

diketonate complex has been calculated from the ratio τ_{obs}/τ_{rad} and the pertinent value is tabulated in Table 3.1. The radiative lifetime (τ_{rad}), $^5D_0$ lifetime (τ_{obs}), energy transfer efficiency (Φ_{sens}), and overall quantum yield ($\Phi_{overall}$) for the developed europium complex is also presented in Table 3.1. Most importantly, the current results disclose that the newly developed europium complex exhibits impressive quantum yield ($\Phi_{overall}$ = 25 %) in the solution state under biological pH conditions, which is found to be the highest so far reported for visible light excited europium complex systems (Table 3.1). The luminescent quantum yields value ($\Phi_{overall}$ = 28 %) observed in the present study are in line with the recently published studies on lysosome targetable Eu^{3+} complexes.[1b, 10c, 11b]

Table 3.1. Photophysical parameters Radiative lifetime (τ_{rad}), $^5D_0$ lifetime (τ_{obs}), intrinsic quantum yield (Φ_{Ln}) energy transfer efficiency (Φ_{sens}), and overall quantum yield ($\Phi_{overall}$) for selected europium complexes.

Complex	τ_{rad} **(ms)**	τ_{obs} **(ms)**	Φ_{Ln} **(%)**	Φ_{Sens} **(%)**	$\Phi_{Overall}$ **(%)**	λ_{exc} **(nm)**
Eu(pfphOCH$_3$IN)$_3$(DDXPO)	1.7	0.398	23	~100	25±3	405
[a] **[EuL^1]$^{3-}$** *1b*	-	1.050	-	-	26	355
[a] **[EuL^3]$^{3+}$** 1b	-	1.030	-	-	17	355
[b] **[EuL^9]$^{3-}$** *11b*	-	1.040	-	-	26	355
[c] **[Eu$_2$(L^{C2})$_3$]** 10c	6.9	2.430	36	58	21	405
[c] **[Eu$_2$ (L^{C5})$_3$]** 10c	6.7	3.300	35	26	8.9	405

[a] In water at pH 6.5 (Ref. 1b); [b] In water at pH 6.5 (Ref.11b); [c] In tris-HCl buffer at pH 7.4 (Ref. 10c).

3.4.4. The photostability of the Eu(pfpHOCH$_3$IN)$_3$(DDXPO)

The photostability of the complex **4** was inspected by means of measuring photoluminescence intensity at 612 nm in a buffer solution of pH 7.2 [% DMSO: % HBSS =0.01: 99.99; c = 2.5 x 10^{-5} M] at 298 K, as a function of irradiation time. λ_{exc} = 405 nm, for 5 h and the results are given in figure 3.6. These results validated that the emission intensity of the complex at 612 nm is remains approximately the same after 5 h of continuous irradiation. This indicates the stability of the Eu^{3+} complex towards photoirradiation.

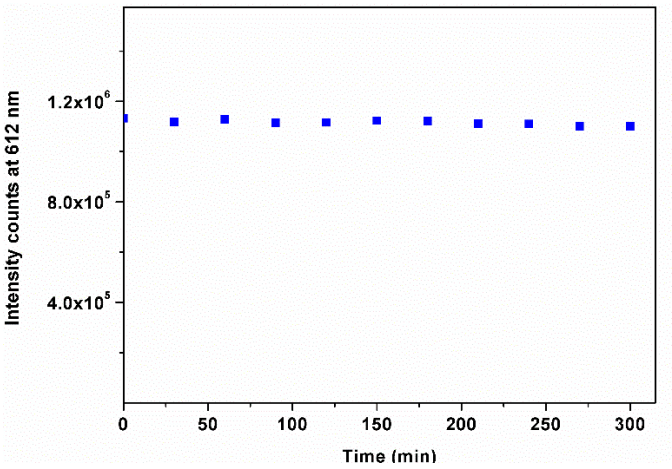

Figure 3.6. Photoluminescence intensity of complex **4** at 612 nm in a buffer solution of pH 7.2 [% DMSO: % HBSS =0.01: 99.99; c = 2.5 x 10^{-5} M] at 298 K, as a function of irradiation time. λ_{exc} = 405 nm.

3.4.5. Cell-imaging properties of Eu(pfphOCH$_3$IN)$_3$(DDXPO)

To evaluate the cytotoxic effects, the cytotoxicity of the developed europium complex was evaluated using the methyl thiazolyl tetrazolium (MTT) assay in mouse pre-adipocyte cell lines (3T3L1) and the results are depicted in figure 3.7.

Upon incubation with different concentrations of europium complex from 0.0 to 125µM for 24 h, no significant differences in the cell proliferation of the cells were observed. The cellular viability was greater than 99%. It is noted that when the concentration of the complex increased to 125µM, the cell viability still remained above 90%. The results of the MTT assay clearly demonstrate that the europium compound is non-cytotoxic.

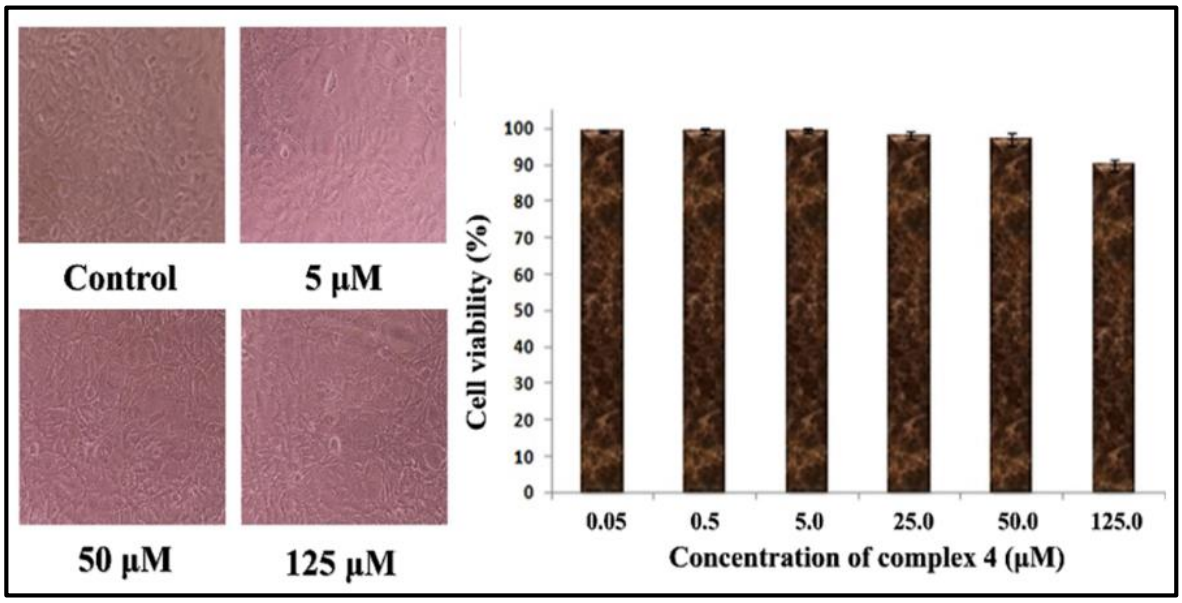

Figure 3.7. The change in cell viability after incubating 3T3L1 cells with different concentration of Eu(pfphOCH$_3$IN)$_3$(DDXPO) (representative images shown) and the graphical representation showing cell viability assessed by MTT assay.

In the subsequent experiments, the 3T3L1 cells were grown on plastic-bottomed cell culture µ-dishes and incubated with a solution of the europium complex in DMEM (0.5-50µM) for 24 h at 37°C. The luminescence images recorded with an excitation wavelength of 405 nm are shown in figure 3.8. Bright spots start to appear in the cytoplasm of the cells for an incubation concentration

as low as 0.5 µM. The results demonstrated that the luminescence intensity of the cells increases with an increase in the concentration of the europium complex (figure 3.9). The uptake of the europium compound at an incubation concentration of 25µM was investigated versus time and emission from the europium compound can be detected after 30 min (Figure 3.8). Another interesting feature of the developed europium complex is its chemical stability at ambient temperatures and requires less incubation time (2 h) as compared to commercial lysosome tracker, CellLight® Lysosome-GFP (16 h).

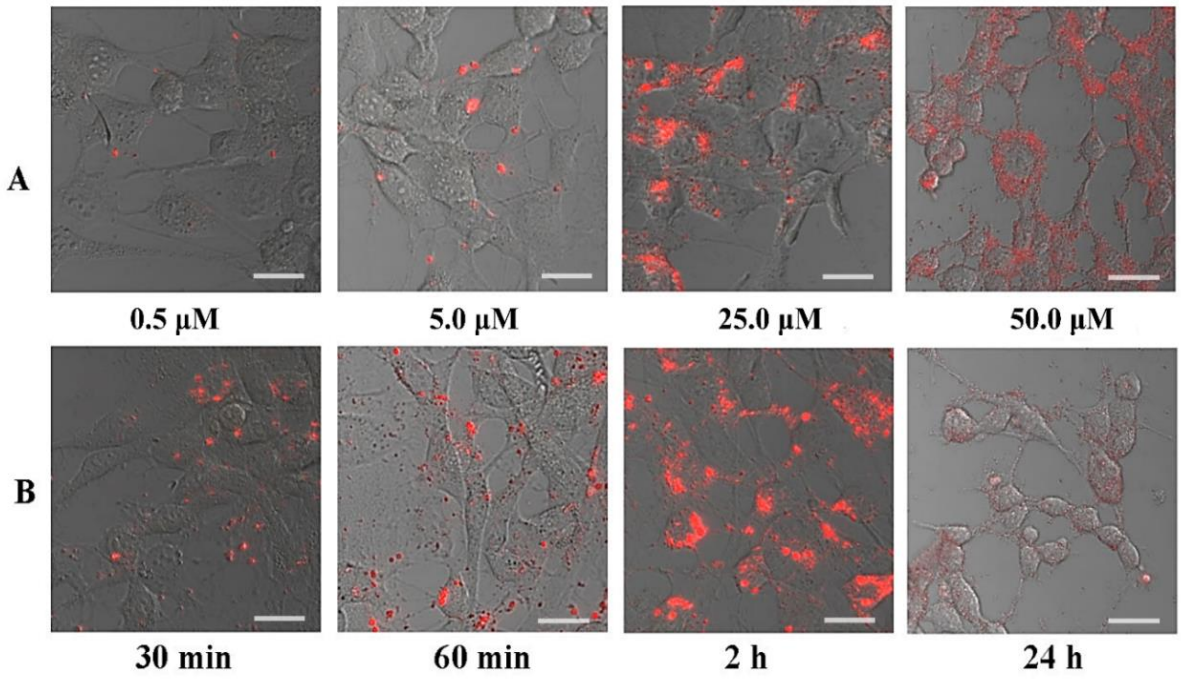

Figure 3.8. Eu(pfphOCH$_3$IN)$_3$(DDXPO) was incubated with 3T3L1 cells at different concentration and time intervals. Lane A shows the luminescence emitted by compound at different concentration after 24 h incubation. Lane B is the images of luminescence from cells after an incubation of 25 µM Eu(pfphOCH$_3$IN)$_3$(DDXPO) at different time intervals. Scale bars: 10 µm.

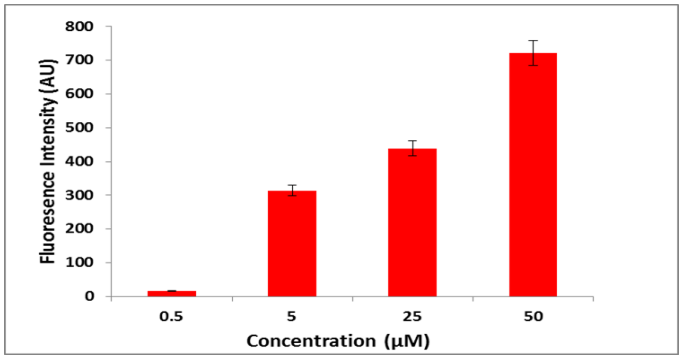

Figure 3.9. The intensity of the complex Eu(pfphOCH$_3$IN)$_3$(DDXPO) in the cells versus the incubation concentration of the complex **4**.

In order to understand the sub-cellular localization of the europium complex, a lysosome targeted green fluorescent protein (CellLight® Lysosome-GFP, BacMam 2.0) was used for the co-localization experiments. The 3T3L1 cells were first loaded with lysosome tracker and incubated at 37 °C for 16 h. Subsequently, the cells loaded with the Lysosome-GFP were incubated with 25 µM of the europium complex for 2 h and the results were examined under a microscope using an appropriate filter. The green fluorescent signals representing the lysosome tracker in the 3T3L1cell line were examined by exciting with 488 nm and emission monitoring at 510 nm (Figure 3.10b). On the other hand, red luminescence signals of the europium complex were obtained at a 405 nm excitation and by emission monitoring at 612 nm (Figure 3.10c). The extensive overlapping with lysosome tracker green indicated that the lysosome is probably the main cite of the europium complex accumulation (Figure 3.10d). Further, the merged image of Channel 1 and Channel 2 (Figure 3.10e) showed the vast overlap between the red luminescence of europium complex and the

green luminescence of Lyso-Tracker Green in the cells. Moreover, the luminescence intensity profile of europium complex and Lysosome-GFP Green in the interest linear region across 3T3L1 cells are in very close synchrony (Figure 3.10f). The colocalization coefficient, *A*, was calculated by using Pearson's method to evaluate the colocalization of complex **4** relative to the commercial probe (Lysosome-GFP).[24] All of these results demonstrated the specific-localization of the developed europium complex in lysosome of the cells, suggesting that europium complex could truly be used as a probe for tracking the intracellular lysosome.

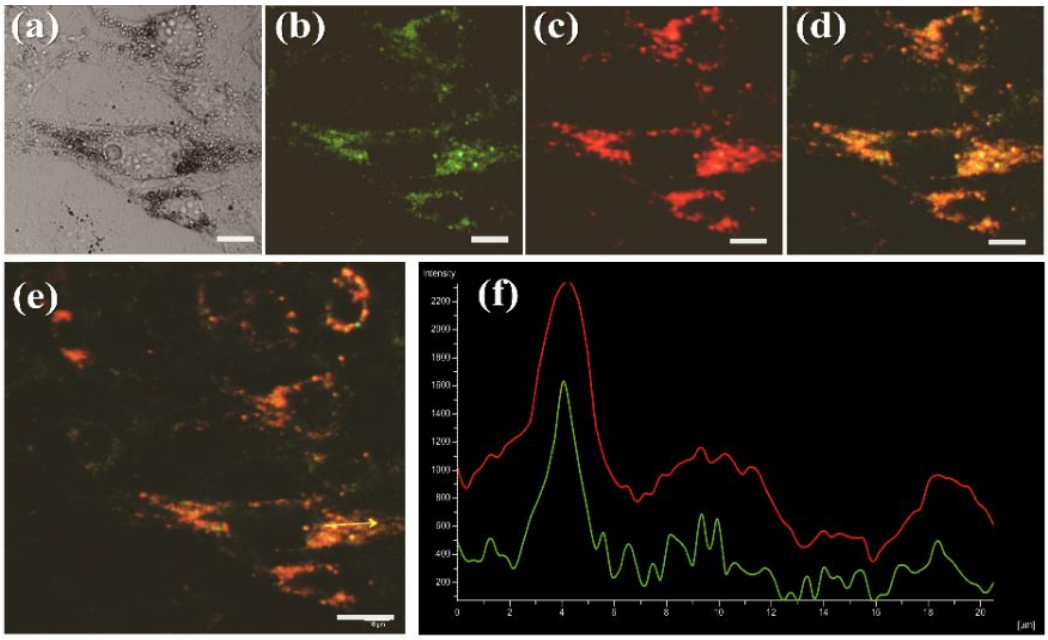

Figure 3.10. Co-localization imaging of the 3T3L1 cells incubated with complex **4** and lysosome-GFP. **a**) the bright field image; **b**) luminescence image of GFP tagged lysosomal protein d(Ex.488/Em.520); **c**) luminescence image of Eu(pfphOCH$_3$IN)$_3$(DDXPO) (Ex.405/Em.612); **d**) merged image of b and c; **e**) representative image from which the luminescence emission intensity of both (GFP & complex **4**) is measured (region showed along the arrow line) and **f**) the graphical representation of luminescence intensity of lysosome-GFP (green) and Eu(pfphOCH$_3$IN)$_3$(DDXPO) (red). Scale bars: 10 μm.

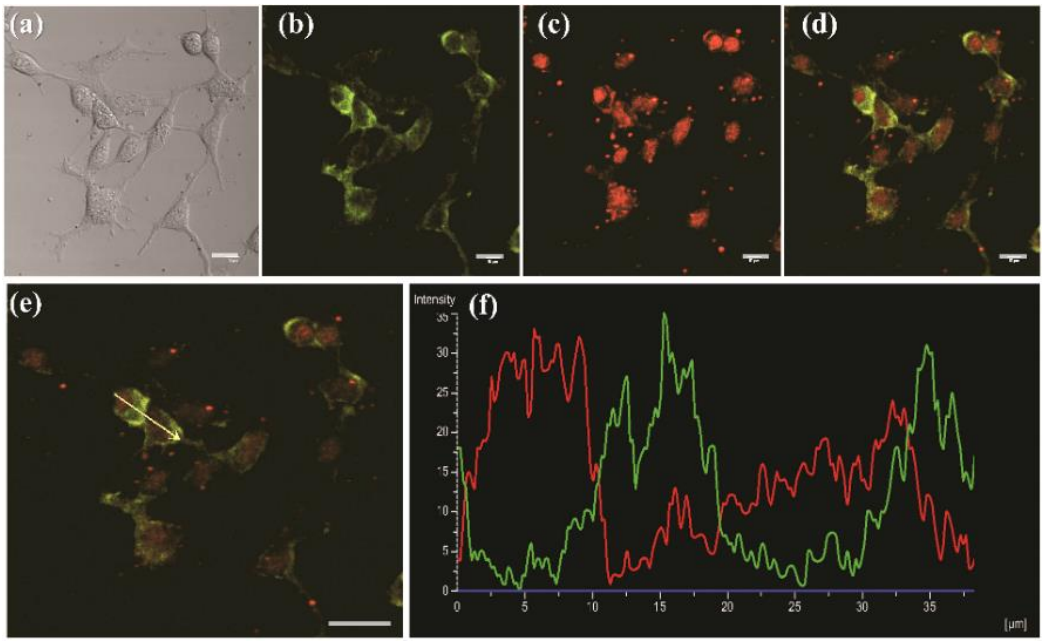

Figure 3.11. Co-localization imaging of the3T3L1 cells incubated with complex **4** and Mito-GFP. **a**) the bright field image; **b**) luminescence image of GFP tagged mitochondrial protein (Ex.488/Em.520) **c**) luminescence image of $Eu(pfphOCH_3IN)_3(DDXPO)$ (Ex.405/Em.612) **d**) the merged image of b and c; **e**) representative image from which the luminescence emission intensity of both (GFP & complex **4**) is measured (region showed along the arrow line) and **f**) the graphical representation of luminescence intensity of GFP (green) and $Eu(pfphOCH_3IN)_3$ (DDXPO) (red). Scale bars: 10 µm.

To further figure out the europium complex localization, the mitochondria targeted green fluorescent protein (CellLight mito-GFP, BacMam 2.0) was also examined whether the europium complex can be localise within the other subcellular domains (Fig.3.11). It can be clearly observed from the Fig.3.11e and 3.11f that no co-localization of the europium complex with mitochondria tracker green. Moreover, the colocalization coefficient, (*A*) of the complex **4** relative to the commercial probe (mito-GFP) is found to be lower (A = 0.46).[24]

3.5. Conclusions

- A unique bright luminescent europium coordination compound with excellent biocompatibility has been developed that serves as a selective bioprobe for particular organelles within the cells.

- The designed europium compound showed distinct advantages of visible-light excitation wavelength and remarkable quantum yield and luminescence lifetime values, which enabled it to be successfully utilized for visible-light excited luminescence cell imaging applications.

- Strikingly, the europium luminescent compound showed no observed cytotoxicity, high photostability and remains localized in the lysosomes of the 3T3L1 cells.

- The results demonstrated in the current study highlights that the developed luminescent europium compound has potential applications in live-cell imaging.

3.6. References

1. (a) M. C. Heffern, L. M. Matosziuk and T. J. Meade, *Chem. Rev.*, 2014, **114**, 4496-4539; (b) S. J. Butler, L. Lamarque, R. Pal and D. Parker, *Chemical Science*, 2014, **5**, 1750-1756; (c) M. L. P. Reddy, V. Divya and R. Pavithran, *Dalton Trans.*, 2013, **42**, 15249-15262; (d) L. Prodi, E. Rampazzo, F. Rastrelli, A. Speghini and N. Zaccheroni, *Chem. Soc. Rev.*, 2015, **44**, 4922-4952; (e) A. J. Amoroso and S. J. A. Pope, *Chem.*

Soc. Rev., 2015, **44**, 4723-4742; (f) J.-C. G. Bünzli, *Chem. Rev.*, 2010, **110**, 2729-2755; (g) M. Sy, A. Nonat, N. Hildebrandt and L. J. Charbonniere, *Chem. Commun.*, 2016, **52**, 5080-5095; (h) E. J. New, A. Congreve and D. Parker, *Chemical Science*, 2010, **1**, 111-118.

2. (a) J. Feng and H. Zhang, *Chem. Soc. Rev.*, 2013, **42**, 387-410; (b) M. L. P. Reddy and S. Sivakumar, *Dalton Trans.*, 2013, **42**, 2663-2678; (c) K. Binnemans, *Chem. Rev.*, 2009, **109**, 4283-4374; (d) C. Piguet and J.-C. G. Bünzli, *Chem. Soc. Rev.*, 1999, **28**, 347-358; (e) J.-C. G. Bünzli, A.-S. Chauvin, H. K. Kim, E. Deiters and S. V. Eliseeva, *Coord. Chem. Rev.*, 2010, **254**, 2623-2633; (f) A. de Bettencourt-Dias, P. S. Barber and S. Viswanathan, *Coord. Chem. Rev.*, 2014, **273–274**, 165-200; (g) Y. Ma and Y. Wang, *Coord. Chem. Rev.*, 2010, **254**, 972-990; (h) N. Sabbatini, M. Guardigli and J.-M. Lehn, *Coord. Chem. Rev.*, 1993, **123**, 201-228.

3. (a) X. Wang, H. Chang, J. Xie, B. Zhao, B. Liu, S. Xu, W. Pei, N. Ren, L. Huang and W. Huang, *Coord. Chem. Rev.*, 2014, **273–274**, 201-212; (b) J.-C. G. Bünzli, *J. Lumin.*, 2016, **170**, 866-878; (c) J.-C. G. Bünzli, *Interface Focus*, 2013, **3**; (d) C. P. Montgomery, B. S. Murray, E. J. New, R. Pal and D. Parker, *Acc. Chem. Res.*, 2009, **42**, 925-937.

4. (a) S. V. Eliseeva and J.-C. G. Bünzli, *New J. Chem.*, 2011, **35**, 1165-1176; (b) L. Armelao, S. Quici, F. Barigelletti, G. Accorsi, G. Bottaro, M. Cavazzini and E. Tondello, *Coord. Chem. Rev.*, 2010, **254**, 487-505; (c) L. D. Carlos, R. A. S. Ferreira, V. de Zea Bermudez, B. Julian-Lopez and P. Escribano, *Chem. Soc. Rev.*, 2011, **40**, 536-549; (d) J.-C. G. Bünzli and C. Piguet, *Chem. Soc. Rev.*, 2005, **34**, 1048-1077; (e) N. M. Shavaleev, S. V. Eliseeva, R. Scopelliti and J.-C. G. Bünzli, *Inorg. Chem.*, 2015, **54**, 9166-9173.

5. (a) S. Biju, N. Gopakumar, J.-C. G. Bünzli, R. Scopelliti, H. K. Kim and M. L. P. Reddy, *Inorg. Chem.*, 2013, **52**, 8750-8758; (b) K. Miyata, Y. Konno, T. Nakanishi, A. Kobayashi, M. Kato, K. Fushimi and Y. Hasegawa, *Angew. Chem.*, 2013, **52**, 6413-6416; (c) J. Yuasa, T. Ohno, H. Tsumatori, R. Shiba, H. Kamikubo, M. Kataoka, Y.

Hasegawa and T. Kawai, *Chem. Commun.*, 2013, **49**, 4604-4606; (d) V. Divya, V. Sankar, K. G. Raghu and M. L. P. Reddy, *Dalton Trans.*, 2013, **42**, 12317-12323; (e) S. Sivakumar and M. L. P. Reddy, *J. Mater. Chem.*, 2012, **22**, 10852-10859; (f) S. Sivakumar, M. L. P. Reddy, A. H. Cowley and R. R. Butorac, *Inorg. Chem.*, 2011, **50**, 4882-4891; (g) T. M. George, S. Varughese and M. L. P. Reddy, *RSC Adv.*, 2016, **6**, 69509-69520; (h) V. Divya, S. Biju, R. L. Varma and M. L. P. Reddy, *J. Mater. Chem.*, 2010, **20**, 5220-5227; (i) A. R. Ramya, M. L. P. Reddy, A. H. Cowley and K. V. Vasudevan, *Inorg. Chem.*, 2010, **49**, 2407-2415; (j) A. R. Ramya, D. Sharma, S. Natarajan and M. L. P. Reddy, *Inorg. Chem.*, 2012, **51**, 8818-8826; (k) V. Divya, R. O. Freire and M. L. P. Reddy, *Dalton Trans.*, 2011, **40**, 3257-3268; (l) T. V. U. Gangan, S. Sreenadh and M. L. P. Reddy, *J. Photochem. Photobiol. A*, 2016, **328**, 171-181; (m) T. V. U. Gangan and M. L. P. Reddy, *Dalton Trans.*, 2015, **44**, 15924-15937.

6. (a) M. Soulié, F. Latzko, E. Bourrier, V. Placide, S. J. Butler, R. Pal, J. W. Walton, P. L. Baldeck , B. Le Guennic, C. Andraud, J. M. Zwier, L. Lamarque, D. Parker and O. Maury, *Chem. Eur. J.*, 2014, **20**, 8636-8646; (b) S. V. Eliseeva and J.-C. G. Bünzli, *Chem. Soc. Rev.*, 2010, **39**, 189-227.

7. (a) F. J. Steemers, W. Verboom, D. N. Reinhoudt, E. B. van der Tol and J. W. Verhoeven, *J. Am. Chem. Soc.*, 1995, **117**, 9408-9414; (b) P. P. Lima, M. M. Nolasco, F. A. A. Paz, R. A. S. Ferreira, R. L. Longo, O. L. Malta and L. D. Carlos, *Chem. Mater.*, 2013, **25**, 586-598; (c) D. B. Ambili Raj, S. Biju and M. L. P. Reddy, *J. Mater. Chem.*, 2009, **19**, 7976-7983; (d) D. B. A. Raj, B. Francis, M. L. P. Reddy, R. R. Butorac, V. M. Lynch and A. H. Cowley, *Inorg. Chem.*, 2010, **49**, 9055-9063; (e) T. M. George, M. J. Sajan, N. Gopakumar and M. L. P. Reddy, *J. Photochem. Photobiol. A*, 2016, **317**, 88-99.

8. (a) J. Wu, G. Wang, D. Jin, J. Yuan, Y. Guan and J. Piper, *Chem. Commun.*, 2008, 365-367; (b) J. Wu, Z. Ye, G. Wang, D. Jin, J. Yuan, Y. Guan and J. Piper, *J. Mater. Chem.*, 2009, **19**, 1258-1264.

9. (a) D. Maurel, J. Kniazeff, G. Mathis, E. Trinquet, J.-P. Pin and H. Ansanay, *Anal. Biochem.*, 2004, **329**, 253-262; (b) J. M. Zwier, H. Bazin, L. Lamarque and G. Mathis, *Inorg. Chem.*, 2014, **53**, 1854-1866; (c) M. Rajendran, E. Yapici and L. W. Miller, *Inorg. Chem.*, 2014, **53**, 1839-1853; (d) S. Petoud, S. M. Cohen, J.-C. G. Bünzli and K. N. Raymond, *J. Am. Chem. Soc.*, 2003, **125**, 13324-13325; (e) J. Xu, T. M. Corneillie, E. G. Moore, G.-L. Law, N. G. Butlin and K. N. Raymond, *J. Am. Chem. Soc.*, 2011, **133**, 19900-19910; (f) B. Alpha, J.-M. Lehn and G. Mathis, *Angew. Chem.*, 1987, **99**, 259-261.

10. (a) S. V. Eliseeva, G. Auböck, F. van Mourik, A. Cannizzo, B. Song, E. Deiters, A.-S. Chauvin, M. Chergui and J.-C. G. Bünzli, *The J. Phys. Chem. B*, 2010, **114**, 2932-2937; (b) A. S. Chauvin, S. Comby, B. Song, C. D. Vandevyver, F. Thomas and J.-C. G. Bünzli, *Chem. Eur. J.*, 2007, **13**, 9515-9526; (c) E. Deiters, B. Song, A.-S. Chauvin, C. D. B. Vandevyver, F. Gumy and J.-C. G. Bünzli, *Chem. Eur. J.*, 2009, **15**, 885-900.

11. (a) Z. Dai, L. Tian, Y. Xiao, Z. Ye, R. Zhang and J. Yuan, *J. Mater. Chem. B*, 2013, **1**, 924-927; (b) S. J. Butler, M. Delbianco, L. Lamarque, B. K. McMahon, E. R. Neil, R. Pal, D. Parker, J. W. Walton and J. M. Zwier, *Dalton Trans.*, 2015, **44**, 4791-4803; (c) M. Li and P. R. Selvin, *J. Am. Chem. Soc.*, 1995, **117**, 8132-8138; (d) P. Kadjane, M. Starck, F. Camerel, D. Hill, N. Hildebrandt, R. Ziessel and L. J. Charbonnière, *Inorg. Chem.*, 2009, **48**, 4601-4603; (e) M. Starck, P. Kadjane, E. Bois, B. Darbouret, A. Incamps, R. Ziessel and L. J. Charbonnière, *Chem. Eur. J.*, 2011, **17**, 9164-9179.

12. (a) N. N. Katia, A. Lecointre, M. Regueiro-Figueroa, C. Platas-Iglesias and L. J. Charbonnière, *Inorg. Chem.*, 2011, **50**, 1689-1697; (b) S. Mizukami, K. Tonai, M. Kaneko and K. Kikuchi, *J. Am. Chem. Soc.*, 2008, **130**, 14376-14377; (c) G. Piszczek, B. P. Maliwal, I. Gryczynski, J. Dattelbaum and J. R. Lakowicz, *J. Fluoresc.*, 2001, **11**, 101-107; (d) V.-M. Mukkala, C. Sund, M. Kwiatkowski, P. Pasanen, M. Högberg, J. Kankare and H. Takalo, *Helv. Chim. Acta*, 1992, **75**, 1621-1632.

13. (a) L. Tian, Z. Dai, Z. Ye, B. Song and J. Yuan, *Analyst*, 2014, **139**, 1162-1167; (b) V. Divya, V. Sankar, K. G. Raghu and M. L. P. Reddy, *Dalton Trans.*, 2013, **42**, 12317-

12323; (c) J. Sun, B. Song, Z. Ye and J. Yuan, *Inorg. Chem.*, 2015, **54**, 11660-11668; (d) L. Zhang, L. Tian, Z. Ye, B. Song and J. Yuan, *Talanta*, 2013, **108**, 143-149; (e) G. L. Law, K. L. Wong, C. W. Y. Man, S. W. Tsao and W. T. Wong, *J. Biophotonics*, 2009, **2**, 718-724.

14. (a) S. J. Butler and D. Parker, *Chem. Soc. Rev.*, 2013, **42**, 1652-1666; (b) S. Pandya, J. Yu and D. Parker, *Dalton Trans.*, 2006, 2757-2766; (c) J. W. Walton, A. Bourdolle, S. J. Butler, M. Soulie, M. Delbianco, B. K. McMahon, R. Pal, H. Puschmann, J. M. Zwier, L. Lamarque, O. Maury, C. Andraud and D. Parker, *Chem. Commun.*, 2013, **49**, 1600-1602; (d) V. Placide, D. Pitrat, A. Grichine, A. Duperray, C. Andraud and O. Maury, *Tetrahedron Lett.*, 2014, **55**, 1357-1361.

15. M. Starck, R. Pal and D. Parker, *Chem. Eur. J.*, 2016, **22**, 570-580.

16. O. V. Vieira, R. J. Botelho and S. Grinstein, *Biochem. J.*, 2002, **366**, 689-704.

17. (a) L. He, Y. Li, C.-P. Tan, R.-R. Ye, M.-H. Chen, J.-J. Cao, L.-N. Ji and Z.-W. Mao, *Chemical Science*, 2015, **6**, 5409-5418; (b) L. He, S.-Y. Liao, C.-P. Tan, Y.-Y. Lu, C.-X. Xu, L.-N. Ji and Z.-W. Mao, *Chem. Commun.*, 2014, **50**, 5611-5614; (c) L. He, C.-P. Tan, R.-R. Ye, Y.-Z. Zhao, Y.-H. Liu, Q. Zhao, L.-N. Ji and Z.-W. Mao, *Angew. Chem.*, 2014, **53**, 12137-12141; (d) X. Zhu, W. Lu, Y. Zhang, A. Reed, B. Newton, Z. Fan, H. Yu, P. C. Ray and R. Gao, *Chem. Commun.*, 2011, **47**, 10311-10313; (e) L. Murphy, A. Congreve, L.-O. Palsson and J. A. G. Williams, *Chem. Commun.*, 2010, **46**, 8743-8745; (f) Y.-M. Ho, N.-P. B. Au, K.-L. Wong, C. T.-L. Chan, W.-M. Kwok, G.-L. Law, K.-K. Tang, W.-Y. Wong, C.-H. E. Ma and M. H.-W. Lam, *Chem. Commun.*, 2014, **50**, 4161-4163.

18. (a) S. R. Meech and D. Phillips, *J. Photochem.*, 1983, **23**, 193-217; (b) D. F. Eaton, *Pure Appl. Chem.*, 1988, **60**, 1107–1114; (c) G. A. Crosby and J. N. Demas, *The J. Phys. Chem.*, 1971, **75**, 991-1024.

19. J. K. Wilson, J. M. Sargent, A. W. Elgie, J. G. Hill and C. G. Taylor, *Br. J. Cancer*, 1990, **62**, 189-194.

20. (a) A. F. A. W. Woodward, A. R. Morales, J. Yu, A. F. Moore, A. D. Campiglia, E. V. Jucov, T. V. Timofeeva and K. D. Belfield, *Dalton Trans.*, 2014, **43**, 16639; (b) P. He, H. H. Wang, H. G. Yan, W. Hu, J. X. Shi and M. L. Gong, *Dalton Trans.*, 2010, **39**, 8919-8924.

21. (a) S. Sivakumar, M. L. P. Reddy, A. H. Cowley and K. V. Vasudevan, *Dalton Trans.*, 2010, **39**, 11690-11691; (b) A. R. Ramya, S. Varughese and M. L. P. Reddy, *Dalton Trans.*, 2014, **43**, 10940-10946.

22. S. Biju, Y. K. Eom, J.-C. G. Bünzli and H. K. Kim, *J. Mater. Chem. C*, 2013, **1**, 3454-3466.

23. (a) M. H. V. Werts, R. T. F. Jukes and J. W. Verhoeven, *Phys. Chem. Chem. Phys.*, 2002, **4**, 1542-1548; (b) N. M. Shavaleev, S. V. Eliseeva, R. Scopelliti and J.-C. G. Bünzli, *Inorg. Chem.*, 2010, **49**, 3927-3936; (c) B. Francis, C. Heering, R. O. Freire, M. L. P. Reddy and C. Janiak, *RSC Adv.*, 2015, **5**, 90720-90730; (d) B. Francis, D. B. A. Raj and M. L. P. Reddy, *Dalton Trans.*, 2010, **39**, 8084-8092.

24. (a) X. Chen, Y. Bi, T. Wang, P. Li, X. Yan, S. Hou, C. E. Bammert, J. Ju, K. M. Gibson, W. J. Pavan and L. Bi, *Sci. Rep.*, 2015, **5**, 9004; (b) X. Wang, D. M. Nguyen, C. O. Yanez, L. Rodriguez, H.-Y. Ahn, M. V. Bondar and K. D. Belfield, *J. Am. Chem. Soc.*, 2010, **132**, 12237-12239.

Chapter 4

Bright Red Luminescence and Triboluminescence from PMMA-Doped Polymer Film Materials Supported by Eu^{3+}-Triphenylphosphine Based β-Diketonate and 4,5-Bis(Diphenylphosphino)-9,9-Dimethylxanthene Oxide

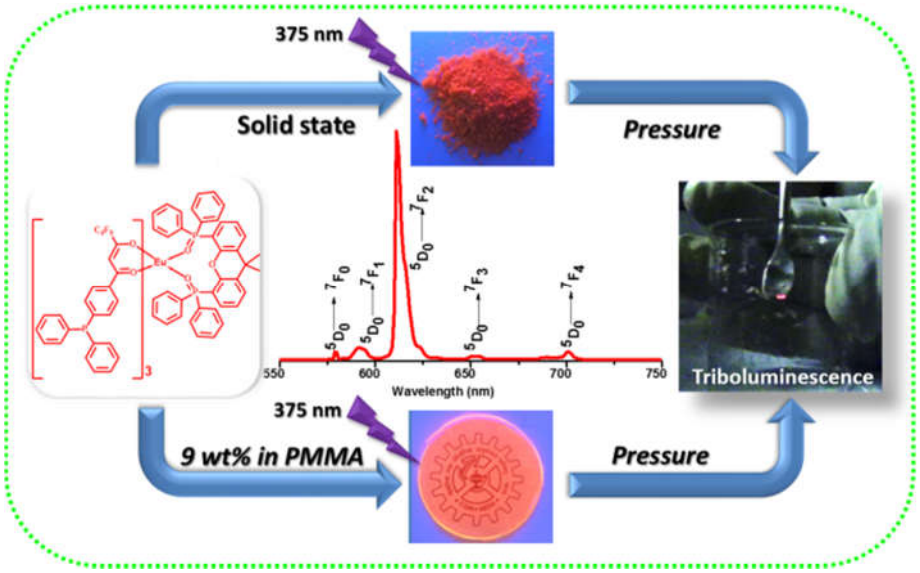

4.1. Abstract

Herein, a new β-diketonate ligand, namely, 1-(4-(diphenylphosphino)phenyl)-4,4,5,5,5-pentafluoropentane-1,3-dione (DPPFH) has been synthesized and utilized for the construction of an antenna complex of Eu^{3+} [$Eu(DPPF)_3(DDXPO)$] in the presence of a chelating ligand, 4,5-bis(diphenylphosphino)-9,9-dimethylxanthene oxide (DDXPO). The developed Eu^{3+} compound has been well characterized and investigated the photophysical properties. The designed Eu^{3+} complex displays bright red luminescence upon irradiation at the ligand-centered band at 375 nm with a quantum yield of 39% in the solid-state. Interestingly, the ternary Eu^{3+} complex also

exhibits brilliant triboluminescence in the daylight, which could be useful in the design of pressure and damage detection probes. In addition, the newly obtained Eu^{3+} complex was embedded into a PMMA matrix to form highly luminescent films having quantum yields as high as 45–50%. These plastic materials display enhanced thermal stability as compared to parent compound. The ground state coordination geometry of the typical Eu^{3+} complex was calculated using the Sparkle/RM1 model. The excellent agreement between the experimental and theoretically predicted photophysical data, attesting the efficacy of the theoretical approach implemented in the LUMPAC software (http://lumpac.pro.br).

T. M. George, S. J. Sajan, N. Gopakumar and M. L. P. Reddy; *J. Photochem. Photobiol. A,* **2016**, 317, 88–99.

4.2. Introduction

Luminescent Eu^{3+} coordination compounds based on β-diketones are seeing an unprecedented surge of interest in view of their outstanding applications in lighting, telecommunications, analytical sensors, security inks, anticounterfeiting tags, biomedical imaging, and solar energy conversion.[1] Due to the Laporte forbidden nature and intra-configurational character of the 4f transitions, the luminescence from Eu^{3+} ions is typically highly monochromatic, exhibits long-lived luminescent lifetimes.[2] The β-diketone ligand class is currently emerging as one of the important "antennas" in terms of high harvest emissions because of the effectiveness of the energy transfer from this ligand to the Ln^{3+} cation.[3] In part, this is due to the fact that the π–π* transition for β-diketones is intense and occurs over a significant range of wavelengths that is appropriate for lanthanide luminescence sensitization. As a consequence, a large number of Eu^{3+}-β-diketonate complexes have been investigated and these data are

covered in excellent review articles.[1k, 1l, 4] However, in view of the poor thermal stability, moisture sensitivity and feeble mechanical strength, the Eu^{3+}-β-diketonate complexes are always difficult to find potential applications in many of the optoelectronic technologies as luminescent materials. These inherent problems can be overcome by encapsulating the luminescent Eu^{3+}-β-diketonate complexes in suitable solid matrixes including polymers[1f, 5], sol–gel silica[3f, 6], mesoporous materials[7] and even in carbon nanotubes.[8]

The incorporation of luminescent Eu^{3+} complexes into polymers display several distinct advantages for the development of molecular materials, especially, thermal and chemical stability, flexibility, versatility, biocompatibility, hydrophobic–hydrophilic balance and the characteristic luminescence of lanthanide ions.[1e-h, 4a, 5, 9] All of these features offer an excellent opportunity for developing a new class of highly luminescent materials. Notably, poly-(methyl methacrylate) (PMMA) is a popular polymer matrix for use as a host for luminescent lanthanide complexes.[9c, 10] It is also recognized as a low-cost polymer, which has no light absorption longer than 250 nm. Furthermore, the carbonyl groups of PMMA can interact with Eu^{3+} ions and substitute the water molecules, thus reduces high frequency oscillators and in turn enhances the luminescence intensity.

Triphenylphosphine unit has well recognized as electron-transporting materials in Organic Light Emitting Diodes (OLEDs) due to their light-harvesting ability and

high thermal stability.[11] It is well documented that the replacement of C–H bonds in a β-diketonate ligand with lower-energy C–F oscillators is able to lower the vibration energy of the ligand, which decreases the energy loss caused by ligand vibration and enhances the emission intensity of the lanthanide ion. Further, due to the heavy-atom effect, which facilitates intersystem crossing, the lanthanide-centered luminescent properties are enhanced.[12] Based on these facts, herein, a new β-diketone ligand, namely, 1-(4-(diphenylphosphino)phenyl)-4,4,5,5,5-pentafluoropentane-1,3-dione has been designed by incorporating a rigid triphenylphosphine moiety as well as highly fluorinated alkyl group. The synthesized ligand has been used for the construction of a novel antenna complex of Eu^{3+} [$Eu(DPPF)_3(DDXPO)$] in the presence of a chelating ligand, 4,5-bis(diphenylphosphino)-9,9-dimethylxanthene oxide. The developed Eu^{3+} complex has been well characterized and investigated its photoluminescence properties. Furthermore, in the current study, the developed Eu^{3+} ternary complex has been embedded into PMMA films, characterized and evaluated their photophysical properties. Interestingly the developed ternary Eu^{3+} complex and its corresponding PMMA films also exhibit strong triboluminescence, which could be useful in the design of pressure and/or damage detection probes.

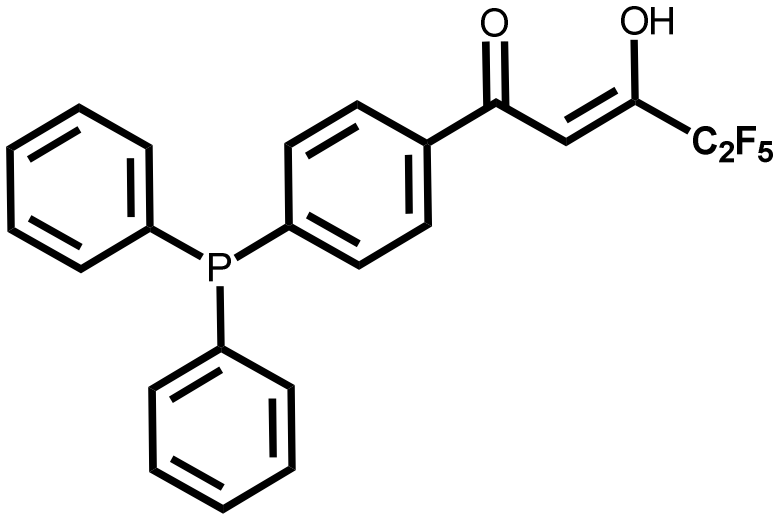

Figure 4.1. Structure of the ligand DPPFH.

4.3. Experimental Section

4.3.1. Materials and characterization

The following chemicals were acquired commercially and used without further purification: Europium(III) nitrate hexahydrate, 99.99% (Alfa Aesar); gadolinium(III) nitrate hexahydrate, 99.99% (Sigma-Aldrich); triphenylphosphine, 98% (Sigma-Aldrich); 4-bromooacetophenone 99% (Sigma-Aldrich); sodium hydride 60% dispersion in mineral oil (Sigma-Aldrich); ethyl pentafluoropropionate, 98% (Sigma-Aldrich); 4,5-bis(diphenylphosphino)-9,9-dimethylxanthene, 97% (Sigma-Aldrich); poly(methyl methacrylate), 98% (Sigma-Aldrich); palladium(II)acetate (Sigma-Aldrich). All the other chemicals used were of analytical reagent grade without further purification.

Elemental analyzes were performed with an Elementar - vario MICRO cube elemental analyzer. A Perkin-Elmer Spectrum two FT-IR spectrometer using KBr was used to obtain the IR spectral data and a Bruker 500 MHz NMR spectrometer was used to record the ^{1}H NMR (500 MHz), ^{13}C NMR (125.7 MHz) and ^{31}P NMR (202.44 MHz) spectra of the new compounds in chloroform-d solution. The chemical shifts are reported in parts per million relative to tetramethylsilane, $SiMe_4$ for ^{1}H NMR and ^{13}C NMR spectra and with respect to 85% phosphoric acid for ^{31}P NMR spectra. Electrospray ionization (ESI) mass spectra were recorded on a Thermo Scientific Exactive Benchtop LC/MS Orbitrap Mass Spectrometer. Matrix assisted laser desorption ionization time-of-flight (MALDI-TOF) mass spectra were recorded on KRATOS analytical spectrometer (Shimadzu Inc.) and the thermogravimetric analyses were performed on a TG/DTA-6200 (SII Nano Technology Inc., Japan). X-ray powder patterns of the samples were measured using X-ray powder diiffractometer (X'pert Pro PANalytical) using Cu−Kα radiation within the 2θ range 5 to 35°. FT-Raman spectra of the solid samples placed on a glass plate were recorded on a HR800 Lab RAM confocal Raman Spectrometer operating at 20 mW laser power using a Peltier cooled CCD detector. The laser source had an excitation wavelength of 633 nm and an acquisition time of 30 seconds using a 50 X objective. The molar absorption coefficient (ε) of the developed ligand and the corresponding lanthanide complexes were measured in THF solution on a UV-vis spectrophotometer (Shimadzu, UV-2450). The photoluminescence (PL) spectra were recorded on a Spex-Fluorolog FL22

spectrofluorimeter equipped with a double grating 0.22 m Spex 1680 monochromator and a 450W Xe lamp as the excitation source operating in the front face mode. The lifetime measurements were carried out at room temperature using a Spex 1040D phosphorimeter. The overall quantum yield ($\Phi_{overall}$) was measured using an integrating sphere in a SPEX Fluorolog spectrofluorimeter. The PL quantum yields of thin films ($\Phi_{overall}$) were determined using a calibrated integrating sphere system. A Xe-arc lamp was used to excite the thin film samples that were placed in the sphere. All samples were prepared by drop casting the material placed between two glass coverslips. The quantum yields were determined by comparing the spectral intensities of the lamp and the sample emission as reported in the literature.[13] Using this experimental setup and the integrating sphere system, the solid state fluorescence quantum yield of a thin film of the standard green OLED material tris-8-hydroxyquinolinolato aluminium (Alq_3) was determined to be 0.40, which is consistent with previously reported values.[14] Each sample was measured several times under slightly different experimental conditions. The estimated error for the quantum yields is (± 10%). Triboluminescence (TL) spectra were recorded at room temperature by exciting the samples impulsively using a technique in which loads of different weights (0.1−0.6 kg) were dropped onto the samples, which were placed on a transparent Lucite plate, from different heights (5−15 cm) using a guiding cylinder. The luminescence was monitored by an RCA 931 photomultiplier tube (PMT) positioned below the transparent plate. The PMT was connected to a Scientific HM205 storage oscilloscope. The TL spectra were recorded

using a grating monochromator MDR-41 having 1500 lines/mm in 400-1000 nm range .[15]

4.3.2. Synthesis of 1-(4-(diphenylphosphino)phenyl)ethanone

1-(4-(Diphenylphosphino)phenyl)ethanone was synthesized according to previous literature reports as described in Scheme 4.1.[16] Bromoacetophenone (1.0 mmol), triphenylphosphine (603 mg, 2.3 mmol) and palladium(II) acetate (22.4 mg, 0.1 mmol, 10 mol%) were charged to a Teflon screw-capped Schlenk flask. Evacuated and backfilled with nitrogen three cycles. The solution was heated to 115°C for 24 h. The reaction mixture was then cooled down and dichloromethane was added. The residue was purified by column chromatography on silica gel eluting with ethyl acetate and hexane (0.5:10) to obtain the pure product. Yield: 75%. ^{1}H NMR ($CDCl_3$, 500 MHz) δ (ppm): 7.95 (d, 2H, J = 8 Hz) 7.29 (m, 12H), 2.48 (s, 3H); ^{13}C NMR (125 MHz, $CDCl_3$) δ (ppm): 197.79, 144.40, 136.83, 136.16, 134.08, 133.91, 132.10, 128.09, 127.29, 77.26-76.75 ($CDCl_3$), 26.87; ^{31}P NMR (202.44 MHz, $CDCl_3$) δ (ppm): -5.07; m/z = 305.22 $(M+H)^+$.

4.3.3. Synthesis of the ligand 1-(4-(diphenylphosphino)phenyl)-4,4,5,5,5-pentafluoropentane-1,3-dione (DPPFH)

The ligand DPPFH was synthesized by a modified Claisen condensation procedure according to Scheme 4.1. 1-(4-(diphenylphosphino)phenyl)ethanone (1 mmol) and ethyl pentafluoropropionate (1 mmol) were added to 20 mL of dry tetrahydrofuran (THF) and stirred for 10 min at 0 °C in an ice bath. To this solution, sodium hydride (2 mmol) was added in an inert atmosphere and stirred for 30 min followed by further stirring at 70 °C for 12 h. To the

resulting solution, 2 M HCl (50 mL) was added, and extracted twice with dichloromethane (2×35 mL). The organic layer was separated and dried over Na_2SO_4, and the solvent was evaporated. The crude product thus obtained is then purified by column chromatography on silica gel with a mixture of ethyl acetate and hexane (1:10) as the eluent to get the product as a yellow solid. Yield: 75%. Elemental analysis (%): calculated for $C_{23}H_{16}F_5PO_2$ (450.18): C 61.34, H 3.58; Found: C 61.41, H 3.63. ^{1}H NMR ($CDC1_3$, 500 MHz) δ (ppm): 14.98 (broad, enol–OH), 7.87 (d, 2H, J = 8 Hz), 7.39 (m, 12H), 6.61 (s, 1H). ^{13}C NMR (125 MHz, $CDCl_3$) δ (ppm): 185.24, 179.15, 146.48, 135.68, 134.00, 133.61, 133.47, 132.38, 129.42, 128.87, 128.81, 127.34, 93.63, 77.28-76.78 ($CDCl_3$). ^{31}P NMR (202.44 MHz, $CDCl_3$) δ (ppm): -4.39. FT-IR (KBr) ν_{max} (cm^{-1}): 2923, 1590, 1438, 1328, 1242, 1195, 1072, 798; m/z = 450.94 $(M+H)^+$.

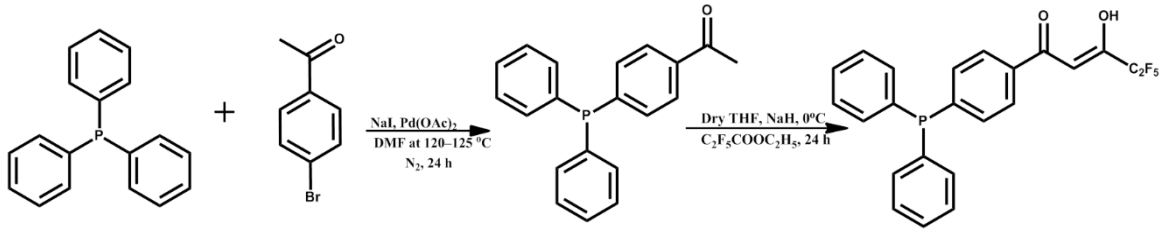

Scheme 4.1. Synthetic procedure for the ligand DPPFH.

4.3.4. Synthesis of the ligand 4,5-Bis(diphenylphosphino)-9,9-dimethylxanthene oxide (DDXPO)

The corresponding phosphine (5.0 mmol) was dissolved in 10 mL of 1,4-dioxane solution, to which 1.0 mL of 30% H_2O_2 (10.5 mmol) was added dropwise with vigorous stirring. The resultant mixture was then stirred for 2 h and then 10 mL of water was

added to the reaction mixture to arrest the reaction. The mixture was extracted with 3 × 30 mL of dichloromethane. The oily phase was then washed with 2 × 30 mL of water to remove 1,4-dioxane. The dichloromethane layer was dried with Na_2SO_4. The solvent was removed in vacuo. The product was recrystallized from dichloromethane. Yield: 95%. Elemental analysis (%): calculated for $C_{39}H_{32}O_3P_2$ (610.18): C 76.71, H 5.28; Found: C 76.52, H 5.40. ^{1}H NMR ($CDCl_3$, 500 MHz) δ (ppm): 7.61 (d, 2 H, J = 7.5 Hz), 7.41 (m, 12 H), 7.30 (m, 8 H), 6.99 (t, 2 H), 6.80–6.76 (m, 2 H), 1.70 (s, 6 H). ^{31}P NMR ($CDCl_3$, 202.44 MHz) δ (ppm): 30.97. FT-IR (KBr) ν_{max} (cm^{-1}): 1727, 1670, 1436, 1401, 1229, 1191, 1114, 875, 785, 746, 719, 694. m/z = 611.31 $(M+H)^+$.

4.3.5. Synthesis of complexes $Ln(DPPF)_3(H_2O)_2$ [Ln = Eu (1) and Gd (2)]

To a solution of DPPFH (6 mmol) in THF, added 6 mmol of NaOH in water and stirred for 5 min. To this mixture, 2 mmol of $Ln(NO_3)_3{\cdot}6(H_2O)$ in 2 mL water was added dropwise and stirred for 24 h at room temperature (Scheme 4.2). The reaction mixture was extracted with $CHCl_3$ and crude products were obtained after solvent evaporation. The products were purified by recrystallization from chloroform solution and used for further analysis and photophysical studies.

$Eu(DPPF)_3(H_2O)_2$ (1). Elemental analysis (%): calculated for $C_{69}H_{49}F_{15}P_3O_8Eu$ (1535.98): C 53.95, H 3.22 Found: C 53.89, H 3.19. FT-IR (KBr) ν_{max} (cm^{-1}): 3434, 2922, 1614, 1470, 1327, 1218, 1145, 1075, 745. m/z = 1518.14 $[Eu(DPPF)_3(H_2O)]^+$. ^{31}PNMR ($CDCl_3$, 202.44 MHz) δ (ppm): -4.77.

$Gd(DPPF)_3(H_2O)_2$ (2). Elemental analysis (%): calculated for $C_{69}H_{49}F_{15}P_3O_8Gd$ (1541.27): C 53.77, H 3.20. Found: C 53.65, H 3.27. FT-IR (KBr) ν_{max} (cm^{-1}): 3442, 2925, 1621, 1472, 1327, 1213, 1122, 1016, 748. m/z = 1523.10 $[Gd(DPPF)_3(H_2O)]^+$.

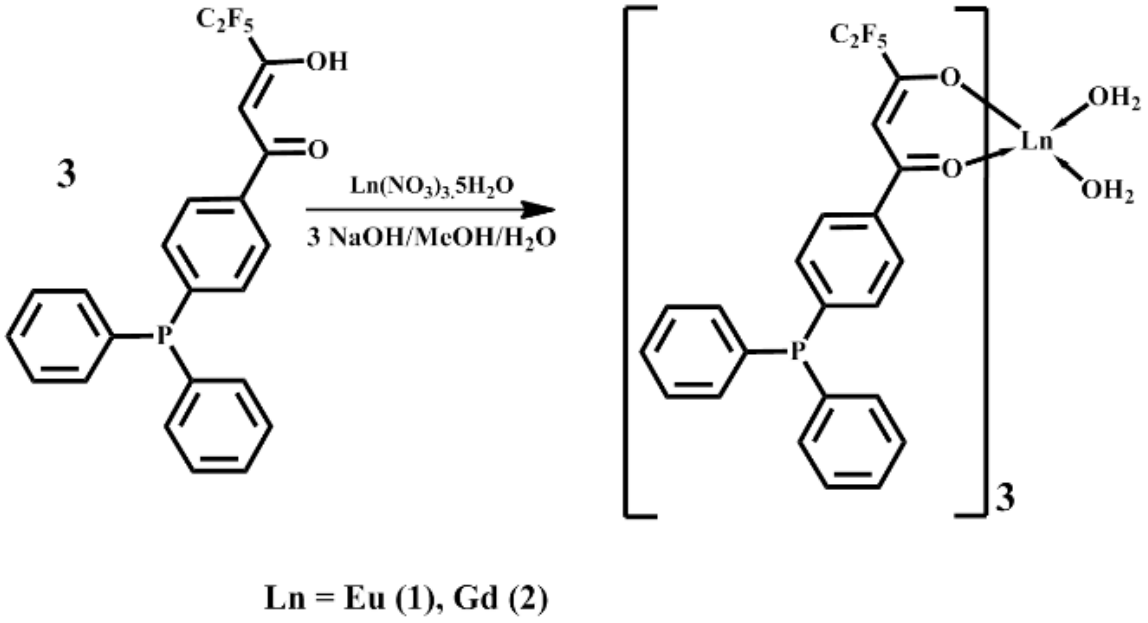

Scheme 4.2. Synthesis of the Ln^{3+} (Ln = Eu and Gd) binary complexes.

4.3.6. Synthesis of $Eu(DPPF)_3(DDXPO)$ ternary complex

Ternary Eu^{3+} complex was prepared by stirring equimolar solutions of complex **1** and DDXPO in $CHCl_3$ solution for 12 h at 70°C. The products were isolated by solvent evaporation and purified by recrystallization from a chloroform mixture. The synthesis procedure is illustrated in scheme 4.3.

$Eu(DPPF)_3(DDXPO)$ (3). Elemental analysis (%): calculated for $C_{108}H_{77}F_{15}P_5O_9Eu$ (2110.57): C 61.46, H 3.68; Found: C 61.39, H 3.63. IR (KBr) ν_{max} (cm^{-1}): 3061, 1621,

1519, 1437, 1327, 1183, 1119, 1016, 695. m/z = 1345.83 $[Eu(DPPF)_2(DDXPO)]^+$. ^{31}PNMR ($CDCl_3$, 202.44 MHz) δ (ppm): -4.77, -88.42.

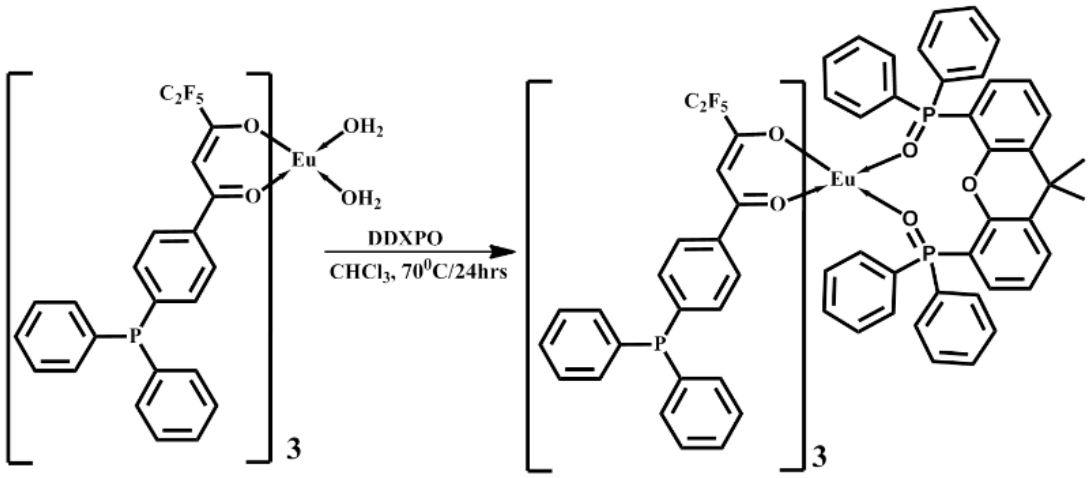

Scheme 4.3. Synthesis of the Eu^{3+} ternary complex.

4.3.7. Synthesis of Eu^{3+} complex-doped PMMA polymer films.

The PMMA polymer was doped with the Eu^{3+} complex **3** in the proportions 5, 7, 9, 11 and 13% (w/w). The PMMA powder was dissolved in chloroform, followed by addition of the required amount of complex **3** in chloroform solution, and the resulting mixture was heated at 40 °C for 30 min. The polymer film was obtained after evaporation of excess solvent at 60 °C.[17]

4.4. Results and Discussion

4.4.1. Synthesis and characterization of the DPPFH ligand and Ln^{3+} complexes 1-3

The β-diketonate ligand (DPPFH) was synthesized from the 1-(4-(diphenylphosphino)phenyl) ethanone and ethylpentafluoropropionate ester by a

modified Claisen condensation reaction with an overall yield of 75%. The protocols used for the synthesis are outlined in scheme 4.1. The ligand, was characterized by ^{1}H NMR, ^{13}C NMR, ^{31}P NMR, FT-IR, and mass spectroscopic (FAB-MS) methods, as well as by elemental analysis. ^{1}H NMR analysis shows that the β-diketonate ligand mainly exists as enol form in chloroform solution. The chelating ligand 4,5-bis(diphenylphosphino)-9,9-dimethylxanthene oxide (DDXPO) was synthesized according to reported procedure described elsewhere.[3e, 5] The Ln^{3+} (Eu^{3+}, Gd^{3+}) complexes were prepared as illustrated in schemes 4.2 and 4.3. The developed lanthanide complexes (**1-3**) were characterized by FT-IR, mass spectroscopy (FAB-MS), and elemental analysis. The elemental analysis and FAB-MS studies disclosed that the central Ln^{3+} ion is coordinated to three β-diketonate ligands. In the case of ternary complex **3**, one molecule of the bidentate phosphine oxide, DDXPO is also present in the coordination sphere.

The FT-IR spectra of complexes **1** and **2** exhibit a broad absorption in the 3000−3500 cm^{-1} region, indicates the existence of solvent molecules in the coordination sphere of the Ln^{3+} ion. The absence of this broad band in the 3000−3500 cm^{-1} region in complex **3** inferred that the solvent molecules have been successfully displaced by the bidentate phosphine oxide ligand. The carbonyl stretching frequency for the β-diketonate ligand, DPPFH (1590 cm^{-1}) is shifted to higher wavenumbers in complexes **1−3** (1614 cm^{-1} for **1**; 1621 cm^{-1} for **2**; 1621 cm^{-1} for **3**), thus indicating the

coordination of the carbonyl oxygen to the Ln^{3+} ions. The P=O stretching frequency of DDXPO at 1191 cm^{-1} shifted to 1183 cm^{-1} in complex **3** confirms the involvement of the P=O bond of DDXPO in complex formation. The upfield shift of P=O resonance in ^{31}P NMR spectra of the complex **3** as compared to that of the free ligand, further supports the coordination of DDXPO with the Eu^{3+}.

The thermal behavior of the complexes **1-3** were investigated by means of thermo-gravimetric analysis (TGA) under nitrogen atmosphere, and the thermograms are given in the figures 4.2 and 4.3. The complexes **1** and **2** undergoes a mass loss of approximately 2% (Calcd: 2.08%) in the first step (120 to 160°C), which corresponds to the elimination of the coordinated water molecules. In contrast, complex **3** is stable up to 340°C, above which it decomposes. This implies that the replacement of coordinated water molecules in complex **1** by the bidentate phosphine oxide ligand, significantly enhances the thermal stability of the ternary complex with DDXPO. These results are in good agreement with the FT-IR data. The total weight loss occurred in the thermal analysis of all these complexes are much lower than that calculated value for the non-volatile lanthanide oxide, indicating the partial sublimation of these complexes under atmospheric pressure, which is commonly observed in the case of fluorinated *β*-diketonate complexes. These residual masses correspond to the formation of non-volatile europium oxyfluoride.[5]

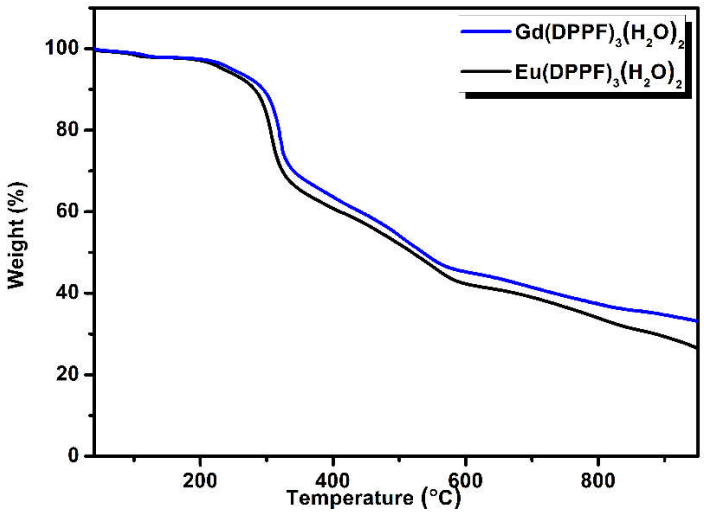

Figure 4.2. Thermogravimetric curves for the complexes **1** and **2**.

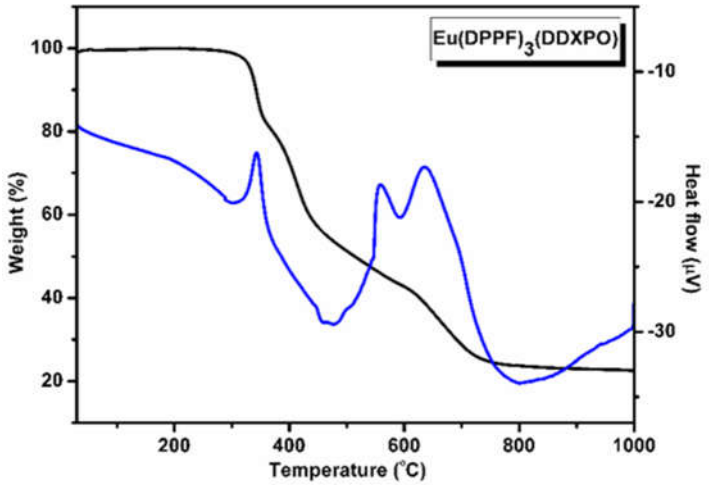

Figure 4.3. Thermogravimetric curve for the complex **3**.

4.4.2. Geometry optimization of Eu^{3+} complexes (1) and (3) by the Sparkle/RM1 model

Our attempts to grow single crystals for the Eu^{3+} complexes **1** and **3** were not fruitful. Therefore in the present study the molecular structures of the designed complexes were optimized using the theoretical models described elsewhere.[18] The optimized molecular structures of the typical Eu^{3+} complexes **1** and **3** predicted by Sparkle/RM1 model[18b]

are displayed in figures 4.4 and 4.5, respectively. The geometry optimization was performed with the semiempirical Sparkle model implemented in MOPAC2012.[18c] The optimization of the ground state geometry by the Sparkle/RM1 model allows accurate geometry prediction as ab initio/ECP (effective core potential) calculations on lanthanide complexes, while being hundreds of times faster.[19] The keywords used were RM1, SPARKLE, PRECISE, GNORM = 0.25, T = 10D, GEO-OK and XYZ. The singlet and triplet excited state energies were determined by using the semiempirical INDO/S-CIS (Intermediate Neglect of Differential Overlap/Spectroscopic-Configuration Interaction Single)[20] method implemented in ORCA.[21] The spherical atomic coordinates calculated *via* Sparkle/RM1 coordination polyhedron of these compounds are summarized in tables 4.1 and 4.2. In complex **1**, the central Eu^{3+} ion is surrounded by eight oxygen atoms, two are furnished from the water molecules and the remaining six oxygen atoms from the three *β*-diketonate ligands. On the other hand, in complex **3**, the central Eu^{3+} ion is coordinated with eight oxygen atoms, six are from the three bidentate *β*-diketonate ligands, and the other two oxygen atoms from the chelated phosphine oxide (DDXPO). The coordination geometry of the metal centre is best described as distorted square-antiprism in both the complexes. In complex **1** the average bond length between the Eu^{3+} ion and the *β*-diketonate oxygen atoms is 2.448 Å, which is shorter than that of the average bond length between the Eu^{3+} ion and the water oxygen atoms is 2.474 Å. In complex **3** the average bond length between the Eu^{3+} ion and the *β*-diketonate oxygen atoms is 2.470 Å. On the other hand, shorter average

bond length between the Eu^{3+} ion and the bidentate phosphine oxide oxygen atoms is noted (2.401 Å) in **3**. It is interesting to note that the predicted bond lengths are in good agreement with the single crystal X-ray analysis data of Eu^{3+}-*β*-diketonate complexes reported earlier from our laboratory.[5] This shows the efficacy of the theoretical model followed in the current study.

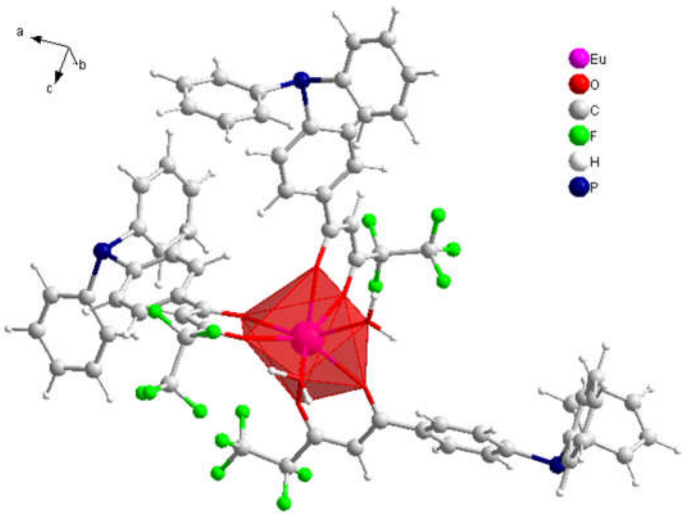

Figure 4.4. The ground state geometry of the complex **1** calculated using the Sparkle/RM 1 model.

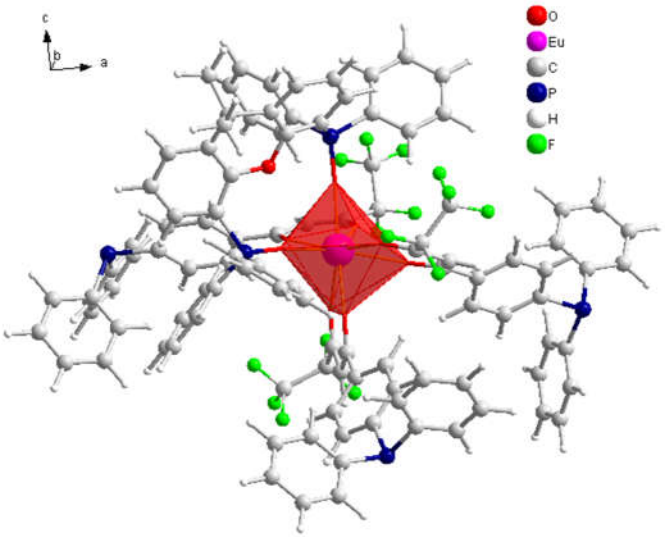

Figure 4.5. The ground state geometry of the complex **3** calculated using the Sparkle/RM 1 model.

Table 4.1. Spherical atomic coordinates calculated *via* Sparkle/RM1 coordination polyhedron of the complex **1.**

Atoms	**R (Å)**	**θ (°)**	**Φ (°)**
Eu	0.00000	0.000	0.000
O(2)(DPPFH)	2.44790	95.926	3.854
O(3)(DPPFH)	2.45147	61.710	311.443
O(4)(DPPFH)	2.44692	52.101	85.504
O(5)(DPPFH)	2.44897	73.207	152.103
O(6)(DPPFH)	2.44640	153.512	104.512
O(7)(DPPFH)	2.44831	144.788	273.954
O(8)(H_2O)	2.47596	104.954	208.625
O(9)(H_2O)	2.47132	38.303	240.858

Table 4.2. Spherical atomic coordinates calculated *via* Sparkle/RM1 coordination polyhedron of the complex **3.**

Atoms	**R (Å)**	**θ (°)**	**Φ (°)**
Eu	0.00000	0.000	0.000
O(2)(DPPFH)	2.46067	108.155	8.749
O(3)(DPPFH)	2.47584	79.109	315.136
O(4)(DPPFH)	2.47251	83.981	80.023
O(5)(DPPFH)	2.47179	85.437	140.990
O(6)(DPPFH)	2.47011	154.788	125.809
O(7)(DPPFH)	2.46672	142.754	274.880
O(8)(DDXPO)	2.40267	76.446	221.515
O(9)(DDXPO)	2.39825	4.299	30.225

4.4.3. Electronic Spectroscopy

Figure 4.6 displays the UV-vis absorption spectra of the free ligands DPPFH, DDXPO and their corresponding Eu^{3+} complexes (**1** and **3**) recorded in THF (c = 1 $\times 10^{-5}$ M) solution at 298 K. The maximum absorption band at 350 nm for β-diketonate ligand and the corresponding complexes, which are attributable to singlet-singlet (n-π^*) enolic absorption of the β-diketonate.[3d, 7a, 8a, 9b] A hump observed around 260 nm in DPPFH and complexes is due to singlet-singlet π-π^* absorption of the aromatic rings in the β-diketonate ligand.[22] The absorption maximum observed around 280 nm in DDXPO and the hump observed in the above region in complex **3** is due to the singlet-singlet π-π^* absorption of the ancillary ligand DDXPO.[5] The electronic transitions of the aromatic moiety of the β-diketonate ligand (peak at ca. 250-280 nm) and the chelated bidentate phosphine oxide (peak at ca. 250-300 nm) units are overlapped. The spectral shapes of the complexes are found to be similar to that DPPFH, highlighting that the coordination of Eu^{3+} ion does not significantly influence the energy of the singlet levels of the β-diketonate ligand. The estimated molar absorption coefficient values of the complexes **1-3** at 350 nm are found be 4.12 $\times$ 10^4, 4.15 $\times$ 10^4, and 4.25 $\times$ 10^4 L mol^{-1} cm^{-1}, respectively. These values are found to be about three times higher than that of the ligand (1.3 $\times$ 10^4 L mol^{-1} cm^{-1} at 350 nm), indicating the presence of three β-diketonate ligands in the corresponding complexes. Further, the large molar absorption coefficient values noted in the present systems clearly indicates that the developed new ligand has a strong ability to absorb light.

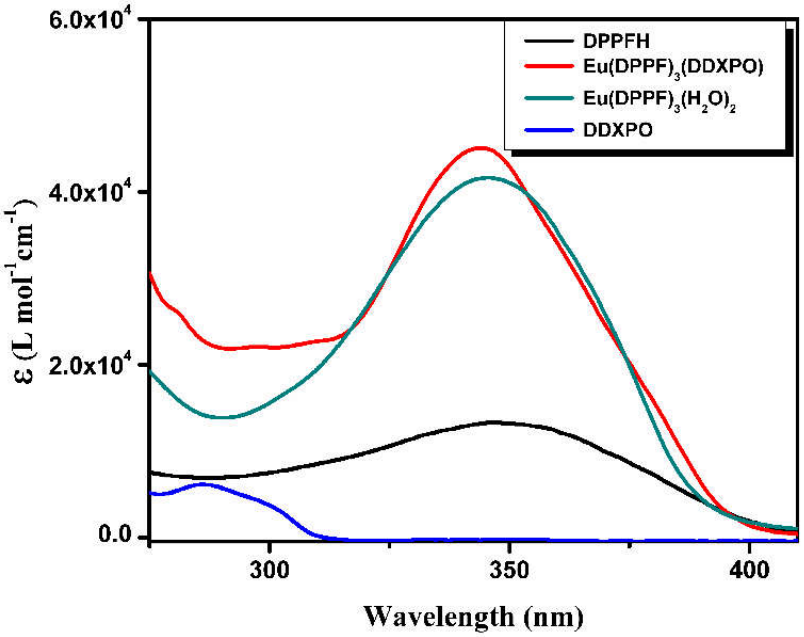

Figure 4.6. UV–vis absorption spectra of the ligands DPPFH and DDXPO and complexes **1** and **3** in THF (c = 1 × 10^{-5} M) solution at 298K.

4.4.4. Photophysical properties

4.4.4.1. Solid-state photoluminescence (PL) properties of Eu^{3+} complexes

The solid-state excitation and emission spectra of Eu^{3+} complexes **1** and **3** recorded at room temperature (298 K) are depicted in figure 4.7. The excitation profiles were recorded by monitoring the intense $^5D_0 \rightarrow {}^7F_2$ (612 nm) transition of the Eu^{3+} ion. The excitation spectra of the compounds exhibit a broad band between 275-400 nm region, which is due to the π–π* electronic transitions of the coordinated ligands. The absence of any absorption bands corresponding to f-f transitions of the Eu^{3+} ion proves that the luminescence sensitization *via* excitation of the ligand is effective. The ambient-temperature emission spectra of the Eu^{3+} complexes **1** and **3** excited at their excitation maxima (λ_{exc} = 375 nm) display characteristic narrow emission bands arising from the

intra-configurational $^5D_0 \rightarrow {}^7F_J$ (J = 0-4) transitions of the Eu^{3+} ion.[3d, 5, 22-23] Among the emission peaks, the intense $^5D_0 \rightarrow {}^7F_2$ peak points to a highly polarizable chemical environment around the Eu^{3+} ion and is responsible for the observed red emission. Moreover, the presence of a single and sharp peak at 580 nm ($^5D_0 \rightarrow {}^7F_0$) indicates the existence of single chemical environment around the Eu^{3+} ion of the point group symmetry C_s, C_n or C_{nv}.[3d, 3f, 5, 8a, 22-23] It is clear from the emission spectrum that the luminescence intensity of the ternary complex **3** was significantly enhanced (2.5-fold) as compared to the precursor complex **1**, by the displacement of water molecules from the coordination sphere by the rigid chelate phosphine oxide (DDXPO). The absence of ligand based emission in the region 385-500 nm, indicates an efficient ligand-to-metal energy transfer process.

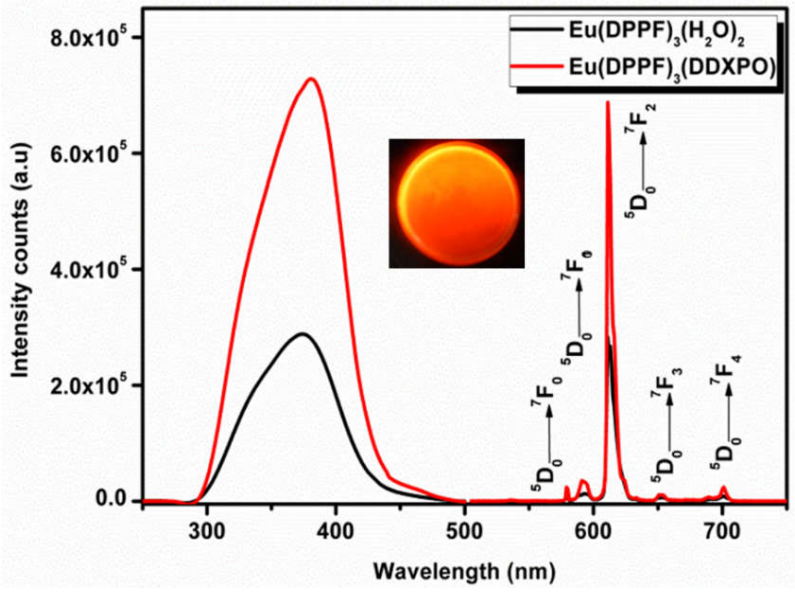

Figure 4.7. Room temperature (298 K) excitation and emission spectra of complexes **1** and **3** in the solid state.

The luminescence decay times (τ_{obs}) for the Eu^{3+}-*β*-diketonate complexes (**1** and **3**) were measured at room temperature using an excitation wavelength that maximizes the Eu^{3+} emission intensity and were monitored by the most intense emission band at 612 nm. The lifetime profiles for all the complexes fitted with single exponential, clearly demonstrate the presence of one emissive Eu^{3+} centre. Typical decay profiles for the complexes are displayed in figure 4.8. The corresponding lifetime values are listed in Table 4.3. The shorter $^5D_0$ lifetime noted for Eu^{3+} complex **1** may be due to the dominant non-radiative decay channels associated with vibronic coupling on account of the presence of water molecules in the coordination sphere.[24] This value is essentially temperature dependent, (τ_{obs} = 330 μs at 298 K; 503 μs in 77 K) showing approximately 2-fold enhancement, while going from 298 to 77 K, thereby reflecting the presence of thermally activated deactivation processes. This effect has been well-documented for several other hydrated Eu^{3+}-*β*-diketonate complexes.[25] On the other hand, the lifetime value of the ternary complex **3** is found to be significantly higher (557 μs) than the corresponding binary complex (330 μs). This may be due to the dramatic decrease of the non-radiative decay rates as compared to the precursor complex. However, the lifetime value of the ternary complex is almost independent of temperature (τ_{obs} = 557 μs at 298 K; 578 μs in 77 K).

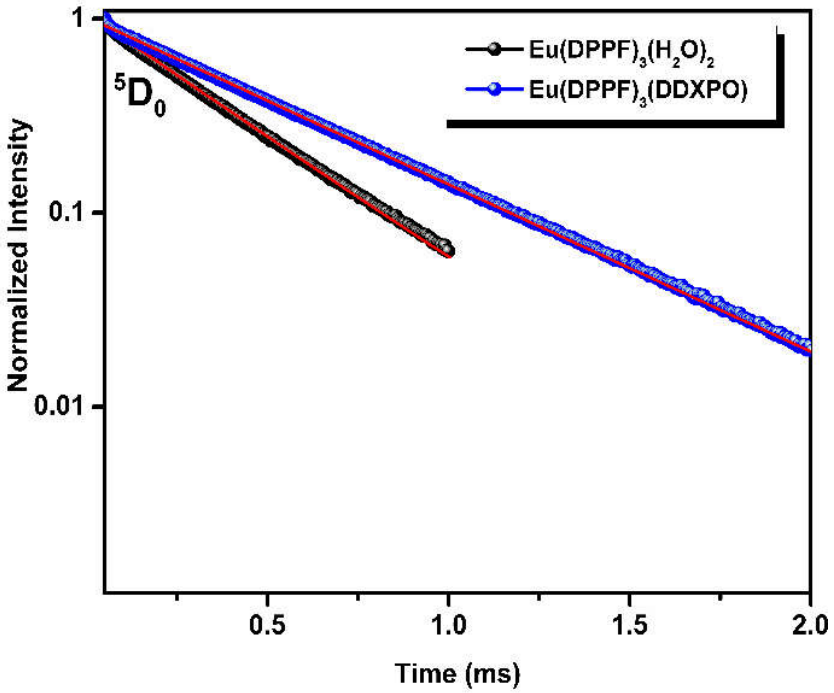

Figure 4.8. Experimental luminescence decay profiles for complexes **1** and **3** in solid state monitored at approximately 612 nm and excited 375 nm.

Table 4.3. Comparison of experimental and theoretical intensity parameters (Ω_λ , where λ = 2, 4 and 6), radiative (A_{RAD}) and non-radiative (A_{NR}) rates intrinsic quantum yield (Φ_{Ln}, %) and overall quantum yield ($\Phi_{Overall}$, %) for complex **1** and **3**.

Complex	$\Omega_2/10^{-20}$ cm^2	$\Omega_4/10^{-20}$ cm^2	$\Omega_6/10^{-20}$ cm^2	A_{RAD} (s^{-1})	A_{NR} (s^{-1})	Φ_{Ln}(%)	Φ_{Sens}(%)	$\Phi_{overall}$ (%)
1[a]	20.36	2.90	-	739	2292	24	67	18
1[b]	20.35	2.90	0.2620	705	2325	23	-	23
3[a]	22.11	4.62	-	825	971	46	84	39
3[b]	22.11	4.62	0.4375	783	1012	44	-	43

[a] = Experimental, = [b] Sparkle/RM1.

In order to get better insight into the quantum efficiency of the developed Eu^{3+} complexes, it was necessary to analyze the emission spectrum in terms of eqn. 1,

$$\Phi_{overall} = \Phi_{sens} \times \Phi_{Ln} = \Phi_{sens} \times (\tau_{obs}/\tau_{rad}) \quad \textbf{(1)}$$

Where $\Phi_{overall}$ and Φ_{Ln} represent the ligand-sensitized and intrinsic luminescence quantum yields of Eu^{3+}; Φ_{sens} represents the efficiency of the ligand-to-metal energy transfer, τ_{obs} and τ_{rad} are the observed and the radiative lifetimes of Eu^{3+} ($^5D_0$).[1f, 26] The intrinsic luminescence quantum yields of Eu^{3+} cannot be estimated experimentally due to the low absorption intensities of direct f-f excitation.[27] Therefore, the radiative lifetime of Eu^{3+} ($^5D_0$) can be estimated using the following relationship.

$$1/\tau_{rad} = A_{MD,0} \times n^3 \times (I_{tot}/I_{MD}) \quad \textbf{(2)}$$

where n represents the refractive index (1.5) of the medium. $A_{MD,0}$ is the spontaneous emission probability for the $^5D_0 \rightarrow {}^7F_1$ transition in *vacuo* (14.65 s^{-1}), and I_{tot}/I_{MD} signifies the ratio of the total integrated intensity of the corrected Eu^{3+} emission spectrum to the integrated intensity of the magnetic dipole $^5D_0 \rightarrow {}^7F_1$ transition.[28] The intrinsic quantum yield for the designed Eu^{3+}-β-diketonate complexes (**1** and **3**) has been calculated from the ratio τ_{obs}/τ_{rad} and the values are given in table 4.3. The overall quantum yields ($\Phi_{overall}$), radiative (A_{RAD}) and non-radiative (A_{NR}) decay rates and energy transfer efficiencies (Φ_{sens}) are also presented in Table 4.3. It is clear from the Table 3 that complex **1**, having water molecules in the coordination sphere exhibits lower quantum yield. This is due to the presence of O–H oscillators in the system, which effectively quenches the luminescence of the Eu^{3+} ion. The replacement of solvent molecules by the chelating phosphine oxide molecule results in an approximately 2-

fold increase in the overall quantum yield of Eu^{3+}-β-diketonate complexes (from 18 to 39 % in complex **3**). The substantial contribution of the chelating phosphine oxide to the overall sensitization of Eu^{3+}-centred luminescence in complex **3** is confirmed by (i) an increase in the intrinsic quantum yield by a factor of 2 which results from the removal of quenching effects of the O-H vibrations and (ii) the significant enhancement of Φ_{sens} from 67 to 84 %. This is in accordance with the substantial decrease of the non-radiative decay rate (A_{NR}) from 2292 to 971 s^{-1}.

The experimental intensity parameters (Ω_2 and Ω_4) for the developed Eu^{3+} complexes (**1** and **3**) were determined from the corresponding emission spectra, based on the $^5D_0 \rightarrow {}^7F_2$ and $^5D_0 \rightarrow {}^7F_4$ electronic transitions of the Eu^{3+} ion, and they are estimated according to the following eqn. 3.

$$\Omega_{\lambda} = \frac{4e^2\omega^3 A_{0J}}{3\hbar\chi \left\langle {}^7F_J \left\| U^{(\lambda)} \right\| {}^5D_0 \right\rangle^2} \qquad \textbf{(3)}$$

where A_{0J} is the coefficient of spontaneous emission for the $^5D_0 \rightarrow {}^7F_J$ transition, χ is the Lorentz local-field correction term (given by $\chi = (n(n^2 + 2)^2)/9$, where n is the refractive index of the medium (in this case, n = 1.5)), and U is the square reduced matrix element whose values are 0.0032, 0.0023, and 0.0002 for λ = 2, 4, and 6, respectively.[29] The transition $^5D_0 \rightarrow {}^7F_6$ is not observed experimentally; thus, the experimental Ω_6 parameter cannot be estimated. Theoretical values of the intensity parameters were obtained using module#3 of Lumpac software.[30] The experimental and theoretical values of intensity parameters are presented in

Table 4.3. It is interesting to note that there is an excellent agreement between the experimental and theoretical intensity parameter values, which demonstrates the efficacy of the theoretical models followed in the present study. The Ω_6 parameter was only determined theoretically, since the $^5D_0 \rightarrow {}^7F_{5,6}$ transitions are not noticed experimentally. The high Ω_2 values observed in both the Eu^{3+} complexes can be explained on the basis of hypersensitive behaviour of the $^5D_0 \rightarrow {}^7F_2$ transition.[31] This suggests that the dynamic coupling mechanism is quite operative in these complexes, and the chemical environment is highly polarisable. On the other hand, the Ω_4 parameter is less sensitive to the coordination sphere than Ω_2. However, these values reflect on the chemical environment rigidity surrounding the Eu^{3+} cation.[22]

The theoretical singlet and triplet energies, energy transfer and back transfer rates to the $^5D_4$ level from the singlet state (S_1), energy transfer and back-transfer rates to the $^5D_1$ and $^5D_0$ levels from the ligand triplet state (T_1) and R_L parameters obtained from the Lumpac software are summarized in table 4.4.[32] For the complex **1**, the energies of the singlet and triplet states calculated for the Sparkle/RM1 structure using the INDO/S-CIS method [20a, 33] are 34,918 cm^{-1} and 22,279 cm^{-1}, respectively. The same physical quantities obtained using the complex **3** structure are 36,017 cm^{-1} and 25,028 cm^{-1}, respectively. The R_L parameter is the distance from Eu^{3+} ion nucleus to the donor state located at the organic ligands. This quantity has been calculated by eqn. 4

$$R_L = \frac{\sum_i c_i^2 R_{L,i}}{\sum_i c_i^2} \qquad \textbf{(4)}$$

Where c_i being the molecular orbital coefficient of the atom *i* contributing to the ligand state (triplet or singlet) involved in the energy transfer, and $R_{L,i}$ corresponding to the distance from atom *i* to the Eu^{3+} ion. The two complexes show favorable R_L values for obtaining efficient energy transfer rates. It is clear from Table 4.4 that the theoretically predicted triplet energy transfer rate of Eu^{3+} complexes **1** and **3** is found to be significantly larger than the singlet energy transfer rate. On the other hand, it is interesting to note that the back energy transfer rates in complex **3** are found to be extremely low.

Table 4.4. Calculated values of excited state singlet and triplet energies, R_L values, intramolecular energy transfer (W_{ET}) and back-transfer (W_{BT}) rates for complexes **1** and **3**.

Parameters		**$Eu(DPPF)_3(H_2O)_2$ (1)**	**$Eu(DPPF)_3(DDXPO)$ (3)**
Singlet energy (cm^{-1})		34918	36017
***R_L* Singlet (Å)**		8.1005	6.3268
Triplet energy (cm^{-1})		22279	25028
***R_L* Triplet (Å)**		7.4420	7.5524
Singlet→$^5D_4$	$W_{ET1}(s^{-1})$	6.00×10^{2}	9.14×10^{2}
	$W_{BT1}(s^{-1})$	3.21×10^{-13}	2.51×10^{-15}
Triplet→ $^5D_1$	$W_{ET2}(s^{-1})$	5.44×10^{8}	9.66×10^{7}
	$W_{BT2}(s^{-1})$	9.16×10^{1}	3.05×10^{-6}
Triplet→ $^5D_0$	$W_{ET3}(s^{-1})$	4.09×10^{8}	1.16×10^{7}
	$W_{BT3}(s^{-1})$	1.69×10^{-2}	5.20×10^{-9}

4.4.4.2. Intramolecular energy transfer in the Eu^{3+} complexes

In order to understand the energy transfer process in the newly derived Eu^{3+} complexes, the energy levels of the relevant electronic states of the ligands have been determined. The singlet (S_1) and triplet (T_1) energy levels of DPPFH was estimated by referring to its wavelength of UV-vis absorption edge and the lower wavelength emission edge of the corresponding phosphorescence spectra of the Gd^{3+} complex **2** (Figure 4.9). The S_1 and T_1 of DPPFH are found to be 25,906 and 21,186 cm^{-1}, respectively. The S_1 (31,847 cm^{-1}) and T_1 (23,470 cm^{-1}) levels of chelating phosphine oxide were obtained from our previous publication.[3e] Thus, the energy gap between the Eu^{3+} state ($^5D_0$ = 17,250 cm^{-1}) and the donor ligands turns out to be 3936 and 6220 cm^{-1} for DPPFH and DDXPO, respectively. This suggests that the triplet states of the *β*-diketone and ancillary ligands are energetically compatible with an efficient energy transfer process. Furthermore, the $^5D_1$ Eu^{3+} emitting state, located at approximately 18,800 cm^{-1}, is critically close to the triplet energy level of the DPPFH. The corresponding energy gaps $\Delta E(T_1-{}^5D_1)$ = 2111 cm^{-1} (DPPFH) and 4400 cm^{-1} (DDXPO) are too high to allow thermal back-energy transfer from the central Eu^{3+} ion.[34] According to Reinhoudt's empirical rule [35], that the intersystem crossing process becomes effective when $\Delta E(S_1\text{-}T_1)$ is around 5000 cm^{-1} and hence the intersystem crossing process is effective for the newly designed *β*-diketone ligand (4720 cm^{-1}).[3b, 3c] Based on the preceding observations, the schematic

representation of energy level diagram showing the possible energy transfer pathways for the typical Eu^{3+} complex (**3**) is depicted in figure 4.10.

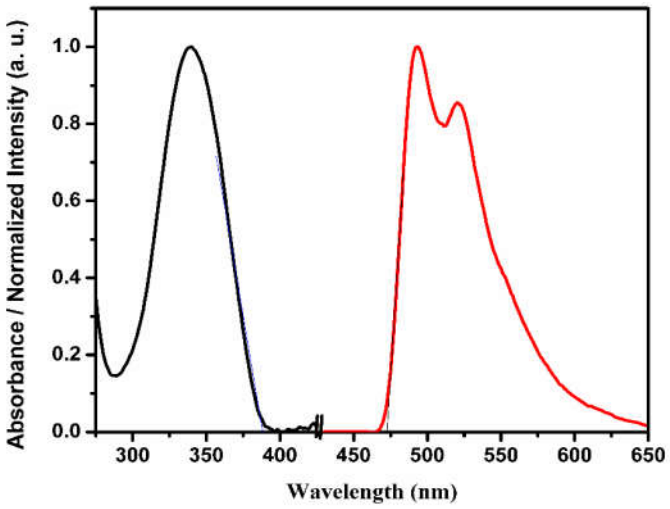

Figure 4.9. UV–vis absorption spectrum at 298 K (black) and 77 K phosphorescence spectra (red) of the $Gd(DPPF)_3(H_2O)_2$ complex.

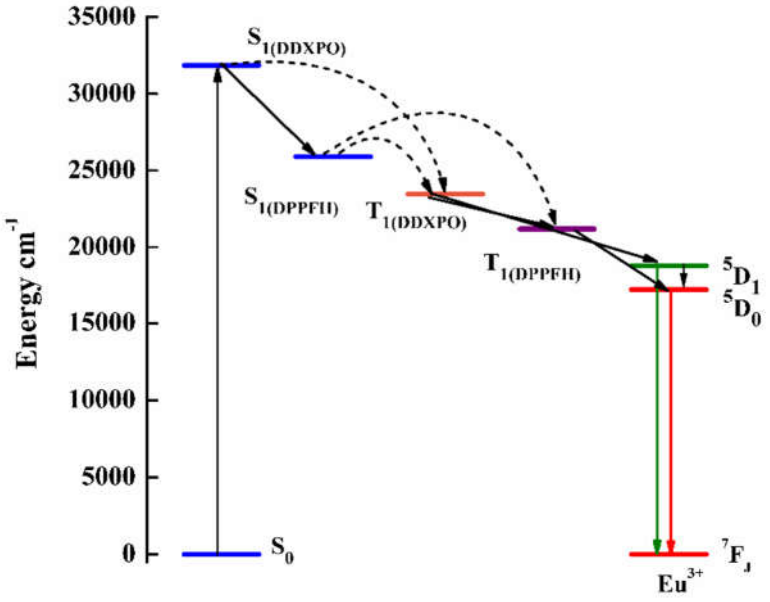

Figure 4.10. Schematic energy level diagram and energy transfer processes for the complex **3**. S_1 represents the first excited singlet state and T_1 represents the first excited triplet state.

4.4.4.3. Luminescent properties analysis for Eu^{3+} complex doped PMMA polymer film

The investigation of quantitative photophysical data of polymer films derived from Eu^{3+}-*β*-diketonate complexes embedded in PMMA are crucial for the realization of practical optical applications in light emitting devices[9a], active waveguides[36] and biomedical actuators[1e] and sensors [37]. Hence in the present study, we describe the incorporation of newly designed luminescent $Eu(DPPF)_3(DDXPO)$ (**3**) complex into PMMA matrix, a well-known, low-cost and easily prepared polymer of excellent optical quality. The PMMA polymer was doped with $Eu(DPPF)_3(DDXPO)$ (**3**) in the proportions of 5, 7, 9, 11 and 13% (w/w) and characterized by FT-IR and Raman spectroscopic studies. The FT-IR spectra of precursor pure $Eu(DPPPF)_3(DDXPO)$ and embedded Eu^{3+} complex in PMMA (Complex **3** at 9% in PMMA) have been recorded in the 400-4000 cm^{-1} region to understand the extent of miscibility of the complex in PMMA and the results are shown in figure 4.11. The characteristic bands of pure PMMA, i.e, C—O—C symmetric stretching, O—CH_3 deformation, —CH_3 asymmetric stretch and O—CH_2 asymmetric stretch, occur at 990, 1384, 2949 and 2993 cm^{-1}, respectively.[38] In addition, an intense and sharp peak at 1733 cm^{-1} noted can be assigned to carbonyl group. In the doped polymer PMMA film, all the PMMA peaks are shifted toward lower wavenumbers, indicating the influence of ligand molecules on the microenvironment of the PMMA host and the mutual interaction between them. Further, the absorption peaks become sharper after the incorporation of the complex. This signifies the alignment of a large number of molecules having the same

orientation.[9c] The Raman shifts of Eu^{3+} complex (**3**) can be attributed to 1603 cm^{-1} (ν C=O), 1549 cm^{-1} (ν_{as} COO-), 1104 cm^{-1}(ν_{as} CF_3−) and 1006 cm^{-1} (ring deformation).[39] PMMA film doped with Eu^{3+} complex, exhibit superimposed Raman shifts (figure 4.12) of both the species.

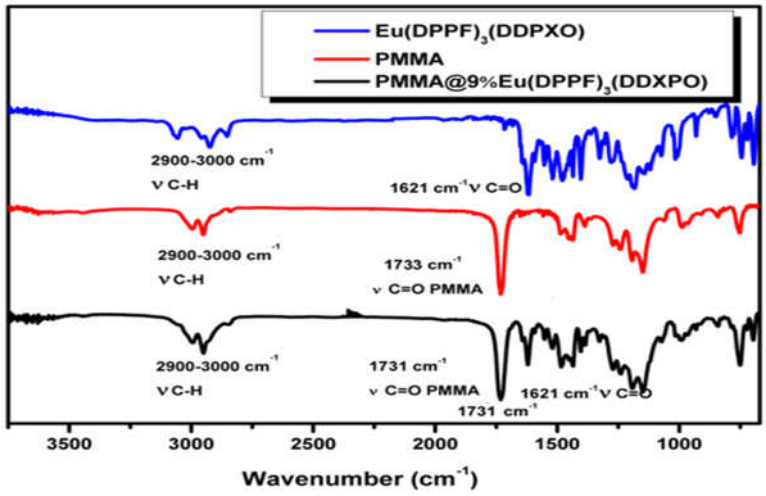

Figure 4.11. FT-IR Spectra for the complex $Eu(DPPF)_3(DDXPO)$, PMMA and PMMA film doped with complex **3**.

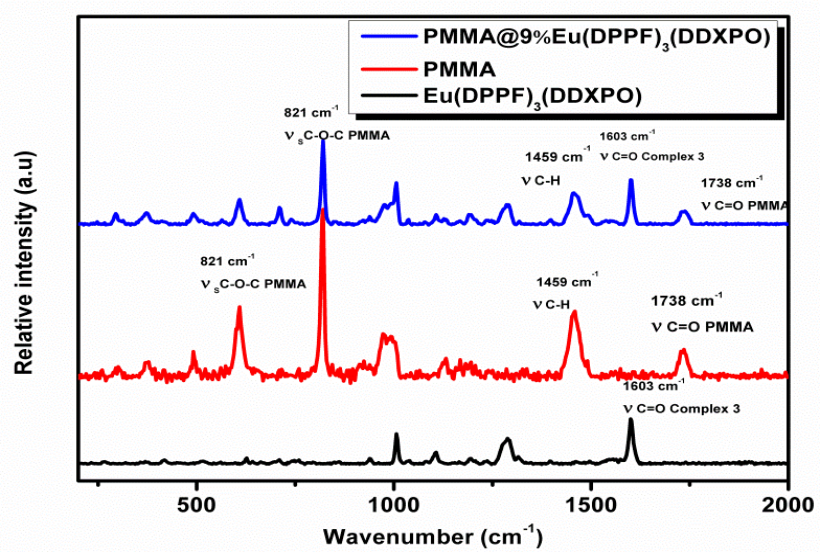

Figure 4.12. Raman Spectra for the complex $Eu(DPPF)_3(DDXPO)$ PMMA and PMMA film doped with complex **3**.

The thermal stabilities of the developed complex $Eu(DPPF)_3(DDXPO)$ and the PMMA@9 (9% complex **3** in PMMA) film were evaluated by TG and DTA measurements and the results are depicted in figures 4.3 and 4.13. The DTA curve shows that the thermal stability of the Eu^{3+} ternary complex (340°C decomposition temperature) has been significantly improved after incorporating into polymer film (424°C decomposition temperature). It can be noted from the TG curve of PMMA@9 that the PMMA began to decompose at 357°C. Further when the temperature reached 490°C the polymer has departed from the hybrid material. The results demonstrate that the thermal stability of the Eu^{3+} complex embedded PMMA film has been enhanced.

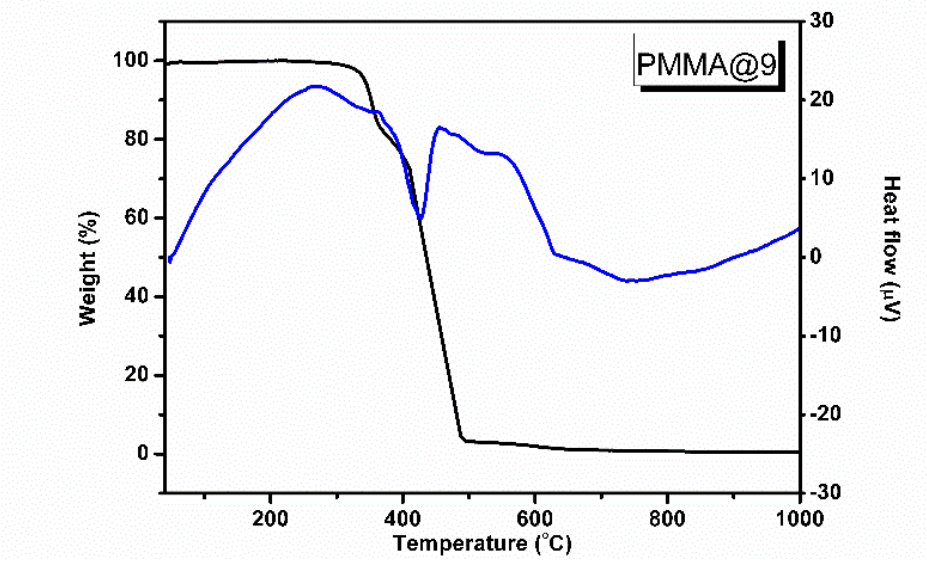

Figure 4.13. Thermogravimetric analysis for the PMMA film doped with complex **3.**

Figure 4.14 shows the excitation spectra of PMMA polymer films doped with complex **3** at different concentrations [5 (PMMA @5), 7 (PMMA @7), 9 (PMMA @9),

11 (PMMA @11), and 13% (w/w)(PMMA @13)] recorded at 298K by monitoring the emission at 612 nm. The excitation spectra are dominated by an intense broad band in the region 300-400 nm which can be assigned to absorptions of PMMA and triphenylphosphine based β-diketonate ligand. The emission spectra of PMMA doped with Eu^{3+} complex **3** at various concentrations and excited at 375 nm exhibit five emission bands that are assigned to characteristic $^5D_0 \rightarrow {}^7F_J$ (J = 0-4) transitions of Eu^{3+}. It can be noted from the emission profiles that the luminescent intensity of the Eu^{3+} at 612 nm increases with increasing Eu^{3+} concentration and reaches a maximum at a Eu^{3+} concentration of 9%. A further increase in the Eu^{3+} concentration [PMMA @11, PMMA @13], in PMMA matrix diminishes the luminescence intensity. It is well documented that the energy transfer between the Eu^{3+} ions generates a non-radiative process, which accounts for the decrease in the emission intensity of Eu^{3+}, notably at high Eu^{3+} concentration in the PMMA film.[40] Interestingly, the emission intensity at 612 nm peak for all the films embedded with Eu^{3+} complexes is found to be higher than that of the precursor complex (**3**). This can be attributed to the phenomenon that PMMA enhances the light absorption cross-section and hence more energy can be transferred to the central Eu^{3+} ion based on the higher emission intensity. The intensity ratio (A_{21}) between the intensity of the $^5D_0 \rightarrow {}^7F_2$ transition over the intensity of the $^5D_0 \rightarrow {}^7F_1$ transition amounts to 12.06 and 13.69 for complex **3** being conditioned in powder and as a dopant in a film of PMMA, respectively. The moderate enhancement in the

intensity parameter in the doped films shows that the local symmetry of the Eu^{3+} ion in the molecular complex **3** is retained whatever the chemical conditions used.[41]

The luminescence decay profiles of the doped films were obtained by monitoring the emission at the hypersensitive $^5D_0 \rightarrow {}^7F_2$ transition (612 nm) and excited at 375 nm (Figure 4.15). These data were fitted with a first-order exponential decay function and the lifetime values (τ) of the emitter $^5D_0$ level of the PMMA doped systems were determined and are given in Table 4.5. All the τ values of the doped polymer systems are found to be higher than that of the precursor complex (**3**), thus indicating that the radiative processes are operative in all the doped polymer films.

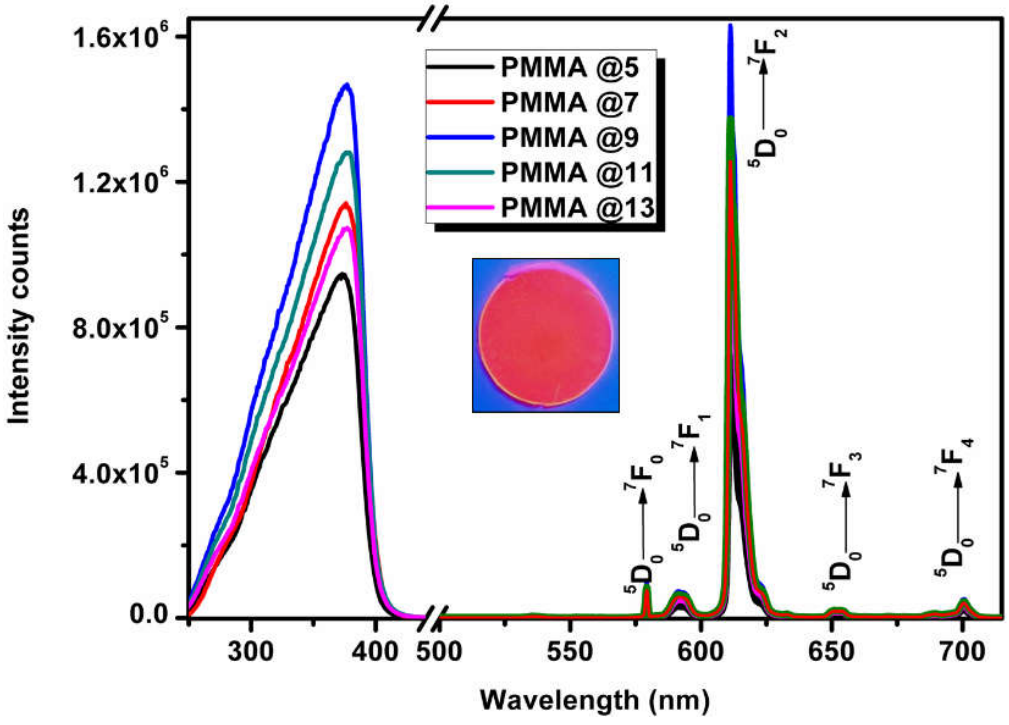

Figure 4.14. Excitation and emission spectra of PMMA films doped with 5, 7, 9, 11 and 13% (w/w) of $Eu(DPPF)_3(DDXPO)$. The data were recorded at 298 K.

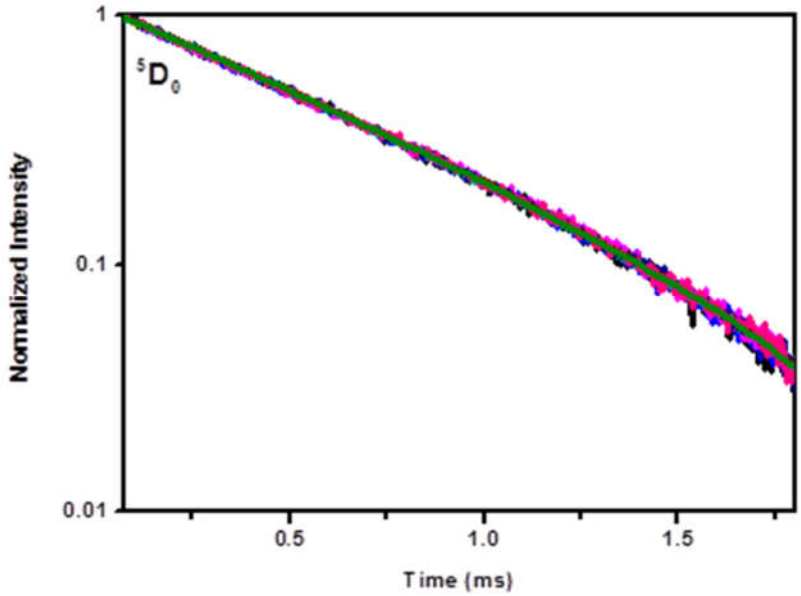

Figure 4.15. $^5D_0$ decay profiles for Eu^{3+} complex **3** doped into PMMA polymer where emission monitored around 612 nm. The straight lines are the best fits (r^2 = 0.999) considering single-exponential behavior.

Table 4.5. Luminescence Parameters for complex **1, 3** and PMMA films doped with various amounts of the complex **3**, at 298 K.

Complex	A_{21}	A_{RAD} (Sec^{-1})	A_{NR} (Sec^{-1})	τ_{obs} (μs)	Φ_{Ln} (%)	Φ_{Sens} (%)	$\Phi_{Overall}$ (%)
$Eu(DPPF)_3(H_2O)_2$	11.52	739	2292	330±3	24	67	18±3
$Eu(DPPF)_3(DDXPO)$	12.06	825	971	557±2	46	84	39±4
PMMA 5	13.73	1111	415	655±2	72	58	42±4
PMMA 7	13.39	1080	448	654±2	73	61	45±4
PMMA 9	13.64	1181	408	654±2	71	71	50±4
PMMA 11	13.16	1105	416	657±2	73	66	48±4
PMMA 13	13.34	1070	458	654±2	70	67	47±4

The overall quantum yields determined by the absolute method, radiative and non-radiative decay rates, intrinsic quantum yields and energy transfer efficiencies of the PMMA films doped with Eu^{3+} complex **3** at different concentrations are listed in

Table 4.5. All the PMMA doped films exhibit excellent intrinsic quantum yields in the range 70-72% and are found to be significantly higher than that of the precursor complex (46%). This can be explained on the basis of radiative and non-radiative decay rates noted for the doped films. The non-radiative decay rates have been significantly lowered in the doped films as compared to complex **3**. The PMMA film doped with complex **3** (50%) exhibits good overall quantum yield as compared to complex **3** (39%). Thus, the preserved rigidity in complex structure in PMMA could be the origin of the enhanced overall quantum yield. Further, the improved photophysical properties of the PMMA doped films may arise from the enhanced encapsulation of Eu^{3+} centre minimizing the detrimental effect of the C-H oscillators in the PMMA matrix that potentially provide non-radiative decay pathways for the Eu^{3+} excited state. The photographs of PMMA films doped with 9% (w/w) of $Eu(DPPF)_3(DDXPO)$ under normal light and UV illumination (365 nm) are displayed in figure 4.16.

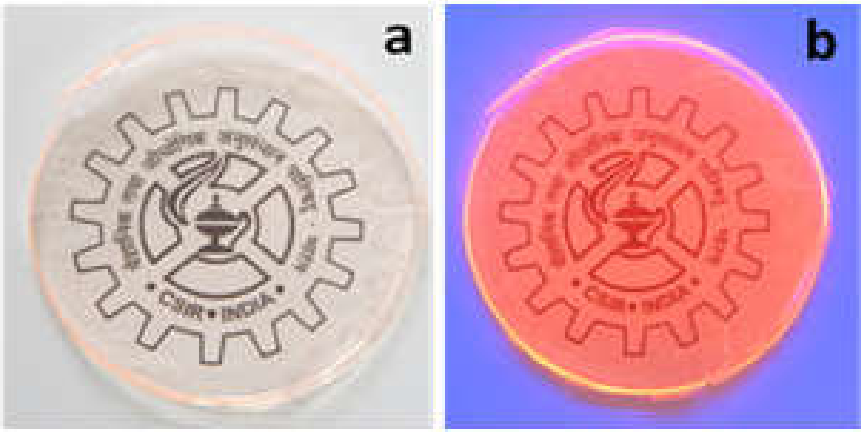

Figure 4.16. Photographs of PMMA films doped with 9% (w/w) of $Eu(DPPF)_3(DDXPO)$ (a) under normal light (b) under UV illumination (365 nm).

4.4.5. Triboluminescence

Triboluminescence is defined as the emission of light upon fracture of the material, the excitation energy being produced by the mechanical grinding of the microcrystals of the lanthanide compounds. Eliseeva and co-workers have reported on triboluminescent Eu^{3+} coordination with low-vibrational-frequency hexafluoroacetylacetonato ligands.[42] Hasegawa *et al*. [43] reported brilliant triboluminescence from a lanthanide coordination polymer with low-vibrational-frequency and non-centrosymmetric structural networks. The ability of the Eu^{3+} complex (**3**) and the corresponding complex embedded polymer film to generate triboluminescence (TL) is ascertained by the spectra recorded under by applying mechanical pressure on the samples. Figure 4.17 shows the triboluminescence spectra for complex **3** and the complex embedded polymer film at 298K. Both the TL spectra match the overall pattern of the photoluminescence spectra, indicating that TL involves Eu^{3+} excited state ($^5D_0$). The TL of complex **3** is quite intense, as indicated by the short dropping heights (Section **4.3.1**) and by the fact that, it is visible to the naked eye in daylight allowing detection using inexpensive, compact detectors. On the other hand, there is a slight decrease in the triboluminesence intensity for the complex doped polymer film than the complex **3.** This might be due to the decrease in the short range order observed in hybrid polymer film compared with the solid state (Figure 4.18). The two peaks observed for the complex **3** at 6.90° and 19.56° were broadened in the presence of PMMA, which is evident from the XRD pattern.

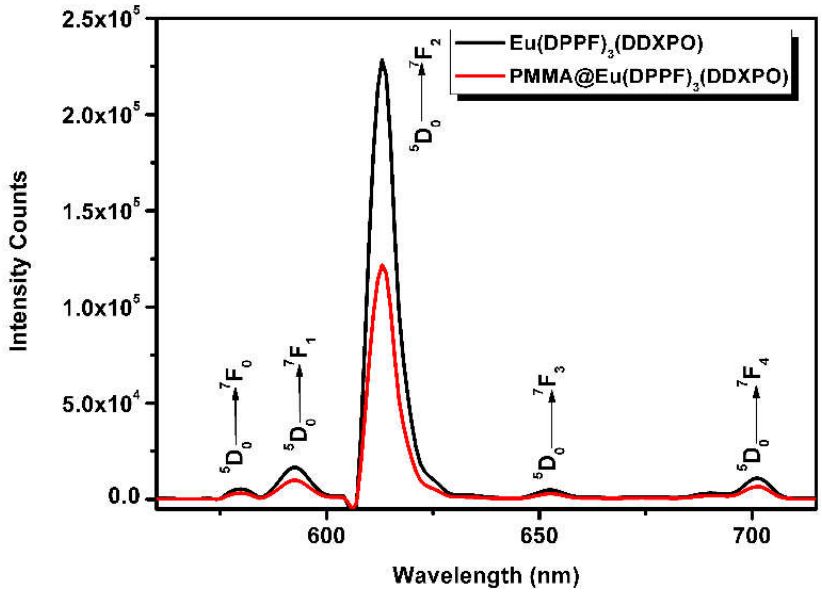

Figure 4.17. Triboluminescence (TL) spectra (uncorrected) of complex **3** and 9% complex **3** doped PMMA film recorded at 298K.

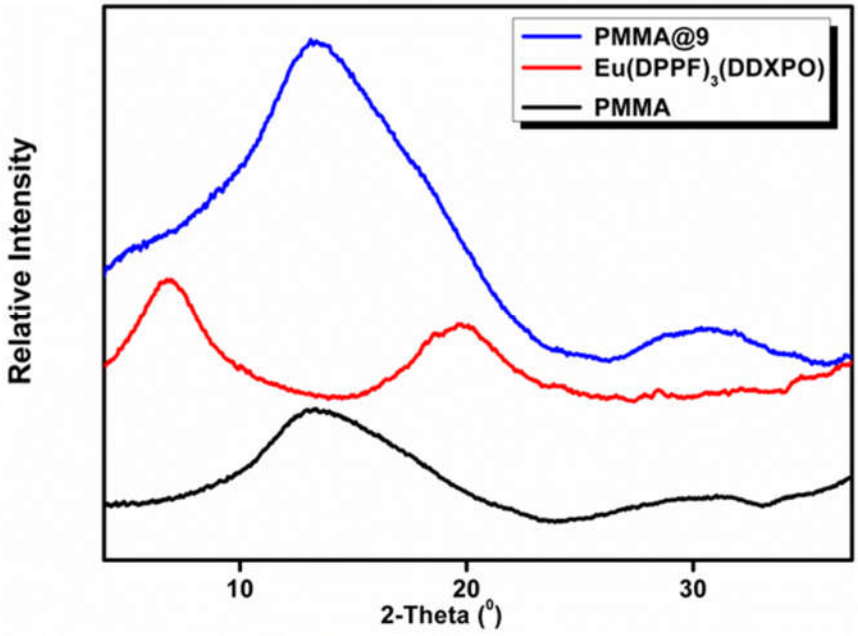

Figure 4.18. Powder XRD pattern for the complex $Eu(DPPF)_3(DDXPO)$, PMMA and PMMA@9 films.

Highly luminescent lanthanides β-diketonates are prone to display this type of luminescence, and several examples are well documented.[3a, 42] Taking into consideration of the impressive thermal stability (340°C), the developed Eu^{3+} complex is potentially well suited as smart optical sensor.

4.5. Conclusions

- A new triphenylphosphine based polyfluorinated β-diketonate ligand was developed and utilized for the construction of a Eu^{3+} ternary complex in the presence of a chelating phosphine oxide.
- The developed Eu^{3+}-β-diketonate complex possesses high molar absorption coefficient (4.25×10^4 L mol^{-1} cm^{-1} at 350 nm) and displays strong red emission (solid state quantum yield = 39%) upon irradiation at the ligand-centered band in the range 300−400 nm.
- Notably, the developed Eu^{3+}-β-diketonate complex also exhibits impressive triboluminescence in the daylight, which may find potential applications in developing smart optical probes.
- Additionally, the newly designed europium complex was embedded into PMMA polymer films, which is shown to exhibits greater thermal stability (424°C decomposition temperature) and high photoluminescence quantum yield (50%) as compared to the precursor complex (340°C decomposition temperature).

- The PMMA films doped with the Eu^{3+}-β-diketonate complex show promising PL efficiency and therefore have potential applications as polymer light-emitting diodes and active polymer optical fibers.
- The theoretical photophysical properties such as radiative and non-radiative decay rates, intrinsic and overall quantum yields and intensity parameters of the developed Eu^{3+} complex calculated using the Sparkle/RM1 model are in excellent agreement with the experimental values, clearly demonstrates the validity of the theoretical models.

4.6. References

1. (a) J.-C. G. Bünzli, *Coord. Chem. Rev.*, 2015, **293**, 19-47; (b) M. L. P. Reddy and S. Sivakumar, *Dalton Trans.*, 2013, **42**, 2663-2678; (c) J.-C. G. Bünzli and S. V. Eliseeva, *Chem. Sci.*, 2013, **4**, 1939; (d) W. Xiaohui, C. Hongjin, X. Juan, Z. Baozhou, L. Botong, X. Shuilin, P. Wenbo, R. Na, H. Ling and H. Wei, *Coord. Chem. Rev.*, 2014, **273-274**, 201212; (e) L. D. Carlos, R. A. Ferreira, Z. Bermudez Vde and S. J. Ribeiro, *Adv. Mater.*, 2009, **21**, 509-534; (f) J. Rocha, L. D. Carlos, F. A. Paz and D. Ananias, *Chem. Soc. Rev.*, 2011, **40**, 926-940; (g) S. J. Butler and D. Parker, *Chem. Soc. Rev.*, 2013, **42**, 1652-1666; (h) C. Yuanjing, C. Banglin and Q. Guodong, *Coord. Chem. Rev.*, 2014, **273**, 76-86; (i) J.-C. G. Bünzli, *J. Coord. Chem.*, 2014, **67**, 3706-3733; (j) J. Andres, R. D. Hersch, J.-E. Moser and A.-S. Chauvin, *Adv. Funct. Mater.*, 2014, **24**, 5029-5036; (k) T. Datao, Z. Wei, L. Yongsheng, Z. Haomiao and C. Xueyuan, *Coord. Chem. Rev.*, 2014, **273-274**, 1329; (l) M. L. Reddy, V. Divya and R. Pavithran, *Dalton Trans.*, 2013, **42**, 15249-15262; (m) X. Huang, S. Han, W. Huang and X. Liu, *Chem. Soc. Rev.*, 2013, **42**, 173-201.

2. (a) A. R. Ramya, D. Sharma, S. Natarajan and M. L. Reddy, *Inorg. Chem.*, 2012, **51**, 8818-8826; (b) A. R. Ramya, M. L. Reddy, A. H. Cowley and K. V. Vasudevan, *Inorg. Chem.*, 2010, **49**, 2407-2415.

3. (a) S. Biju, N. Gopakumar, J. C. G. Bünzli, R. Scopelliti, H. K. Kim and M. L. P. Reddy, *Inorg. Chem.*, 2013, **52**, 8750-8758; (b) V. Divya, S. Biju, R. L. Varma and M. L. P. Reddy, *J. Mater. Chem.*, 2010, **20**, 5220-5227; (c) V. Divya, R. O. Freire and M. L. P. Reddy, *Dalton Trans.*, 2011, **40**, 3257-3268; (d) V. Divya, V. Sankar, K. G. Raghu and M. L. P. Reddy, *Dalton Trans.*, 2013, **42**, 12317-12323; (e) D. B. A. Raj, S. Biju and M. L. P. Reddy, *Dalton Trans.*, 2009, **36**, 7519-7528; (f) T. V. Usha Gangan and M. L. P. Reddy, *Dalton Trans.*, 2015, **44**, 15924-15937.

4. (a) W. Xiaohui, C. Hongjin, X. Juan, Z. Baozhou, L. Botong, X. Shuilin, P. Wenbo, R. Na, H. Ling and H. Wei, *Coord. Chem. Rev.*, 2014, **273**, 201-212; (b) L. Armelao, S. Quici, F. Barigelletti, G. Accorsi, G. Bottaro, M. Cavazzini and E. Tondello, *Coord. Chem. Rev.*, 2010, **254**, 487-505; (c) B.-D. Ana de, S. B. Patrick and V. Subha, *Coord. Chem. Rev.*, 2014, **273**, 165-200; (d) P. A. Vigato, P. Valentina and T. Sergio, *Coord. Chem. Rev.*, 2009, **253**, 1099-1201; (e) B. Koen, *Chem. Rev.*, 2009, **109**, 4283-4374.

5. D. B. A. Raj, B. Francis, M. L. P. Reddy, R. R. Butorac, V. M. Lynch and A. H. Cowley, *Inorg. Chem.*, 2010, **49**, 9055-9063.

6. Y. Qiao, H. Chen, Y. Lin, Z. Yang, X. Cheng and J. Huang, *J. Phys. Chem. C*, 2011, **115**, 7323-7330.

7. (a) B. Francis, D. B. Ambili Raj and M. L. Reddy, *Dalton Trans.*, 2010, **39**, 8084-8092; (b) D. B. A. Raj, S. Biju and M. L. P. Reddy, *J. Mater. Chem.*, 2009, **19**, 7976-7983; (c) X. M. Guo, X. M. Wang, H. J. Zhang, L. S. Fu, H. D. Guo, J. B. Yu, L. D. Carlos and K. Y. Yang, *Microporous Mesoporous Mater.*, 2008, **116**, 28-35; (d) L. J. Jia, J. Y. Shen, Z. Y. Li, D. R. Zhang, Q. Zhang, G. P. Liu, D. D. Zheng and X. N. Tian, *Int. J. Pharm.*, 2013, **445**, 12-19; (e) A. V. S. Lourenco, C. A. Kodaira, E. R. Souza, M. C. F. C. Felinto, O. L. Malta and H. F. Brito, *Opt. Mater.*, 2011, **33**, 1548-1552.

8. (a) V. Divya and M. L. P. Reddy, *J. Mater. Chem. C*, 2013, **1**, 160-170; (b) L. Maggini, M. Liu, Y. Ishida and D. Bonifazi, *Adv. Mater.*, 2013, **25**, 2462-2467; (c) X. Xin, M.

Pietraszkiewicz, O. Pietraszkiewicz, O. Chernyayeva, T. Kalwarczyk, E. Gorecka, D. Pociecha, H. Li and R. Hołyst, *Carbon*, 2012, **50**, 436-443.

9. (a) L. L. Beecroft and C. K. Ober, *Chem. Mater.*, 1997, **9**, 1302-1317; (b) K. Binnemans, *Chem. Rev.*, 2009, **109**, 4283-4374; (c) W. Li, P. Yan, G. Hou, H. Li and G. Li, *Dalton Trans.*, 2013, **42**, 11537-11547.

10. E. B. Gibelli, J. Kai, E. E. S. Teotonio, O. L. Malta, M. C. F. C. Felinto and H. F. Brito, *J. Photochem. Photobiol., A*, 2013, **251**, 154-159.

11. W. Jinshan, X. Xinjun, T. Yuan, Y. Chuang, L. Ronghua and L. Lidong, *J. Mater. Chem. C*, 2015, **3**, 2856-2864.

12. Y. Hasegawa, Y. Wada and S. Yanagida, *J. Photochem. Photobiol., C*, 2004, **5**, 183-202.

13. (a) B. K. Shah, D. C. Neckers, J. Shi, E. W. Forsythe and D. Morton, *Chem. Mater.*, 2006, **18**, 603-608; (b) J. C. de Mello, H. F. Wittmann and R. H. Friend, *Adv. Mater.*, 1997, **9**, 230-232.

14. N. S. S. Kumar, S. Varghese, N. P. Rath and S. Das, *J. Phys. Chem. C*, 2008, **112**, 8429-8437.

15. B. P. Chandra and J. I. Zink, *Phys. Rev. B*, 1980, **21**, 816-826.

16. F. Y. Kwong, C. W. Lai, M. Yu and K. S. Chan, *Tetrahedron*, 2004, **60**, 5635-5645.

17. O. Moudam, B. C. Rowan, M. Alamiry, P. Richardson, B. S. Richards, A. C. Jones and N. Robertson, *Chem. Commun.*, 2009, **43**, 6649-6651.

18. (a) J. D. L. Dutra, T. D. Bispo and R. O. Freire, *J. Comput. Chem.*, 2014, **35**, 772-775; (b) M. A. M. Filho, J. D. L. Dutra, G. B. Rocha, R. O. Freire and A. M. Simas, *RSC Adv.*, 2013, **3**, 16747-16755; (c) J. P. Stewart, *Stewart Comput. Chem. Version 13.113W*, MOPAC2012, Colorado. Springs.

19. R. O. Freire, G. B. Rocha and A. M. Simas, *J. Mol. Model.*, 2006, **12**, 373-389.

20. (a) J. Ridley and M. Zerner, *Theor. Chim. Acta*, 1976, **42**, 223-236; (b) M. C. Zerner, G. H. Loew, R. F. Kirchner and U. T. Mueller-Westerhoff, *J. Am. Chem. Soc.*, 1980, **102**, 589-599.

21. F. Neese, *Wiley Interdiscip. Rev. Comput. Mol. Sci.*, 2012, **2**, 73-78.

22. V. Divya, R. O. Freire and M. L. P. Reddy, *Dalton Trans.*, 2011, **40**, 3257-3268.

23. S. Biju, Y. K. Eom, J.-C. G. Bünzli and H. K. Kim, *J. Mater. Chem. C*, 2013, **1**, 3454.

24. G. F. de Sá, O. L. Malta, C. de Mello Donegá, A. M. Simas, R. L. Longo, P. A. Santa-Cruz and E. F. da Silva Jr, *Coord. Chem. Rev.*, 2000, **196**, 165-195.

25. A. Dossing, *Eur. J. Inorg. Chem.*, 2005, **2005**, 1425-1434.

26. B.-D. Ana de, *Dalton Trans.*, 2007, **22**, 2229-2241.

27. Z. Ahmed and K. Iftikhar, *J. Phys. Chem. A*, 2013, **117**, 11183-11201.

28. N. M. Shavaleev, S. V. Eliseeva, R. Scopelliti and J. C. Bünzli, *Inorg. Chem.*, 2010, **49**, 3927-3936.

29. J. Guan, B. Chen, Y. Sun, H. Liang and Q. Zhang, *J. Non-Cryst. Solids*, 2005, **351**, 849-855.

30. O. L. Malta, M. A. C. dos Santos, L. C. Thompson and N. K. Ito, *J. Lumin.*, 1996, **69**, 77-84.

31. W. T. Carnall, H. Crosswhite and H. M. Crosswhite, *Energy level structure and transition probabilities in the spectra of the trivalent lanthanides in LaF.* , 1978.

32. (a) O. L. Malta, H. F. Brito, J. F. S. Menezes, F. R. Gonçalves e Silva, C. de Mello Donegá and S. Alves Jr, *Chem. Phys. Lett.*, 1998, **282**, 233-238; (b) O. L. Malta, *J.*

Lumin., 1997, **71**, 229-236; (c) F. R. G. e Silva and O. L. Malta, *J. Alloys Compd.*, 1997, **250**, 427-430.

33. (a) R. Pavithran, M. L. P. Reddy, S. A. Junior, R. O. Freire, G. B. Rocha and P. P. Lima, *Eur. J. Inorg. Chem.*, 2005, **2005**, 4129-4137; (b) A. V. M. de Andrade, N. B. da Costa Jr, O. L. Malta, R. L. Longo, A. M. Simas and G. F. de Sá, *J. Alloys Compd.*, 1997, **250**, 412-416.

34. L. Martti, T. Harri, M. Veli-Matti, M. Cristina, C. R.-U. Juan and K. Jouko, *J. Lumin.*, 1997, **75**, 149-169.

35. F. J. Steemers, W. Verboom, D. N. Reinhoudt, E. B. van der Tol and J. W. Verhoeven, *J. Am. Chem. Soc.*, 1995, **117**, 9408-9414.

36. C. Sanchez, B. Julian, P. Belleville and M. Popall, *J. Mater. Chem.*, 2005, **15**, 3559-3592.

37. C. Sanchez, B. Lebeau, F. Chaput and J. P. Boilot, *Adv. Mater.*, 2003, **15**, 1969-1994.

38. J. Jang and J. H. Oh, *Adv. Funct. Mater.*, 2005, **15**, 494-502.

39. P. Martín-Ramos, M. Ramos Silva, F. Lahoz, I. R. Martín, P. Chamorro-Posada, M. E. S. Eusebio, V. Lavín and J. Martín-Gil, *J. Photochem. Photobiol., A*, 2014, **292**, 16-25.

40. (a) Q. Li, T. Li and J. Wu, *J. Phys. Chem. B*, 2001, **105**, 12293-12296; (b) D. F. Parra, A. Mucciolo and H. F. Brito, *J. Appl. Polym. Sci.*, 2004, **94**, 865-870.

41. G. Zucchi, V. Murugesan, D. Tondelier, D. Aldakov, T. Jeon, F. Yang, P. Thuery, M. Ephritikhine and B. Geffroy, *Inorg. Chem.*, 2011, **50**, 4851-4856.

42. V. E. Svetlana, N. P. Dmitry, A. L. Konstantin, S. L. Leonid, G. B. Jean-Claude and P. K. Natalia, *Inorg. Chem.*, 2010, **49**, 9300-9311.

43. Y. Hasegawa, R. Hieda, K. Miyata, T. Nakagawa and T. Kawai, *Eur. J. Inorg. Chem.*, 2011, **2011**, 4978-4984.

Papers Presented at Conferences

1. Bright Red Luminescence and Triboluminescence from PMMA-Doped Polymer Film Materials Supported by Eu^{3+} Triphenylphosphine Based *β*-Diketonate and 4,5-Bis(Diphenylphosphino)-9,9-Dimethylxanthene Oxide. **T. M. George**, S. J. Sajan & M. L. P. Reddy.

   Presented a paper at the poster session in the *International Symposium on Photonic Applications and Nanomaterials (ISPAN-2015)* during 28-30 October **2015** organized by Sree Chitra Tirunal Institute for Medical Sciences and Technology, Thiruvananthapuram.

2. PMMA-Supported Hybrid Materials Doped with Europium Complexes Based on Fluorinated *β*-Diketonate Ligands and 4,5-Bis-(Diphenylphosphino)-9,9-Dimethylxanthene Oxide as Co-Ligand. **T. M. George**, & M. L. P. Reddy.

   Presented a poster at the *National Conference on Analytical Science for Technological Excellence and Environmental Sustainability* organized by the Indian Society of Analytical Scientists, held in Munnar, Kerala, India during September 24-26, **2015**.

3. Highly Luminescent Europium Complexes Supported By Indole-Based Fluorinated *β*-Diketonate Ligands and 4,5- Bis Diphenylphosphine-9,9- Dimethylxanthene Oxide as Co-ligand. **T. M. George**, & M. L. P. Reddy.

   Presented a poster at the *International Conference on Science, Technology and Applications of Rare earths (ICSTAR 2015)* organized by Rare Earths Association of India (REAI) held at Thiruvananthapuram during April 23-25, **2015**. (***Best poster award***).

4. AIPE-Active Green Phosphorescent Iridium(III) Complex Impregnated Test Strips for the Vapor-Phase Detection of 2,4,6-Trinitrotoluene (TNT). K. S. Bejoymohandas, **T. M. George**, & M. L. P. Reddy.

   Presented a poster in the *Indian Society of Analytical Scientists conference (ISAS 2014; Theme - Advanced Technologies for Material Processing and Diagnostics)* held at Kochi. Kerala during September 18-21, **2014**. (***Best poster award***).

5. AIPE-Active Green Phosphorescent Iridium(III) Complex Impregnated Test Strips for the Vapor-Phase Detection of 2,4,6-Trinitrotoluene (TNT). K. S. Bejoymohandas, M.

V. Lucky, P. K Thejus, Alikunhi, **T. M. George**, S. Bhattacharya, S. Natarajan & M. L. P. Reddy.

Presented a poster at the *International Conference on Advanced Functional Material (ICAFM)* organized by CSIR-NIIST, Thiruvananthapuram, India during February 19-21, **2014**.

List of Publications

From the thesis

1. Bright red luminescence and triboluminescence from PMMA-doped Polymer film materials supported by Eu^{3+}-triphenylphosphine based β-diketonate and 4,5-bis(diphenylphosphino)-9,9-dimethylxanthene oxide; **T. M. George**, M. J. Sajan, N. Gopakumar, and M. L. P. Reddy.

   Journal of Photochemistry and Photobiology A: Chemistry, **2016**, 317, 88–99.

2. Near-infrared luminescence of Nd^{3+} and Yb^{3+} complexes using a polyfluorinated pyrene-based β-diketonate ligand; **T. M. George**, S. Varughese, and M. L. P. Reddy.

   RSC Advances, **2016**, 6, 69509–69520.

3. Lysosome targetable luminescent bioprobe based on a europium β-diketonate complex for cellular imaging applications; **T. M. George**, Mahesh S. Krishna, and M. L. P. Reddy.

   Dalton Transactions, **2016,** 45, 18719-18729.

Out of the thesis

1. AIPE-active green phosphorescent iridium(III) complex impregnated test strips for the vapor phase detection of 2,4,6-trinitrotoluene (TNT); K. S. Bejoymohandas, **T. M. George**, S. Bhattacharya, S. Natarajan and M. L. P. Reddy.

   Journal of Materials Chemistry C, **2014**, 2, 515–523.